THESIS FOR THE DEGREE OF DOCTOR OF PHILOSOPHY

d-wave Josephson Junctions
-Dynamics and Applications in the Quantum Regime

Tobias Lindström

Department of Microtechnology and Nanoscience
CHALMERS UNIVERSITY OF TECHNOLOGY
Göteborg, Sweden 2005

d-wave Josephson Junctions
-Dynamics and Applications in the Quantum Regime
Tobias Lindström

ISBN: 91-7291-664-8
Doktorsavhandlingar vid Chalmers Tekniska Högskola,
Ny serie nr: 2346
ISSN: 0346-718x

Technical Report MC2-40
ISSN: 1652-0769

Quantum Device Physics Laboratory
Department of Microtechnology and Nanoscience
Chalmers University of Technology
SE-412 96 Göteborg
Sweden
Phone +46 (0)31-772 1000

Vasastadens Bokbinderi AB
Göteborg, Sweden 2005

d-wave Josephson Junctions
-Dynamics and Applications in the Quantum Regime
TOBIAS LINDSTRÖM
Department of Microtechnology and Nanoscience
Chalmers University of Technology
Göteborg, Sweden 2005

Abstract

The properties of d-wave YBCO Josephson junctions and dc-SQUIDs with high misorientation angles have been studied experimentally . The predominant d-wave symmetry of the pairing wavefunction in high-T_c superconductors has, to a large extent, been a hindrance in applications, but it also makes it possible to fabricate devices with novel properties that may be suitable for applications in the quantum regime; one particulary interesting property is a strong second harmonic component in the current-phase relation of junctions with the electrodes oriented in a node-lobe arrangement; so-called $0°$-$45°$ junctions.

The work has been focused on the properties of grain-boundary $0°$-$45°$ dc-SQUIDs: Their dc-properties as well as the effects of a strong second harmonic component on the dynamics have been studied experimentally and modeled numerically. The experimental results can be explained by taking into account the meandering of the grain boundary which in combination with a strong orientational dependence of the transport properties due to the d-wave symmetry results in interfaces with properties that change dramatically over a length scale of 50-100 nm.

The properties of grain-boundary YBCO $0°$-$45°$ junctions have been studied in the quantum regime. Macroscopic quantum tunneling has been demonstrated in these junctions and microwave spectroscopy is here used to verify the presence of discrete energy levels. The quality factor of the junction has been experimentally determined to 40 ± 10, a much higher value than previously believed to be possible in high-T_c structures.

Finally, the possibility of using high-T_c structures to build qubits is discussed. There is now a renewed interest in this possibility, especially in light of our recent results which demonstrate that the inherent dissipation mechanisms are much less detrimental to coherent phenomena than previously feared.

Keywords: Josephson junctions, high-temperature superconductivity, Andreev states, intrinsic effects, SQUID dynamics,qubits, macroscopic quantum tunnelling, energy levels

To my family

New ideas pass through three periods:
- It can't be done.
- It probably can be done, but it's not worth doing.
- I knew it was a good idea all along!
- Arthur C. Clarke

LIST OF APPENDED PAPERS

This thesis is based on the contents of the following papers:

I. A.Ya. Tzalenchuk, T. Lindström, S.A. Charlebois, E.A. Stepantsov, A.M. Zagoskin, Z. Ivanov and T. Claeson,
"Feasibility studies of ultra-small Josephson junctions for qubits",
IEEE Transactions on Applied Superconductivity **13**, pp. 48-51(2003)

II. T. Lindström, S.A. Charlebois, A.Ya. Tzalenchuk, Z. Ivanov, M.H.S Amin and A.M. Zagoskin,
"Dynamical Effect of an Unconventional Current-Phase Relation in YBCO dc SQUIDs"
Physical Review Letters **90**, 117002 (2003)

III. A.Ya. Tzalenchuk, T. Lindström, S.A. Charlebois, E.A. Stepantsov, Z. Ivanov and A.M. Zagoskin,
"Mesoscopic Josephson Junctions of high-T_c Superconductors"
Physical Review B **68** 100501(R) (2003)

IV. M.H.S. Amin, A.Y. Smirnov, A.M. Zagoskin, T. Lindström, S.A. Charlebois, T. Claeson, and A.Ya. Tzalenchuk,
"Silent Phase Qubit Based on d-wave Josephson junctions"
Physical Review B **71**, 64516 (2005)

V. T. Lindström, J. Johansson, T. Bauch, F.Lombardi and S.A. Charlebois
"Josephson Dynamics of Bicrystal d-Wave YBCO dc-SQUIDs"
Manuscript(2005)

VI. T. Bauch, F. Lombardi, T. Lindström, F. Tafuri, G.Rotoli, T. Claeson and P. Delsing
"Quantum Dynamics of a d-wave YBCO Josephson Junction"
Submitted(2005)

Contents

Definitions of symbols and how they are used in this thesis

Φ_0	Flux quantum $h/2e$
Φ	Total magnetic flux through a loop
Φ_x	Flux generated by an external field
ϕ_x	Normalized flux $2\pi\Phi/\Phi_0$
θ	Phase of the superconducting wavefunction in a electrode
ϕ	Superconducting phase difference across a junction $\theta_2 - \theta_1$
Ψ	Superconducting wavefunction
I	Bias current
I_c	Critical current of a Josephson junction
I_s	Supercurrent
I_m^n	Our notation for the current components in a SQUID, subscript m=1,2 denotes the junction and superscript n=I, II is the 1^{st} or 2^{nd} harmonic.
α_m	I^{II}/I^I for junction m
E_m^n	Free energy for current component n in junction m
η	E_2^I/E_1^I
j_c	Critical current density
β_L	Dimensionless self-inductance
R_N	Normal resistance of a Josephson junction
ρ_N	Normal resistivity
D	Transparency of the interface
T_c	Critical temperature of a superconductor
l	Mean free path of an electron
V	Voltage
U	Free energy
E_J	Josephson energy
E_c	Charging energy of a Josephson junction
λ	Magnetic penetration depth
λ_J	Josephson penetration depth
ω_p	Bias dependent plasma frequency
ω_0	Zero bias plasma frequency
β_c	Damping parameter of a junction
Q	Quality factor

List of Abbreviations

HTS	High-Temperature Superconductor
CPR	Current-Phase Relation
MQT	Macroscopic Quantum Tunnelling
S-state	The superconducting state ($I < I_c$) of a Josephson junction

Chapter 1

Introduction

The discovery of the high-temperature superconductors (HTS) in 1986 [1] was hailed as a revolution in condensed matter physics. Conventional superconductivity had been known for 75 years. Already in 1911 Kamerlingh Onnes noticed a sudden drop in the resistivity of mercury when the temperature dropped below 4.15K. Over the years that followed more elements were found to exhibit superconductivity but always at very low temperatures. Niobium which is superconducting at temperatures below 9.2K has the highest transition temperature of the pure elements. $YBa_2Cu_3O_{7-\delta}$ (YBCO) which is the most common high-temperature superconductor has a transition temperature of about 92K; still very cold but well above 77K which means that it can be cooled by inexpensive liquid nitrogen.

However, the discovery of the high-T_c materials did not mean that research involving conventional superconductivity ceased. They are easily handled, well understood and often well suited for experiments which aim at investigating quantum phenomena. In 1986 a lot of effort was directed towards investigating quantum phenomenon at the macroscopic scale. In this respect superconductors are ideal systems. Macroscopic Quantum Tunnelling (MQT) [2] in general was first discussed theoretically by Leggett in 1980 in conjunction with the ”quantum measurement problem” and had been experimentally observed in a device known as a superconducting Josephson tunnel junction by Voss and Webb in 1981[3]. However, it took a few years before the phenomenon was well understood.

At the time of this writing both high-temperature superconductors and MQT have been around for about 20 years. They have however rarely crossed paths and it was not until recently that it was suggested that also devices made from HTS materials such as YBCO can exhibit MQT. Moreover, it has also been suggested that high-T_c devices may exhibit effects not found in devices made from conventional superconductors.

In this chapter I will introduce a number of important concepts. Starting with a discussion of bulk superconductivity I will then move to the idea of a superconducting wavefunction which is a central point in this thesis. After that the superconducting device known as a ”Josephson junction” will be introduced as well as the concept of ”qubits”. Finally, I will try to motivate the work done in this thesis by bringing all of these concept together in the new idea of a d-wave qubit.

1.1 High Temperature Superconductivity

All known HTS are oxides[1] and have a layered structure. The first material to be discovered in 1986 was La-doped barium cuprate LBCO which has a transition temperature, T_c, of 35 K. A few months later it was shown that the related material YBCO had a T_c of 92K. By now many more materials have been discovered including electron- and hole-doped compounds. However, YBCO together with the bismuth compound BSCCO are still the most important materials for applications, even though the highest T_c is found in mercury compounds.
The structure of the HTS superconductors is quite complex and belongs to a family known as perovskites. All HTS materials have layered structure which includes a number of copper-oxide planes. It is known that the superconductivity occurs in these planes and that the other planes probably serve as "spacers" between the layers and charge reservoirs for the Cu-O planes.
The structure of materials such as YBCO means that it is often useful to think of HTS as being quasi 2-dimensional. This model is especially useful when describing the properties of epitaxial thin films. Most of the physics can be understood by imagining that the film consists of a single plane of Cu-O. Note however that many effects can only be understood by considering the full 3D lattice.

$\mathbf{YBa_2Cu_3O_{7-\delta}}$

YBCO is the most common HTS. It is used both in applications and in basic research. The reason for its popularity is its relatively high T_c (92K) and that it is relatively easy to fabricate high-quality thin films and devices. Over the years many methods for depositing epitaxial YBCO films have been developed, for example Pulsed Laser Deposition (PLD), sputtering, co-evaporation and MBE.
YBCO is a very "typical" HTS in that it is a perovskite with a layered structure as shown in fig. 1.1. The superconducting phase is orthorhombic. In the center of the unit cell there is an yttrium ion surrounded by two Cu-O planes. The superconducting transport takes place in these planes. Above/below the planes there are two additional planes with barium-oxide and finally a layer with CuO_x chains; the base of the unit cell is nearly quadratic, 3.8227x3.8872 Å^2, and the total height is approximately 11 Å.
The stoichiometric phase of YBCO is $YBa_2Cu_3O_6$ which is tetragonal and not superconducting. For YBCO to become superconducting, it must be doped with additional oxygen which will find sites in the interleaved layers, the resulting compound is $YBa_2Cu_3O_{7-\delta}$ where δ must be below 0.6 in order to form the superconducting orthorhombic phase. If $\delta > 0.6$ the compound is in an antiferromagnetic phase. YBCO in the superconducting phase is semi-metallic above T_c, hence it is a rather poor conductor.
From a device point of view the most important lesson from the complicated chemistry of YBCO is that one has to take care to preserve the oxygen content during fabrication. Even an optimally doped film can loose its oxygen if, for example, it is heated too much (the "limit" is around 140° C in normal atmosphere). Another problem is that other commonly used oxide materials such as $SrTiO_3$ can "suck" oxygen from YBCO if deposited on top. This is a serious problem when making multilayered devices. The diffusion length of oxygen in YBCO is rather large even at moderate temperatures which means that it is difficult to preserve the oxygen content in small structures, the linewidth seems to be limited to around 50-100 nm for a 200 nm thick film; structures with a width below that are not superconducting, most likely this is due to oxygen out-diffusion.
The complicated structure of HTS materials like YBCO has hampered the development of applications which would obviously benefit from the use of superconductors operated at liquid

[1] There are non-oxide superconductors with structures similar to the HTS, but T_c is usually very low.

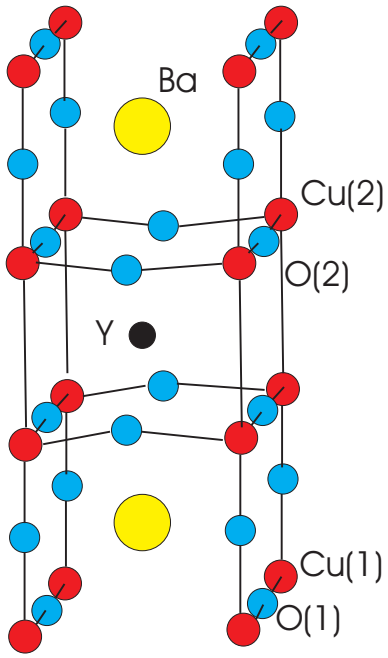

Figure 1.1: The structure of YBCO. The ions labelled with a (1) belong to the chains whereas (2) belong to the superconducting Cu-O planes

nitrogen temperature. The most natural application is cables for power transmission.However, it has unfortunately turned out to be very difficult to make cables that can compete commercially (despite the fact that available HTS cables can carry 150 times as much current as a copper cable of the same dimension) and it is only recently that the development has reached a point where real-world use is viable.

1.1.1 Conventional Superconductivity

It took a long time for a complete theory of conventional superconductivity to be developed. The first theories were phenomenological and assumed the existence of a "superfluid" in the superconductor. A microscopic theory of conventional superconductivity [2] was first published in 1957 by Bardeen, Cooper and Schrieffer[4], it is now simply known as the BCS-theory. Using BCS-theory one can explain most properties of a conventional superconductor.
A superconductor differs from normal materials in that it is characterized by a single, macroscopic, wavefunction. The whole superconductor, no matter the dimensions, is in the same quantum mechanical state; the electrons form a *condensate*. The mechanism behind conventional superconductivity is that two electrons right circumstances can form a Cooper pair; the electrons in each pair having opposite momentum and spin. This happens at a temperature below a critical temperature T_c where a weak *attractive* force -in conventional superconductors mediated by phonons- can act between electrons near the Fermi level. The orbital state of the Cooper pair can have a radius ξ_0 which in conventional superconductors can be very large, of the order of a

[2] With "conventional" we mean low temperature superconductors including MgB_2, another common name is "BCS-superconductor".

micrometer. The Cooper pair is a kind of boson which means that it is possible for many pairs to condense into the same quantum state.
Soon after the discovery of high-temperature superconductivity in 1986 it became clear that the new class of materials can *not* be explained using the simple BCS-theory. HTS and conventional superconductivity do have many things in common, we know for example that the existence of superconductivity in HTS materials is due to the electrons forming Cooper pairs and creating a condensate, just as in BCS-superconductors. There are however also many differences and at present the answer to the question of the microscopic origin of high-temperature superconductivity is beyond our reach. This is still an ongoing debate in solid state physics.

1.1.2 Symmetry and Topology of the Wavefunction in YBCO

The existence of a condensate is the reason for the existence of superconductivity. A superconducting condensate can be described by a singe macroscopic wavefunction $\Psi(\mathbf{r}) = |\Psi(\mathbf{r})|e^{i\phi(\mathbf{r})}$ known as the order parameter. The order parameter is characterized by a phase $\phi(\mathbf{r})$ and a modulus $|\Psi(\mathbf{r})|$ where the quantity $|\Psi(\mathbf{r})|^2$ is a measure of the local superfluid density. The simplest way of understanding the concept of an superconducting order parameter is to consider it to be a description of the centre of mass motion of the Cooper pair. A more formal description [5] can be given by looking at the expectation value $< \Psi^{\dagger}(\mathbf{r'})\Psi(\mathbf{r}) >$, this usually falls of very rapidly as **r'** is separated from **r** because the phase factors from different terms tend to cancel, but in a superconductor this is not the case; the pair function in BCS theory has the property that the condensed pair retains an expectation value even for large $|\mathbf{r'} - \mathbf{r}|$ and this is what is meant by long range phase coherence. It can also be shown that the pair function is an effective wavefunction for a large number of particles.
The BCS theory assumes a singlet (s-wave) pair function [3]. However, it is now generally accepted that the wavefunction in HTS such as YBCO does not have this simple shape. Evidence from many experiments have shown that the wavefunction is not just strongly anisotropic, but also topologically complicated.
The symmetry of the crystal lattice in perovskites such as YBCO limits the number of possible symmetries of the wavefunction to s,p and d (here we are using the same notation as is used to label the electronic orbitals in atomic physics). Using Knight-shift measurement[6] the possibility of p-symmetry was eliminated [4], hence the wavefunction could only have s- or d-wave symmetry. Using phase sensitive techniques such as π-SQUIDs, corner junctions [7] and tricrystal rings[8] it was possible to establish that the phase changes sign as one moves around the Fermi surface and that the gap-function vanishes in the four $< 110 >$ directions. Furthermore, there is a phase change of π for rotation around the z-axis.
Based on symmetry-considerations and experimental data, various forms of the wavefunction have been suggested: Anisotropic s, extended s, d_{xy}, $d_{x^2-y^2}$ and admixtures such as $d + s$ and $d + is$ (i.e. an imaginary s-component), but today most of the scientific community agree that the $d_{x^2-y^2}$-symmetry is the correct form; possibly with an admixture of a very small s-component (which should exist in an orthorhombic crystal[9]). An illustration of a $d_{x^2-y^2}$ wavefunction can be seen in figure 1.2. There are four lobes with alternating sign and four nodes where the gap disappears.

[3] The BCS-theory itself is a very general and pair functions of any symmetry can be used, but when describing conventional superconductors a s-wave function is used

[4] The term "Knight shift" refers to the shift of a NMR resonance line to polarization of conduction electrons.

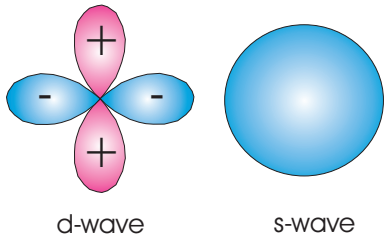

Figure 1.2: Polar diagram of the variation of the gap Δ. *Left*: d-wave symmetry with four lobes and alternating sign of the order parameter. *Right*: s-wave pairing, the gap is isotropic.

1.2 Josephson Junctions

The Josephson Junction (JJ) is a device which was first proposed by Brian Josephson in 1962[10]. In its simplest form it is made made by separating two superconducting electrodes by an insulating layer. Josephson showed that is the layer is thin enough to allow coupling between the wavefunctions in the two electrodes; the device behaves as a superconducting short up to a current threshold, known as the critical current, I_c. For $I > I_c$ the junction becomes resistive and a voltage appears. The properties of Josephson junctions will be discussed in some detail in chapter 3.
The Josephson effect is a very general phenomena which can occur in a wide variety of situations and therefore it was not surprising that the first HTS Josephson junctions were demonstrated soon after the discovery of the HTS superconductors (see for example [11]). At first sight HTS junctions are very similar to conventional junctions and can often be well described by the same models. It is only when the electrodes are arranged so that the d-wave pairing symmetry becomes important that significant differences appear.
Josephson junctions are the basic building block for several devices, the most important one being the dc-**S**uperconducting **QU**antum **I**nterference **D**evice; or "dc-SQUID" for short. The dc-SQUID consists of a superconducting loop interrupted by two Josephson junctions. The importance of the dc-SQUID stems from the fact that it is extremely sensitive to external magnetic fields, it is by far the most sensitive magnetometer available. This is important not only for fundamental studies (which is how it used in this work) but also in applications. These range from medical diagnostics to non-destructive evaluation of materials [12]. There are also many applications of Josephson junctions in e.g. high-speed electronics and sensors for astronomy. Obviously, HTS junctions have an advantage over conventional junctions since they can be operated at relatively high temperatures. However, the complicated material properties that hampered the development of power applications

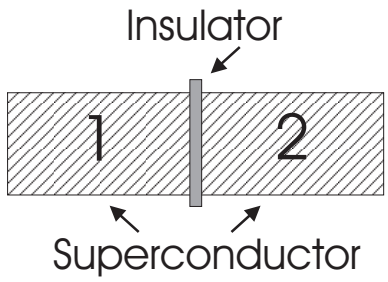

Figure 1.3: Two superconductors separated by a thin insulator, the simplest form of a Josephson Junction.

have had the same effect on applications of HTS junctions and dc-SQUIDs which is why they are still rarely used in real applications.

1.3 Superconducting qubits

One application of superconductivity that has received a lot of attention over the past few years is the *superconducting qubit*. The qubit -short for **qu**antum **bit**- can be though of as a simple "artificial atom" that can be controlled in such a way that it can be used as the basic building block of a quantum computer, a machine originally proposed by theorists such as Feynmann in the 1970s and early 1980s.

The quantum computer is in essence a computer that takes advantage of the possibility of having a two-state system in a "Schrödinger's cat state". The name refers to a famous thought-experiment where a cat is e.g. poisoned with 50% probability as a consequence of some "quantum event" (originally the radioactive decay of a nucleus). According to classical physics we would expect that the cat would either die or survive the experiment. However quantum mechanics tells us that it is in fact possible for the cat to be in a state which is a *superposition* of dead *and* alive until the box is opened and the state of the cat measured. This is of course an apparent paradox, but it turns out to be in essence correct.

The quantum computer uses superposition to perform certain types of calculations very fast, much faster than what is possible with a conventional computer. In a quantum computers the qubits have the job of the "cats" and are two-state systems that are coupled to each other. If we denote the "alive" and "dead" states of our qubits by $|0>$ and $|1>$ we can write the state at any time as $|\Psi>= a|0> +b|1>$ where a and b are complex numbers normalized so that $a^2 + b^2 = 1$. Now, if we couple two qubits together we can denote their states as $|00>$, $|01>$, $|10>$ and $|11>$; this is similar to a two bit register but due to the possibility of superposition we can also have e.g. the state $0.5(|00> +|01> +|10> +|11>)$ representing all four classical states at once. In 1994 Peter Shor [13] presented what is now known as Shor's algorithm which uses a quantum computer to factorize very large numbers, an important problem in mathematics and cryptology. In 2001 Vandersypen et al. [14] implemented Shor's algorithm using a 7-qubit NMR-based quantum computer, this was of course a triumph for qubit-implementations using "real" atoms and molecules but it stretched the technology to the limit. There is today a broad consensus that the only way to build a *useful* quantum computer is to use solid state technology which can be manipulated and designed in ways impossible with e.g. molecules.

In 1999 Nakamura et al [15] demonstrated the first solid state qubit. It was based on a superconducting Cooper pair box operated as a two-state system. Over the past few years a number of other superconducting qubits have been suggested and many have also been implemented. All of them made of Josephson junctions. Originally, the reason for using superconductors was that the existence of the superconducting gap makes the device less sensitive to fluctuations which should make the system more stable; in retrospect it has also turned out to be relatively easy to come up with possible two-state systems to perform experiments. Since any solid state quantum computer needs to be operated at low temperature in order to suppress thermal fluctuations the fact that you need to cool superconductors -usually a good argument against using superconductors in an application- becomes irrelevant.

1.4 Motivation for this work

Even though it is not the central theme of this thesis the possibility of using the d-wave symmetry and its effect on the properties of Josephson junctions to make a HTS qubit is the underlying idea behind the work done during the past five years. Before a d-wave qubit can be realized we need to understand the properties of d-wave Josephson junctions in detail. We also need to know if it is even possible to operate such junctions in the quantum regime.
Hence, when this work started there were a number of questions that needed to be answered

- Is it possible to fabricate HTS devices with the right properties?
- What are the effects of the d-wave symmetry on the transport properties of Josephson junction and SQUIDs?
- Can HTS junctions be operated in the quantum regime? I.e. can they exhibit phenomena such as MQT and energy level quantization?

This thesis aims to answer some of these questions.

Chapter 2

Scope and outline of this thesis

The scope of this thesis is rather broad and covers a wide range of phenomena and properties. I have therefore opted to limit the contents of the thesis to topics directly relevant to the appended papers. Hence, the main idea of the remaining text is to give the background necessary to understand the contents of the papers. Some material that has not previously appeared in print has also been included, mainly numerical simulations that are useful for understanding the experimental data. Hence, what follows is intended to be read at the same time as the relevant papers, these can be found as appendices.
I have divided the remainder of thesis into five main parts:

- Chapter 3 gives a background to the general theory of Josephson junctions and SQUIDs, i.e. properties not directly related to the d-wave symmetry.
- In chapter 4, I describe the experimental methods and equipment used. This chapter also includes an introduction to the properties of YBCO grain boundaries and the three types of grain boundary Josephson junctions used in this work.
- Chapter 5 is the first chapter to deal with my own work. It deals with properties of sub-micron sized YBCO Josephson junctions. In this chapter I also discuss the theory of bound Andreev states and other phenomena related to the effects of the d-wave symmetry on JJ. The contents of this chapter is based on papers I and III.
- Chapter 6 describes modelling and experiments on dc-SQUIDs made from high-angle JJ. The main focus is on how the d-wave symmetry changes the current-phase relation from the conventional $I = I_c \sin\varphi$ to $I = I_c^I \sin\varphi - I_c^{II} \sin 2\varphi$ and how this affects the dynamics of dc-SQUIDs. Our first results in this field can be found in paper II and the topic is discussed in some detail in paper V.
- The most recent results are presented in chapter 7. Here I describe experiments on resonant activation in high-angle biepitaxial junctions. Some basic modelling of this phenomenon is also discussed. Since paper VI is somewhat limited in scope due to length restrictions, chapter 7 is the most extensive in terms of content. I also present some numerical simulations that were used to understand our experimental data as well as some theoretical results.
- In chapter 8 I give a short introduction to the theoretical work presented in paper V in which it is described how high-angle dc-SQUIDs can potentially be used as qubits.

Chapter 3

General Theory of Josephson Junctions

In 1962 [10] Brian Josephson predicted two new effects that can occur when two superconductors are connected through an insulator. In his calculations he showed if there is a difference in phase between the electrodes, a zero voltage supercurrent can flow through the barrier. He also predicted that if the junction is biased with a voltage V a phase difference would evolve in time. These predictions are now known as the dc- and ac Josephson effects respectively. Once these discoveries were experimentally verified the field grew rapidly. Today it is a rich and well-developed field of solid-state physics.

The Josephson effects are very general phenomena. For them to occur it is in principle enough to have two superconducting banks connected via a *weak link*, a region where the superconductivity has been somehow suppressed. Since the effect can occur in such a wide variety of situations the general theory is rather complicated (especially since the mechanisms which carry the supercurrent differ between different types of barriers) and usually the calculations are simplified by assuming that one is working in a certain mathematical limit. Hence, what will be discussed here are only some special cases of a much more general theory. The theory in this chapter was originally developed for Josephson junctions fabricated from conventional superconductors. As will be shown in later chapters the theory for single junctions and dc-SQUIDs outlined here needs to be extended in order to be valid for high-angle HTS junctions where effects of the d-wave symmetry become important.

3.1 Feynman's Derivation of the Josephson Equations

There are many ways to derive the Josephson equations; if e.g. the electrodes are made from BCS superconductors it is possible to derive them directly from the microscopic theory. In his *Lectures* Feynman used another method which does not rely on the details of the microscopic process.

Suppose we have two identical superconductors separated by an thin insulator as depicted in figure (1.3). Assuming there is no applied magnetic field and everything is symmetric [1] we can argue that the superconducting wavefunctions on each side of the junction should be weakly coupled to each other with a strength K. Hence, we can write two coupled equations for the amplitudes on each side

[1] Another, implicit, assumption is that time-reversal symmetry is preserved.

of the insulator

$$i\hbar\frac{\partial\Psi_1}{\partial t} = U_1\Psi_1 + K\Psi_2 \tag{3.1a}$$
$$i\hbar\frac{\partial\Psi_2}{\partial t} = U_2\Psi_2 + K\Psi_1 \tag{3.1b}$$

In equilibrium the energy U_1 is equal to U_2 and nothing happens. If we bias the junction with a voltage V the energies will be shifted so that $U_1 - U_2 = qV$ where q is the charge of the current carrying particle. For convenience we can define zero of energy to be halfway between U_1 and U_2

$$i\hbar\frac{\partial\Psi_1}{\partial t} = \frac{qV}{2}\Psi_1 + K\Psi_2 \tag{3.2a}$$
$$i\hbar\frac{\partial\Psi_2}{\partial t} = -\frac{qV}{2}\Psi_2 + K\Psi_1 \tag{3.2b}$$

In order to solve this system of equations we make to following *ansatz*

$$\Psi_l = \sqrt{\rho_l}e^{il\theta} \tag{3.3a}$$
$$\Psi_m = \sqrt{\rho_m}e^{im\theta} \quad l, m \in \mathbf{Z}$$

By inserting these expressions into eq. 3.2b we get

$$\sqrt{\rho_n}e^{il\theta_1}\left(\frac{i\hbar\dot{\rho}_l}{2\rho_l} - l\hbar\dot{\theta}_1 - \frac{qV}{2}\right) = K\sqrt{\rho_m}e^{im\theta_2} \tag{3.4a}$$
$$\sqrt{\rho_m}e^{im\theta_2}\left(\frac{i\hbar\dot{\rho}_m}{2\rho_m} - m\hbar\dot{\theta}_2 + \frac{qV}{2}\right) = K\sqrt{\rho_n}e^{im\theta_1} \tag{3.4b}$$

By equating the real and imaginary parts we get four equations

$$\dot{\rho}_l = \frac{2K}{\hbar}\sqrt{\rho_m\rho_l}\sin(m\theta_2 - l\theta_1) \tag{3.5a}$$
$$\dot{\rho}_m = -\frac{2K}{\hbar}\sqrt{\rho_m\rho_l}\sin(m\theta_2 - l\theta_1) \tag{3.5b}$$
$$l\dot{\theta}_1 = \frac{K}{\hbar}\sqrt{\frac{\rho_m}{\rho_l}}\cos(m\theta_2 - n\theta_1) - \frac{qV}{2\hbar} \tag{3.5c}$$
$$m\dot{\theta}_2 = \frac{K}{\hbar}\sqrt{\frac{\rho_l}{\rho_m}}\cos(m\theta_2 - l\theta_1) + \frac{qV}{2\hbar} \tag{3.5d}$$

The current through the junction must be equal to the change in density and is therefore equal to $\dot{\rho}_l = -\dot{\rho_m}$. Letting $n\phi = m\theta_2 - l\theta_1$ ($n \in \mathbf{Z}$) we can write this as

$$\frac{2K}{\hbar}\sqrt{\rho_m\rho_l}\sin n\phi = J_n \sin n\phi \tag{3.6}$$

where we have introduced the constant J_n to represent the density of supercurrent flowing through the junction. Now, we have in fact solved the system for an *arbitrary* $n \in \mathbf{Z}$ and have therefore obtained a set of solutions, since the system is linear that means that the most general solution is given by a linear combination of all these solutions

$$J = \sum_{n=1}^{\infty} J_n \sin n\phi \tag{3.7}$$

By calculating the difference $m\dot{\theta}_2 - l\dot{\theta}_1 = n\dot{\varphi}$ we obtain another interesting equation

$$\frac{d\phi}{dt} = \frac{2e}{n\hbar}V \tag{3.8}$$

Where we have used the fact that $q = 2e$ in a superconductor (the charge-carrying "particle" is the Cooper pair). Eq. 3.7 and 3.8 are the celebrated **Josephson equations**, and are known as the dc- and ac Josephson effect respectively. Here we have written the equations in their most general form, usually it is assumed that only the first harmonic gives a contribution to the total current giving

$$I = I_c \sin\phi \tag{3.9}$$

$$\frac{d\phi}{dt} = \frac{2e}{\hbar}V \tag{3.10}$$

where we have written an expression for the total current in the junction and introduced I_c, the *critical current* of the junction. This is the most common form of these equations. Note that ϕ is just the difference in phase between the order parameters in the two electrodes.

3.2 General Properties of the Josephson Current-Phase Relation

Regardless of the material, geometry or transport mechanism giving rise to the Josephson effect in a junction there are several general properties that must be valid for all theoretical models used to describe the process.

- Changing the phase across the junction by 2π should not change the physical state of the junction. Hence, the change must not influence the supercurrent across the junction and the current-phase relation(CPR) is a 2π-periodic function

$$I_S(\phi) = I_S(\phi + 2\pi) \tag{3.11}$$

- Changing the direction of flow of the supercurrent must change the sign of the phase, whence

$$I_S(\phi) = -I_S(-\phi) \tag{3.12}$$

  Equation 3.12 does not hold in junctions where the time-reversal symmetry is broken(TRSB) . There are potentiality several mechanisms that can cause this symmetry to be broken in HTS junction. It was for example shown that the presence of an imaginary subdominant component in the order parameter [16] would cause TRSB. More recently Löfwander *et al.*[17] and Amin [18] *et al.* showed that spontaneous TRSB can also occur in pure d-wave junctions. However, so far there is no clear experimental evidence of TRSB in HTS junctions, more experimental data are needed to resolve this issue. In the following discussion it is assumed that eq. 3.12 holds.

- A dc supercurrent can only flow if there is a change of the phase of the order parameter as one crosses the barrier, this means that if $\phi = 0$ there should be zero supercurrent

$$I_S(2\pi n) = 0,\ n = 0, \pm 1, \pm 2... \tag{3.13}$$

To summarize, the supercurrent in the absence of TRSB must be a symmetric 2π-periodic function. Therefore it can always be expanded in a Fourier series

$$I_S(\phi) = \sum_{n\geq 1} I_n \sin(n\phi) \tag{3.14}$$

This equation is identical to eq. (3.6), the difference being that now we have derived the result based on *general* principles, hence equation (3.6) is actually valid under quite general assumptions.

3.3 Josephson Junctions in Magnetic Field

One of the defining facts of a superconductor is that it screens magnetic fields; an applied field will only penetrate a very short distance, known as the *London penetration depth* λ, into the superconductor before it decays completely. The size of λ varies between different superconductors but is about 130 nm for YBCO. In Josephson junctions there is a similar effect; the Josephson currents will screen magnetic fields from the interior of the junction. The field will penetrate a distance λ_J known as the *Josephson penetration depth*[2]

$$\lambda_J = \sqrt{\frac{\Phi_0}{2\pi J_c \mu_0 (2\lambda + d)}} \tag{3.15}$$

where d is the thickness of the insulating barrier, J_c the critical current density and Φ_0 is the *magnetic flux quantum* which is a constant defined as $h/2e$ and is equal to $2 \cdot 10^{-15}$ Wb. Since λ_J depends on J_c it can vary with orders of magnitude even for junctions made of the same material; in YBCO junctions with $J_c = 10^2 - 10^6$ A/cm^2 it will vary between 0.3-30 μm.
λ_J is very important since it determines the "magnetic size" of the junction, when the width w of the junction is bigger than λ_J we need to take into account its self-field and screening currents when studying how the junction parameters are affected by an external magnetic field. In a junction with w smaller than λ_J the field will penetrate the junction uniformly, the junction is "short", whereas if $w > \lambda_J$ the flux dynamics of the junction starts to be important and the junction is "long".
Unless a junction is very narrow its dynamics will be affected by even relatively moderate fields, this is true even for magnetically short junctions. In other words the junction has a certain width and the properties change as we move along the interface if there is a field-gradient, it is *distributed* [20]. In a conventional rectangular junction with uniform current distribution it is straightforward to describe the effect of the external field. It turns out the critical current through the junction has a familiar dependence on the external flux Φ

$$I_c(\Phi) = I_{c0} \frac{|\sin(\pi\Phi/\Phi_0)|}{|\pi\Phi/\Phi_0|} \tag{3.16}$$

which is nothing else but the well known *Fraunhofer* pattern as can be seen in 3.1. This pattern is identical to what one finds if a beam of light passes through a narrow rectangular slit. However, as will be shown later this formula is just the simplest case of a more general formalism.

[2] In coplanar junction geometry, such as GBJJ, this expression requires some corrections. It was shown [19] that the expression $\lambda_J = \sqrt{\frac{\Phi_0}{2\pi J_c \mu_0 (2(\lambda^2)/w + d)}}$ (w-width) better describes the experimental data. This expression differs from 3.15 by a factor $\sqrt{w/\lambda} \gg 1$.

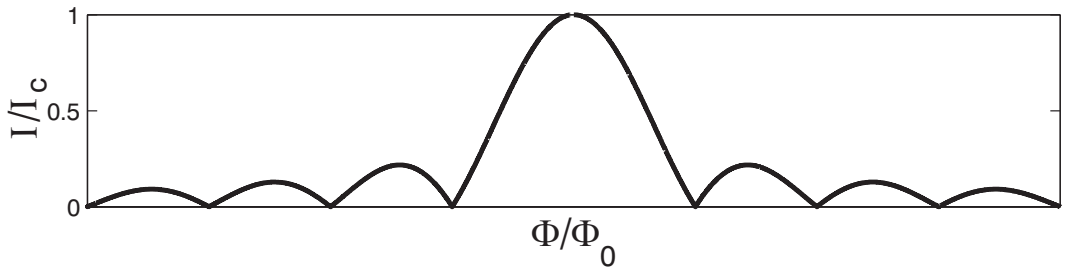

Figure 3.1: The modulation of the critical current as a function of applied magnetic field for a single junction.

3.4 Quantum Interference Devices

One of the unique properties of superconductivity is that it can be described by a *single* wavefunction, even if the superconducting device is macroscopic, coherence is preserved. This has many important implications, one being that if we connect two Josephson junctions to each other using superconducting leads not only will the *amplitude* of the wavefunction describing each junction be important but also the *phase*. The situation is analogous to two water waves colliding; it is not enough to simply sum the amplitudes to get the shape of the resulting wave, one also has to consider their relative phase. Hence the two junctions interact causing what is known as *quantum interference*.

3.4.1 The dc-SQUID

The most common quantum interference device is the dc-SQUID [3]. It consists of two junctions in a superconducting loop, see fig. 3.2.

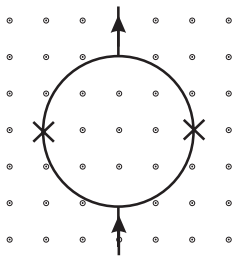

Figure 3.2: A dc-SQUID is created by connecting two Josephson Junctions in a loop. The arrows indicate the direction of the bias current and the symbols $\odot$ the field threading the loop.

Inside a bulk superconductor without holes it can be shown [21] that by using continuity arguments that the total change of the phase along any closed path is

$$\delta\theta = \frac{2e}{\hbar} \oint \mathbf{A} d\mathbf{l} \equiv 0 \tag{3.17}$$

giving rise to the Meissner effect of ideal diamagnetism of superconductors. Making use of the Stokes theorem

[3] The other type is known as the *rf-SQUID*, and only incorporates one junction in the loop

$$\delta\theta = \frac{2e}{\hbar}\oint \mathbf{A}d\mathbf{l} = \frac{2e}{\hbar}\int_S \nabla \times \mathbf{A}dS \tag{3.18}$$

and substituting for $\nabla \times \mathbf{A} \equiv \mathbf{B}$ by definition

$$\delta\theta = \frac{2e}{\hbar}\int_S \mathbf{B}dS = \frac{2e}{\hbar}\Phi = 2\pi\frac{\Phi}{\Phi_0} \equiv 0 \tag{3.19}$$

In a multiply connected superconductor the continuity argument does not hold, but the wave function must still be single-valued. Hence,

$$\delta\theta = 2\pi\frac{\Phi}{\Phi_0} = 2\pi n \tag{3.20}$$

and the internal flux only takes quantized values in multiples of $\Phi_0 = 2 \cdot 10^{-15}$ Wb.
In a dc-SQUID the phase is not continuous, each junction contributing a certain 'jump' which add up to some value ϕ along the closed path.

$$\delta\theta = 2\pi\frac{\Phi}{\Phi_0} + \phi = 2\pi n \tag{3.21}$$

or ignoring multiples of 2π, which lead to physically equivalent conditions,

$$\phi = -2\pi\frac{\Phi}{\Phi_0} \tag{3.22}$$

and the total phase difference across the junctions, ϕ, (summed with the correct signs along the closed path) becomes flux-dependent. As we know from the previous discussion of the Josephson effect, ϕ is intimately related to the critical current, I_c, which is an experimentally measurable quantity. This and the smallness of Φ_0 makes the SQUIDs extremely sensitive sensors of the magnetic flux. What is more important for this work, the phase difference, ϕ, across the junctions of a small SQUID is simply proportional to the magnetic flux Φ. It follows that a dc-SQUID will carry a supercurrent I_s which is periodic in field.

$$I_s = 2I_c\left|\cos\pi\frac{\Phi}{\Phi_0}\right| \tag{3.23}$$

Where is has been assumed that both junctions have the same critical current I_c. The resulting pattern can be seen in figure 3.3.

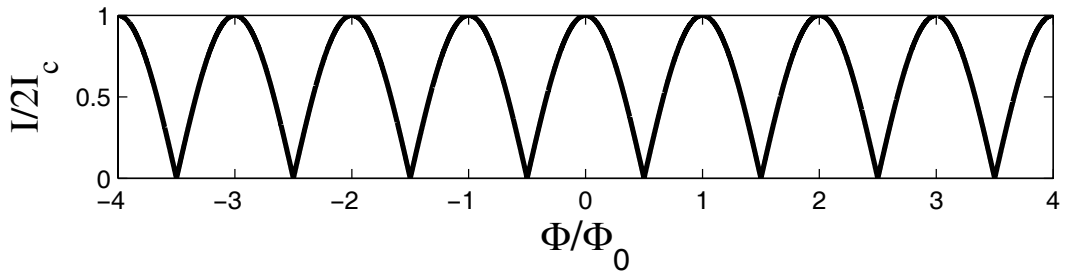

Figure 3.3: The modulation of the critical current as a function of applied magnetic field for a dc-SQUID.

3.5 Dynamics of Junctions and SQUIDs

A very common way of modelling Josephson junctions is to use the so-called resistively shunted junction (RSJ) model, where the junction is described as being composed of a voltage controlled current source (VCC) in parallel with a resistor. By also adding a parallel capacitor, the result is the RCSJ-model which can account for a wide variety of phenomena in Josephson junction. The RCSJ-circuit is composed of the following lumped elements (see figure 3.4).

- A VCC which is governed by the Josephson relations $I = I_s(\varphi)$ and $\dot{\varphi} = 2eV/\hbar$
- A resistor with the value R_N, the normal resistance of the junction.
- A capacitor with a value C, this includes not only the geometrical capacitance but also includes effects of the barrier and any stray capacitance from the substrate.

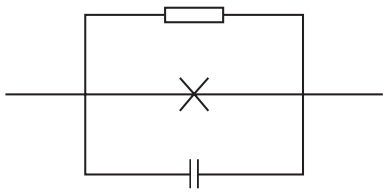

Figure 3.4: The RCSJ-model consists of three lumped elements: R_N, C and a voltage controlled current source. In the simpler RSJ-model the capacitor is absent.

The RCSJ-model is especially useful for the study of dynamics of junctions and SQUIDs, since it is a circuit model it is easy to incorporate for example external inductances.

3.5.1 The tilted washboard model

Using the RCSJ-model we can write a system of two equations that describes the dynamics of a current biased shunted junction [4]. Using the Josephson equations and ordinary circuit theory one gets

$$\frac{d\phi}{dt} = \frac{2e}{\hbar}V \tag{3.24a}$$

$$I = I_s(\phi) + \frac{V}{R_N} + C\frac{dV}{dt} \tag{3.24b}$$

This can also be written as a 2nd order equation for the phase

$$\frac{\hbar C}{2e}\frac{d^2\phi}{dt^2} + \frac{\hbar}{2eR_N}\frac{d\phi}{dt} = I - I_S(\phi) \tag{3.25}$$

which is the equation of motion for a "phase-particle" with mass $M_\phi = (\hbar/2e)^2 C$ moving in a potential

$$U(\phi) = -E_J\cos\phi - \frac{\hbar I}{2e}\phi \tag{3.26}$$

[4] In this section I will assume that the CPR have the simple form $I_S(\phi) = I_c \sin\phi$

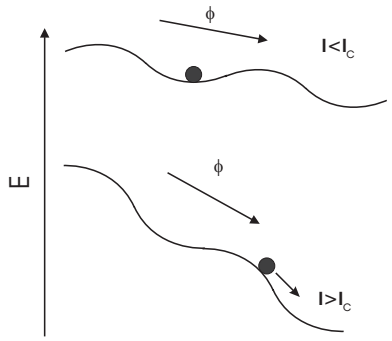

Figure 3.5: The washboard potential model. *Top:* When $I < I_c$ the particle is trapped in minimum. *Bottom:* When $I > I_c$ the well is tilted so much that the particle can roll over the barrier and go into the running state.

where we have introduced E_J, the Josephson energy which is defined as

$$E_J = \frac{\hbar}{2e} I_c \tag{3.27}$$

The tilted washboard model eq. 3.26 is a very useful mechanical analogue of a Josephson junction. In this model the dynamics can be understood as a particle with mass M_ϕ subjected to a drag force $(\frac{\hbar}{2e})^2(1/R)\frac{d\phi}{dt}$ rolling down the potential given by 3.26. This is known as the "running state". Using this model we can also understand how a junction switches from the superconducting ($I < I_c$) to the resistive state ($I > I_c$. When $I < I_c$ the "phase particle" will be trapped in one of the energy minima, but if the "tilt" of the washboard is gradually increased (by pushing more current trough the junction) we will eventually reach a point where the particle is no longer trapped but will travel along the profile of the potential (known as the "running state"). This is illustrated in figure 3.5.
The Josephson energy defined above sets the energy-scale of the problem. It also determines how much the dynamics is affected by external factors such as the temperature and noise (a table with energy conversion factors can be found in appendix A).
The inertia of the phase particle determines what happens once the junction has switched. If the junction goes directly from the supercurrent state (S-state) to some finite voltage > 0 it is said to be *hysteretic* Whether or not the junction is hysteretic is determined by the Stewart-McCumber number

$$\beta_C = \frac{2e}{\hbar} R^2 C I_{C0} \tag{3.28}$$

$\beta_C \ll 1$ means that the junction is overdamped and not hysteretic, $\beta_C \gg 1$ means that the junction is heavily underdamped and hysteretic. E.g. HTS junctions usually have $\beta_C \approx 1$, i.e. they are slightly hysteretic. Figure 3.6 shows an example of a slightly underdamped junction. Note that the term $\frac{\hbar I}{2e}\phi$, which corresponds to the "inertia", will disappear if the capacitance is very small; it will therefore be absent in the RSJ-model.
β_c can be estimated from the current-voltage characterizes using the *Zappe approximation*

$$\beta_c = (\omega_p R_N C)^2 \approx \frac{2 - (\pi - 2)(I_r/Ic_c)}{(I_r/I_c)^2} \tag{3.29}$$

If the junction is overdamped ($\beta_c \ll 1$)we can drop the second order term from the equations. By integrating the result we get the time averaged voltage to be

$$V = R\sqrt{I^2 - I_c^2} \tag{3.30}$$

This is an important equation even though it is simple. It is a fairly good approximation of the behavior of a real junction, the term ”RSJ-like” refers to a junction which exhibits a behavior which can be well described by 3.30.

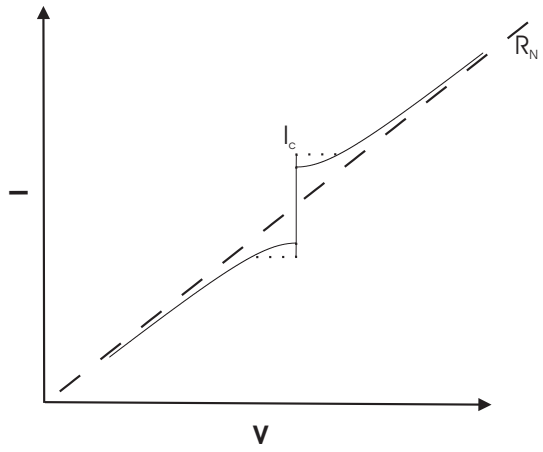

Figure 3.6: An example of an hysteretic (underdamped) IV-curve. The dashed line indicated R_N, the slope of the resistive branch. The switch from the superconducting to the resistive branch has been indicated by a dotted line.

Classical dynamics in the well

Even before the junction has switched, the ”phase particle” undergoes oscillations in the minimum where it is trapped with a frequency $m^{-1}d^2U/d\phi^2$ which is known as the plasma frequency and is given by

$$\omega_p = \sqrt{\frac{2\pi I_{c0}}{\Phi_0 C}}(1-\gamma^2)^{0.25} \tag{3.31}$$

where $\gamma = I/I_c$. The notation for how to write the plasma frequency varies. Here ω_p is the *bias dependent* plasma frequency (in units of s^{-1}) whereas the symbol ω_0 is used for the zero-bias plasma frequency which is a constant for a given junction. The plasma frequency can also be written as

$$\omega_p = \frac{1}{\sqrt{L_J C}} \tag{3.32}$$

where L_J is the bias-dependent *Josephson inductance*

$$L_J = \frac{\Phi_0}{2\pi I_{c0}\sqrt{1-\gamma^2}} \tag{3.33}$$

This formula is often convenient when modelling circuits which include both junctions and other components. In eq. 3.31 the *noiseless critical current* I_{c0} has also been introduced. I_{c0} can be thought of as the critical current in the absence of fluctuations.
Another important parameter related to β_c and ω_p is the Q-value of the junction which is given by

$$Q = \omega_p RC \tag{3.34}$$

which is identical to $\sqrt{\beta_c}$. The Q-value is a measure of the amount of energy dissipated in the junction and will be important in the discussion on macroscopic quantum phenomena. In the RCSJ-model R is just the shunting resistance. However, in real junctions R can differ significantly from the R_N and is best seen as a phenomenological parameter since it also includes the dissipative effects of the environment.

3.5.2 Dynamics of the dc-SQUID

It is straightforward to deduce the governing equations for a dc-SQUID in the same way as for a single junction. If we bias the SQUID above the critical current a voltage will develop across it just as in the case of a single junction. Assuming the junctions are overdamped we can use 3.30 and 3.23 to write

$$V = \frac{R}{2}\sqrt{I^2 - 4I_c^2 \cos^2 \pi \frac{\Phi}{\Phi_0}} \tag{3.35}$$

A plot of this expression can be seen in figure 3.7; as expected it is periodic in field. Experimentally

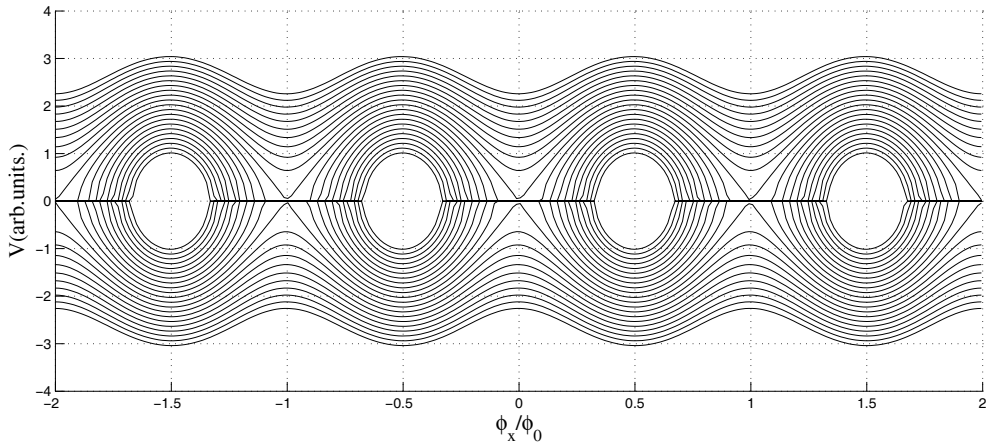

Figure 3.7: The voltage modulation of a dc-SQUID. Each curve corresponds to a bias current $I > I_c$.

the voltage response is measured by biasing the dc-SQUID with a current $I > I_c$ and then measuring how the voltage changes with field. This is the method used when dc-SQUIDs are utilized as highly sensitive magnetometers.

The tilted washboard potential analogy can be carried over to SQUIDs as well [22]. In this case the two junctions are biased to the same voltage, or analogously, the same average washboard slope. The relative phases can be represented by displacement of the two washboards, and this corresponds to the applied flux. The junctions are of course not independent. The relative phase changes adjust themselves to minimize the total energy. This can be modelled by joining the 'phase particles' by a spring; its stiffness representing the SQUID inductance. In the case of small SQUIDs of negligible inductance the spring has to be infinitely stiff. This means that the phase *across* the SQUID does not depend on the magnetic field or, equivalently, the phases of the two junctions are 'locked' to each other. In this respect the small SQUID can be regarded as a single junction with a magnetically adjustable critical current.

Screening effects

In the discussion above it is implicitly assumed that the applied flux Φ_x is equal to the flux enclosed by the loop Φ. However, in general the inductance of the loop can not be neglected and a screening current I_s is flowing in the loop

$$I_s = I_{c1} \sin \phi_1 - I_{c2} \sin \phi_2 \tag{3.36}$$

we also have that $\phi_1 - \phi_2$ is constrained by

$$\phi_1 - \phi_2 = 2\pi\Phi/\Phi_0 \tag{3.37}$$

where

$$\Phi = \Phi_x + LI_s \tag{3.38}$$

In order to quantify the effects of the inductance it is useful to define the dimensionless self-inductance

$$\beta_L = \frac{2\pi L I_c}{\Phi_0} \tag{3.39}$$

When $\beta_L < 1$ the relation between ϕ and ϕ_x is single-valued, in the opposite limit $\beta_L > 1$ there are many possible flux states for a given applied field and and SQUID is said to be hysteretic.
Generally speaking screening effect make the dynamics very complicated and in this work we have therefore used dc-SQUIDs designed to have small β_L.

3.6 The Josephson Junction as a Quantum Well

Consider a Josephson junction in the S-state. The dynamics can be described by considering a potential of the form

$$U(\phi)/E_J = 1 - cos(\phi) - \gamma\phi \tag{3.40}$$

which is just 3.26 written in dimensionless form using the normalized bias current $\gamma = I/I_{c0}$. If we plot this potential we see that it takes the shape of a "bumpy slope" as can be seen in figure 3.8. A state initially prepared in the well can escape to the running state by either being thermally excited *over* or by direct tunnelling *through* the barrier. Note that both the *shape* of the potential and the height of the barrier ΔU are bias dependent and that $\Delta U \to 0$ as $I \to I_{c0}$.
In the RCSJ model considered above it is usually assumed that $I_c \approx I_{c0}$ which works very well for applications at the temperatures where junctions are most often used (e.g. 4.2K for Nb and HTS devices) as long as $E_J \gg k_B T$. However, if $E_J \approx k_B T$ thermal noise must be taken into account since it will cause the junction to switch at a current $I_c < I_{c0}$.
The rate at which the junction switches due to thermal noise is given by an Arrhenius formula

$$\Gamma_t = a_t \frac{\omega_p}{2\pi} \exp\left(-\frac{\Delta U}{k_B T}\right) \tag{3.41}$$

where a_t is a numerical pre-factor ≈ 1 given by [24]

$$a_t = \frac{4}{\left(\sqrt{(1 + \frac{Qk_BT}{1.8\Delta U})} + 1\right)^2} \tag{3.42}$$

If the temperature is so low that $\hbar\omega_p \gg k_bT$ the escape will be dominated by tunnelling *through* the barrier, this is what is known as *Macroscopic Quantum Tunnelling* (MQT). The crossover temperature is given by the expression [25]

$$T^* \asymp \frac{\hbar\omega_p}{2\pi k_B}\left[\left(1+\frac{1}{4Q^2}\right)^{1/2}-\frac{1}{2Q}\right] \tag{3.43}$$

Usually the Q-dependence is small in real junctions and can be neglected which means that the equation for the crossover temperature reduces to

$$T^* = \frac{\hbar\omega_0}{2\pi k_B}(1-\gamma^2)^{1/4} \tag{3.44}$$

In the RCSJ-model this corresponds to the "phase-particle" tunnelling through the barrier ΔU meaning that the junction switches "prematurely" at some current $I < I_{co}$. The switching rate is given by [26]

$$\Gamma_q = Ae^{-B} \tag{3.45}$$

where A and B are variables to be determined. In the WKB-approximation they are given by

$$A = \frac{\omega_p}{2\pi}\left(\frac{864\pi U_0}{\hbar\omega_p}\right)^{1/2} \tag{3.46}$$

$$B = \frac{36}{5}\frac{U_0}{\hbar\omega_p} \tag{3.47}$$

Closer inspection shows that both A and B depend on the damping - i.e. the Q-value - of the junction. However, no analytical expressions for A and B exist for the general case and numerical methods need to be used if accurate values are needed.
Note that both Γ_t and Γ_q are ensemble properties. They can not tell us at which current a junction will switch since that is a stochastic process; we need to record a large number of switching current events in order to be able to extract any information.
One important difference between thermal and quantum escape is that the latter is independent of temperature. This gives us a way to experimentally determine in which regime we are in by measuring the switching rate Γ (or another parameter directly related to Γ such as the width of the switching current histogram); once we enter the quantum regime the rate becomes independent of temperature. There is also a crossover regime with both thermal- and quantum escape. Thus, there will be three "parts" as can be seen in figure 3.9. At high temperatures the width is temperature dependent. If we lover the temperature we reach a crossover regime at T=T^* and finally we enter the MQT regime.
For an in-depth review of experiments on MQT in conventional junctions see, e.g., Martinis et al. [27].

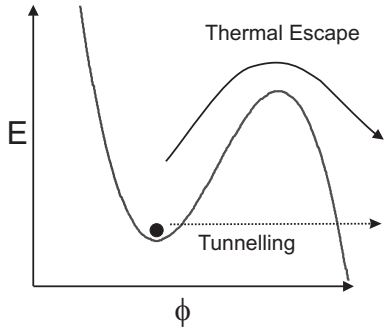

Figure 3.8: The tunnel junction potential has the shape of "bumpy slope" [23], via MQT the junction can escape to the continuum on the right of the barrier.

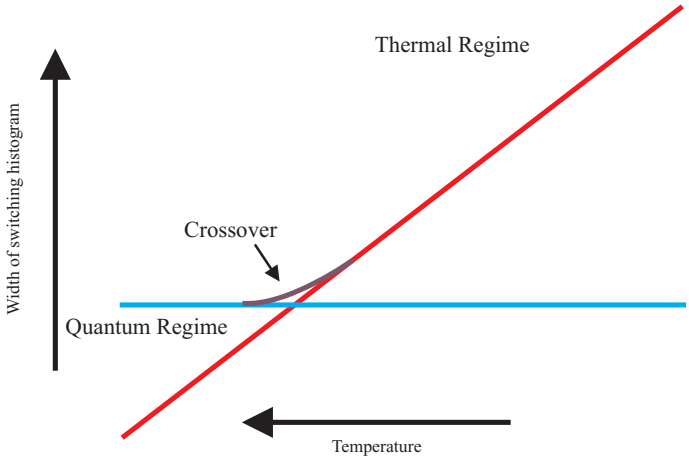

Figure 3.9: Conceptual picture of the temperature dependence of the width of the switching current histogram.

Chapter 4

Experimental Techniques

All our results were obtained from samples fabricated and measured at Chalmers. Sample fabrication was done in the MC2 cleanroom facilities. Here I will briefly discuss the methods used to fabricate our devices as well as give an overview of the types of junctions used in this work.

4.1 Grain Boundary Josephson Junctions

Conceptually, the simplest method to create a Josephson junction is to make a trilayer device consisting of a sandwich with two superconducting electrodes and an insulating barrier, usually in the form of an oxide layer. This structure is similar to the one depicted in figure 1.3. A typical example of a trilayer device is the aluminium (Al) tunnel junction which consists of two layers of Al with an insulating layer of aluminium oxide as the barrier. Due to the complex material prosperities of the high-T_c materials it has proven to be difficult to use trilayer techniques. So called ramp junctions have a structure somewhat similar to trilayer devices (i.e. two electrodes with barrier layer in between) but the fabrication technique is unfortunately quite complicated.
Not long after the discovery of the HTS materials an alternative approach based on the idea of an artificial grain boundary (GB) was therefore developed. This technique itself is conceptually very simple and the method predates HTS since it has been used to study grain boundaries in many materials. Nowadays it is used for many oxides including most perovskites. There are many ways to form Josephson junctions in HTS-materials, the most common types being ramp junctions, biepitaxial junctions, step-edge junctions and bicrystal junctions. Each technique has its advantages but unfortunately none of them can yet be used in large scale applications where a high degree of reproducibility is needed. Roughly speaking, ramp junctions are used in applications such as digital electronics (RSFQ), whereas bicrystal junctions and biepitaxial junctions are used in research (one important exception being applications where only a single dc-SQUID is needed, here bicrystal junctions are often used).
The basic idea of the GB technique is to artificially create a grain boundary acting as a weak link in the superconducting film. In order to understand *why* a GB acts as a weak link we need to briefly review some of the properties of GB in the perovskites. Generally speaking a grain boundary can be considered as a plane of disorder within a single crystal. The degree of disorder is determined by the angle of misfit between the two sides of the plane [28]. The idea is to introduce disorder in a controlled manner and in such a way as to have a well-controlled angle between the crystal axes in the electrodes.

Grain boundary junctions can be fabricated in several ways of which the bicrystal technique is the simplest and I will therefore use that as an example. The starting point for the fabrication is a bicrystal substrate with an artificial grain boundary. The name stems from the fact that the substrate is made by joining two single crystals of different orientations as illustrated in fig 4.1. When e.g. a YBCO-film is grown on top of a substrate, which allows epitaxial growth, the crystal axes of the film will follow those of the substrate, this means that the GB is replicated in the deposited film. At the GB, various types of defects will be created in order to relax the lattice of the film. At low angles, edge dislocations will be created[29] but at higher angles other types of defects are also possible.

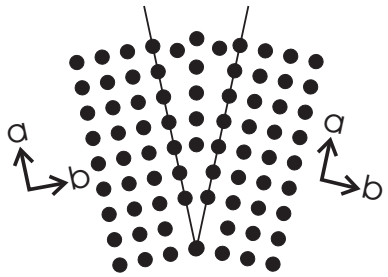

Figure 4.1: A schematic picture of a GB. The fusing of the crystals creates a region of disorder where the two lattices do not coincide.

The reason for the weak link behavior of the GB in YBCO can be found from one or several effects [29]

- Crystallographic misorientation
- Intergranular phases
- Impurities that gather at the GB
- Microcracks
- Changes in stoichiometry

It is very likely that the properties of the barrier will depend on the combined effect of several of these, the relative importance will also depend on the misorientation angle and the type of substrate used.
Many materials are used as substrates for YBCO. The most important materials are $SrTiO_3$ (STO), Y-ZrO_2 (YSZ), MgO, Al_2O_3(Sapphire), $LaAlO_3$ and LaSrAlTaO (LSAT). These are all oxides and most of them have a perovskite structure. It is well known that the transport properties of the GB vary depending on the substrate used. This further underlines the fact that the misorientation angle alone can not explain the properties of the GB.
Grain boundary junctions are classified as being of tilt or twist type according to how the bicrystal is formed [30]. Tilt junctions are formed when the crystal is rotated around an axis in the plane of the grain boundary and twist refers to a rotation perpendicular to the plane.
Being a perovskite, YBCO is very sensitive to oxygen loss and this causes problems when working with GB devices since oxygen tends to diffuse away. This coupled with meandering of the GB makes it hard to beforehand predict the properties of a structure. Parameter spread is usually large in HTS structures, both between nominally identical structures on the same chip and even more so from chip to chip.

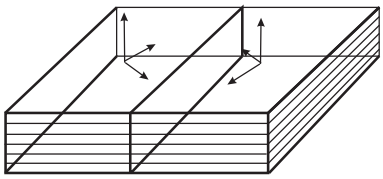

Figure 4.2: A [001]-tilt bicrystal.

4.1.1 Types of junctions used in this work

The common denominator for all three types of junctions used in this work is that they are all based on the idea of the artificial grain-boundary discussed above.

Junctions fabricated on [001]-tilt bicrystal substrates

This is the most common type of grain boundary junction and bicrystal substrates are today commercially available. The different [001]-tilt bicrystals are classified with the help of the angles α and β which refer to the angles the a-axis of the superconducting film on each side of the GB makes with the GB line (see fig. 4.2); in, e.g., a 0°-30° junction one electrode has it s a-axis parallel to the GB line while the other is rotated 30°. Grain boundaries with identical misorientations of the grains with respect to the GB line are said to be *symmetric*, otherwise they are *asymmetric*. A particular case of the later is "asymmetric 45° junction" which is just another way of writing "0°-45° junction". The main reason for using the bicrystal technique is that it enables one to fabricate well-defined grain boundaries with many different misorientations. We have studied the properties of junction fabricated on bicrystals with different misorientation angles (some of the results are discussed in papers I and III) but in this work the focus is on 0°-45° junctions.

Biepitaxial Junctions

In the measurements presented in chapter 7 a *biexpitaxial* JJ was used. This is a techniques used to make grain boundary JJ on ordinary substrates (in this case STO) by first depositing a seed layer of e.g. CeO_2 and then removing it from part of the substrate; when the YBCO is deposited the part of the film that grows on the CeO_2 is rotated 45^o with the respect to the $a-b$ axes of the STO-substrate. Hence, assuming that the film grows epitaxially both directly on the STO and on the CeO_2 the result will be YBCO grown with and without a 45^o rotation of the $a-b$ axes with respect to the substrate (see figure 4.3). By using the same lithographic techniques as for bicrystal devices the film can then be patterned to form junctions where the two parts meet to form a grain boundary. the film can then be patterned to form junctions. Although this scheme is simple in principle real samples are always slightly ' more complex as can be seen in fig 4.3. The samples used in this work were grown on (110) oriented STO which means that there is also a c-axis tilt which affects the junction properties. There are both advantages and drawbacks with the biepitaxial technique compared to the bicrystal technique. The main advantage is that it is possible to make junctions with different misorientation angles on the same substrate and that the junctions are not restricted to lie on a single line. The main drawback is that it is a very difficult technique to use. Another problem is that biepitaxial junctions seem to age (meaning that device properties change, most likely due to oxygen out-diffusion) more rapidly than bicrystal junctions (which rarely change their properties even when stored for several years).

Generally speaking there are a few key differences between biexpitaxial and bicrystal junctions. In the case of the misorientation angles we are interested in (mainly 0°-45°) biepitaxial junctions are normally much less transparent, the critical current density is one- or two orders of magnitude lower than for bicrystal junctions. As has already been mentioned the c-axis tilt also affects the properties and makes any description of the transport even more complicated. It seems likely that the c-axis tilt effectively reduces the damping of the junctions making them hysteretic. Whether this is simply due to the nature of the interface or is related to the orientation of the tunnelling cone (and therefore the d-wave symmetry) is still an open question.

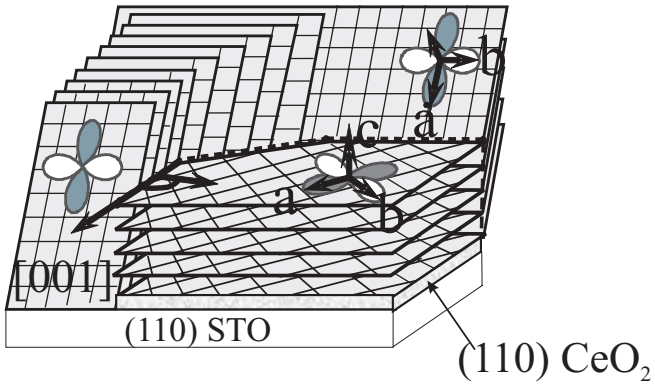

Figure 4.3: Drawing showing a biexptaxial junction as well as the orientation of the lattice.

Tilt-tilt GB junctions

In paper V we introduce a novel type of GB junction with both a [001] *and* [100] tilt. [100]-tilt junctions are, despite being somewhat uncommon, relatively well studied and have properties that might make them suitable in many applications[31]. Since the electrodes have a 0°-0° orientation in the *ab*-plane in a [100]-tilt junction there is nominally no strong effect of the d-wave symmetry. The idea behind the tilt-tilt technique is to make GB junctions with traits both from the biepitaxial and bicrystal technique. As can be seen in 4.4 the structure is very similar to a biepitaxial junction with a c-axis tilt that can be varied by changing the [100] tilt of the substrate. The reason for studying this type of configuration is that for application in the quantum regime it is desirable to have underdamped junctions, ordinary [001]-tilt junctions are mostly overdamped. One major advantage

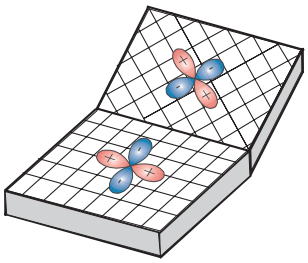

Figure 4.4: A bicrystal substrate with a 45^o rotation around the [001] axis plus an additional tilt around the [100] axis

of this technique is that it allows us to use our well-estabiliched fabrication technique. This allows for a lot of freedom in device design and makes it possible to easily fabricate ,e.g., submicron junctions. Being a new technique there are many things that remain to be investigated; the initial results are, however, very encouraging.

4.2 Device Fabrication

With the exception of one all devices used in this work were fabricated using the same scheme. Since fabrication is somewhat outside the scope of this work, only a summary is given. A more detailed description can be found in paper III.
The choice of substrate was dictated by the fact that it is relatively easy to grow high-quality YBCO-films on STO and bicrystals with a well-defined GB are available. However, the material has one serious drawback which one needs to keep in mind: Its dielectric constant at low temperatures is huge. At 4.2K the low-frequency ϵ_r in a film is at least 2000 [32] but can be as high as 20 000 in bulk samples. ϵ_r is also frequency-dependent. Due to the AC Josephson effect, junctions and SQUIDs are "natural" high-frequency devices and radiate energy. This means that a device can couple electromagnetically to a substrate which can for example result in resonances visible in the IV-curve.
All films used in this work were deposited using Pulsed Laser Deposition (PLD) on 5x5 mm^2 substrates, the film thickness was varied between 150-200 nm. The films were deposited under conditions which give a reasonable compromise between smoothness and critical temperature T_c (in general it is not possible to optimize both at the same time), T_c was usually close to 89K with a steep transition.
Using a rather thick film is crucial when fabricating small structures in any HTS material, the main problem one faces is oxygen out-diffusion and a thick film may reduce this problem. The electrodes leading to the structures can then function as oxygen reservoirs without being depleted themselves.

4.2.1 Lithography

There are many steps involved in the lithography, what follows is a short summary of the most important steps.

- A YBCO film is deposited on the substrate.
- A protective gold layer is deposited.
- The contacts, alignment marks and rulers are defined using e-beam lithography.
- Since the GB is not located exactly in the middle of the chip the pattern needs to be adjusted. The deviation is measured using the rulers and the device drawings are changed accordingly.
- A layer of amorphous carbon (a-carbon) is deposited.
- The pattern is defined in the NiCr using e-beam lithography and NiCr evaporation.
- The pattern is transferred to the carbon layer by a lift-off process.
- The YBCO is milled defining the final pattern. The etch rate of carbon is much lower than than of YBCO, the a-carbon essentially functions as a "hard mask".

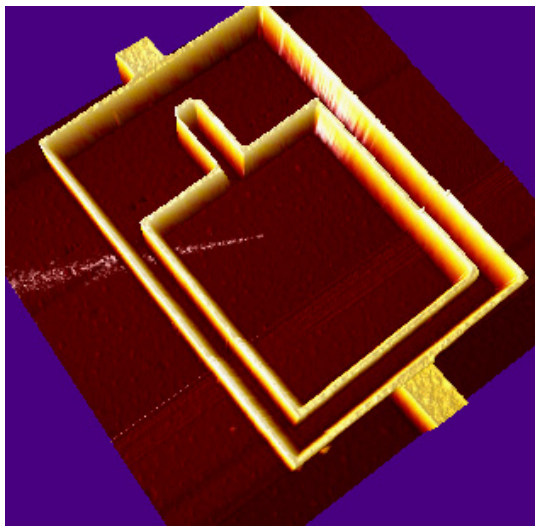

Figure 4.5: A large (20x15 μm^2) SQUID surrounding a smaller one (12x12 μm^2). The depicted area is 25x25 μm^2

A typical device fabricated using this technique can seen in figure 4.5. There are many steps in the fabrication procedure, it is ,however, a quite reliable way to make very small structures in YBCO. 200 nm strips can be made with very high yield. It is possible to define even narrower structures but they are usually not superconducting, probably due to a low oxygen content.

4.2.2 Sample design

Designing SQUIDs for the types of experiments described in this thesis is not straightforward. The main problem is the loop size. Since we are not interested in maximizing the flux sensitivity we can make the loops rather small in order not to make the devices too sensitive to noise. On the other hand it is important to avoid having to use fields which are so high that they start to affect the properties of the junctions themselves. These considerations help us to determine that suitable sizes were 5x5, 10x10 and 15x15 μm^2.
Another important parameter when designing SQUIDs is the loop inductance. In our case it was important to keep the inductance as small as possible since the inductance directly influences the CPR of the SQUID. In order to be sure that the effect of the inductance could be safely neglected, we used the software package 3D-MLSI [33] to solve the problem numerically.
There are about 20 structures (with 44 gold pads) on each sample. Even though the samples were designed for various experiments, the basic design has stayed the same for the duration of this work. Junctions were fabricated with sizes ranging from 0.2-2 μm, the minimum size was set by technological limits whereas the maximum width was choosen in order to make sure that the junctions were in the short limit.

4.2.3 Considerations

From a physical point of view it is important to understand the effect of the fabrication on the properties of the film. Excessive heating at some point could for example lead to oxygen loss resulting in underdoped YBCO. Even though a device made from underdoped YBCO might work, it

would be hard to know how to interpret the results of a measurement since one would be probing properties which might differ a great deal from those of optimally doped YBCO.
We believe that the procedure outlined here, while cumbersome, helps to preserve the integrity of the the film. For the same reason other potentially useful techniques are not used. It is possible to fabricate very narrow structures using a Focused Ion Beam (FIB). However, in the case of FIB there are issues with possible gallium poisoning of the film. It is not fully understood how gallium doping affects the properties of YBCO. So for fundamental studies, it is best to avoid this technique.

4.3 The Measurement setups

Two different setups were used to characterize our samples, a combination of conventional dip-sticks and a He-3 system for temperatures in the range 300 mK-40K and a dilution fridge for temperatures down to 20 mK, the later setup was primarily used for measurements in the quantum regime.

4.3.1 300 mK-90K

Most measurements have been done using a measurement setup known as ”RURIK” at Chalmers. The setup is always evolving as new equipment is added but the basic configuration has been the same for a few years.
The sample is glued to a chip holder and then wedge bonded using gold wires; the chip layout is designed so that it is always possible to do a 4-point measurement on each device. The chip holder is mounted on a dip stick which is then lowered into a magnetically shielded liquid helium cryostat. There is a small magnetic coil in the stick which makes it possible to apply fields of the order of 2 mT.
The devices are always current biased. It is very difficult to voltage bias HTS Josephson junctions and SQUIDs. Several attempts have been made but the end result is always inevitable: The destruction of the device under study. This is due to the fact that the load impedance of most of our devices is too low (often a few Ohms). Voltage biasing is only practical if the devices are relatively high-ohmic. This unfortunately means that it is difficult to directly compare the results with theoretical predictions since they almost always assume voltage bias. Even though this might seem trivial it is actually a big problem.
The biasing is done by connecting a series resistor. Another smaller resistor is used to read out the current flowing through the circuit by measuring the voltage. Both current (indirectly) and voltage are measured by using two battery driven differential pre-amplifiers. The cryostat and pre-amplifiers are kept in a EMI [1] shielded room. The signals are then fed to various measurement devices located at the outside of the shielded room. The measurement electronics is powered from an insulating transformer which separates the measurement ground from the building ground. It also suppresses noise. All measurements are referenced to the wall of the shielded room. A schematic of the setup can be seen in figure 4.6.
The setup consists of

- 2 Princeton Applied Research 5113 differential pre-amplifiers
- 3 HP 3440A multimeters that are used for current-voltage characterization (”IV-measurement”)

[1] **E**lectro**m**agnetic **I**nterference, electromagnetic noise coming from e.g. mobile phones, radio transmitters and computers.

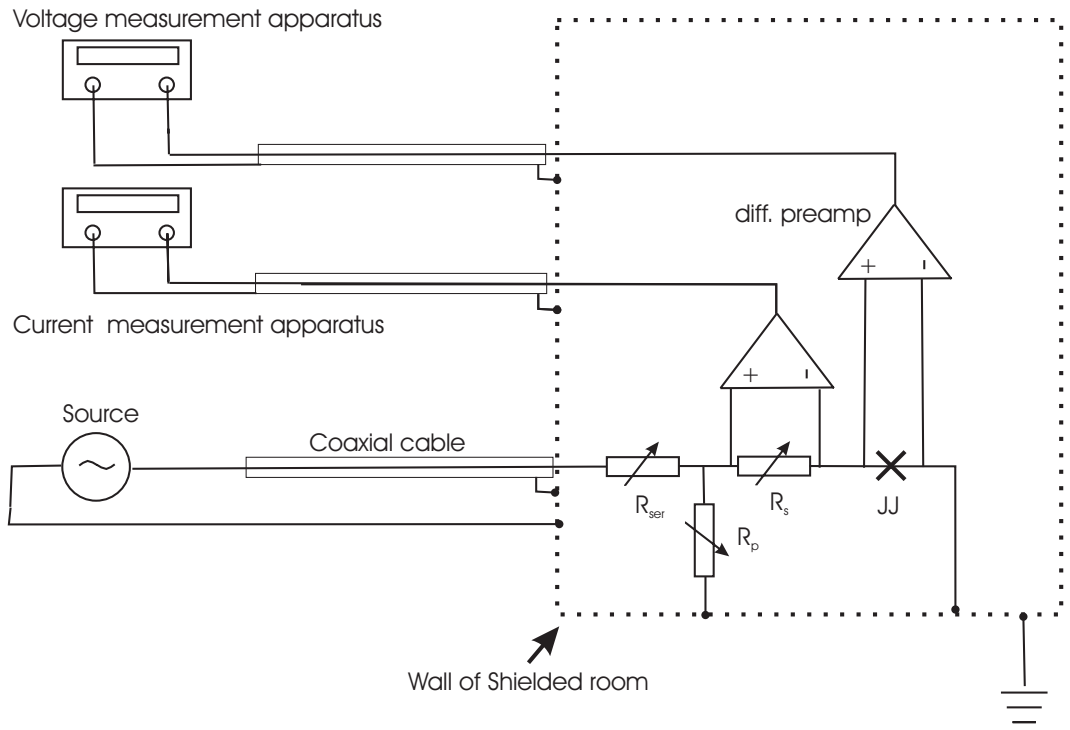

Figure 4.6: The RURIK system. R_{ser} is the series resistance, R_s the resistor used to measure the current, and R_p a resistor which can be connected in parallel with the Josephson junction.

- 1 Agilent 33220A arbitrary function generator used for biasing
- 1 Conductus LTC-21 temperature controller
- 1 Princeton Applied Research 5210 Lock-in amplifier
- 1 Yokogawa 7651 DC Source which is mainly used as current source for the magnetic coil
- 1 Fluke 3380A oscilloscope
- 1 National Instruments PCI-6052E 16-bit 333 kS/s Data Acquisition Card, used for various tasks such as IV-measurements, switching current measurements etc
- An Oxford Heliox ^{3}He cryostat which can reach temperatures of 260 mK

Other types of equipment are also available when needed: Spectrum analyzers, microwave sources (up to 50 GHz), network analyzers etc.
The ^{3}He cryostat is magnetically shielded using a two-layer screen of Niobium and Cryoperm. All control signals (temperature sensors, coil-bias, stepping motor for the Heliox etc) are routed through filtered feed-throughs. One advantage of using this cryostat is that is is possible to stabilize the temperature in the whole range from 260mK to 90 K and it is therefore ideal for measurements on HTS samples. There are also microwave lines, to which it is possible to attach a dipole-antenna, unfortunately the use to these drastically decreased the hold-time at the base-temperature due to the increased heatload.

When used correctly this setup is very suitable for low-noise measurements which is very important in the types of study presented in this theses. Access to a low-noise measurement setup is crucial in this type of experiments since in general the energy scale is set by the free energy of the junction/SQUID, the charging energy and the effective temperature (which is always higher than the bath temperature because of additional noise). An energy-conversion table can be found in Appendix A.

4.4 Measurements below 300 mK

The measurement presented in chapter 7 were all done in an Oxford Model 200 dilution fridge. The cryostat is located in a shielded room and all lines going in and out are filtered. The noise level of this system is extremely low because of the careful multi-stage filtering, the use of battery driven measurement electronics and fiber optic control lines.

4.4.1 Filtering and design of the sample cell

Several types of filtering were used in order to prevent high-frequency noise from reaching the sample, a schematic of the insert can be seen in fig. 4.7. The first filtering state consists of conventional pi-filters at room temperature positioned just at the inputs of the cryostat. From there two twisted pairs (a total of four lines, all control lines for e.g. thermometers where in another tube) go to anchoring points at 4.2K. Stainless-steel powder filters [34] anchored with integrated LC-filters were mounted at 700 mK, followed by another set of filter anchored at 50 mK.
Finally, the lines go through a copper-powder filter integrated in the sample cell (depicted in fig. 4.8), the reason for using copper being to avoid any magnetic impurities in stainless steel powder.
The microwave lines were anchored at 4.2K and 700 mK using 20 and 10 dB attenuator respectively. The coax used was a plated stainless steel cryogenic type [2] which has both good thermal and electrical properties. The response of the whole assembly was reasonably flat from 10 MHz to 40 GHz, the latter being the cut-off frequency for the 2.92mm connectors [3] that were used.
The sample cell itself (depicted in fig 4.8) consists of a copper block. There are four measurement lines that pass through an integrated copper-powder filter. The sample is glued to the copper using silver glue and then bonded to gold pads on a printed circuit board. The cell itself was made as small as possible and has irregular walls in order to minimize problems with standing waves. The microwave excitation is done via coax that has been made into a $\lambda/2$ dipole antenna with a centre frequency of about 10 GHz. When aligned, the antenna is just a few mm above the surface of the sample.

4.4.2 Measurement electronics

The measurement electronics is a mixture of custom-made equipment and commercially available devices. In the measurements presented here the relevant equipment is

- 1 Stanford Research SR560 voltage pre-amplifier
- 3 Keithley 2000/2001 multimeters

[2] ULT03 from Keycom Corp.
[3] RPC-2.92mm from Rosenberger

- Various function generators, mostly used to create timing-waveforms
- 1 Yokogawa 7651 DC Source current source for the magnetic coil
- Temperature controllers etc. for the dilution refrigerator.
- Custom made measurement electronics, including ramp-generator, comparator, sample&hold circuitry etc for switching current measurements.
- 1 National Instruments PCI-6601 20 MHz counter/timer, used for the time-of-flight measurements

The equipment is connected in different ways depending on the application.

Switching current measurements

Most of the results presented in chapter 7 come from *switching current* experiments. In principle these measurements are no different from ordinary IV-measurements, the idea is simply to record at which current the junction/SQUID switches into the running state; this is a stochastic process and the current at which the device switches varies with about 1-2 % of I_{c0}. However, the measurement needs to be done many times, - usually somewhere around 10 000-50 000 times - since we are typically interested in the properties of an *ensemble*. The current variations are typically tens of nA, at most. Hence, these measurements are demanding in that we require them to be fast (in order to complete the measurement in reasonable time), precise, low-noise and also that the system has reasonable long-time stability.
There are several ways to perform this type of measurement. The most straightforward one being to simply measure IV curves and then numerically extract I_c. However, in reality this is far too slow. Another method is to "extract" I_c electronically. The current is swept from zero and a comparator is used to compare the voltage over the junction with some set threshold value (typically a few μV). When the junction switches the comparator gives a trigger signal and the current is captured by a sample&hold circuit which can then be read out using e.g a multimeter. The trigger signal also resets the ramp generator back to zero. This method was initially used in our measurements and was also used to calibrate the Time-of-flight measurements.
A third method uses the fact that it is much easier to measure time than current accurately. In a time-of-flight (TOF) measurement a trigger signal is used to start both the current ramp and a timer at t=T_0. When the junction switches the comparator gives a trigger signal that stops the timer at a time T_1 and resets the current to zero. The signal out is $T_1 - T_0$ and since the current ramp time is known we can calculate the current at which the junction switched. The schematic is shown in fig. 4.9. This measurement technique is fast, accurate and only needs two logic signals to start the sweep/timer and subsequently stop the timer; these signals can be transmitted using fiber-optics meaning that it is possible to completely isolate the sample from, e.g., computers.
It is important to reset the current waveform generator back to zero as soon as possible after the junction has switched, The reason is that when the junction is in the running state it is resistive, meaning it will start to heat and therefore change its properties.

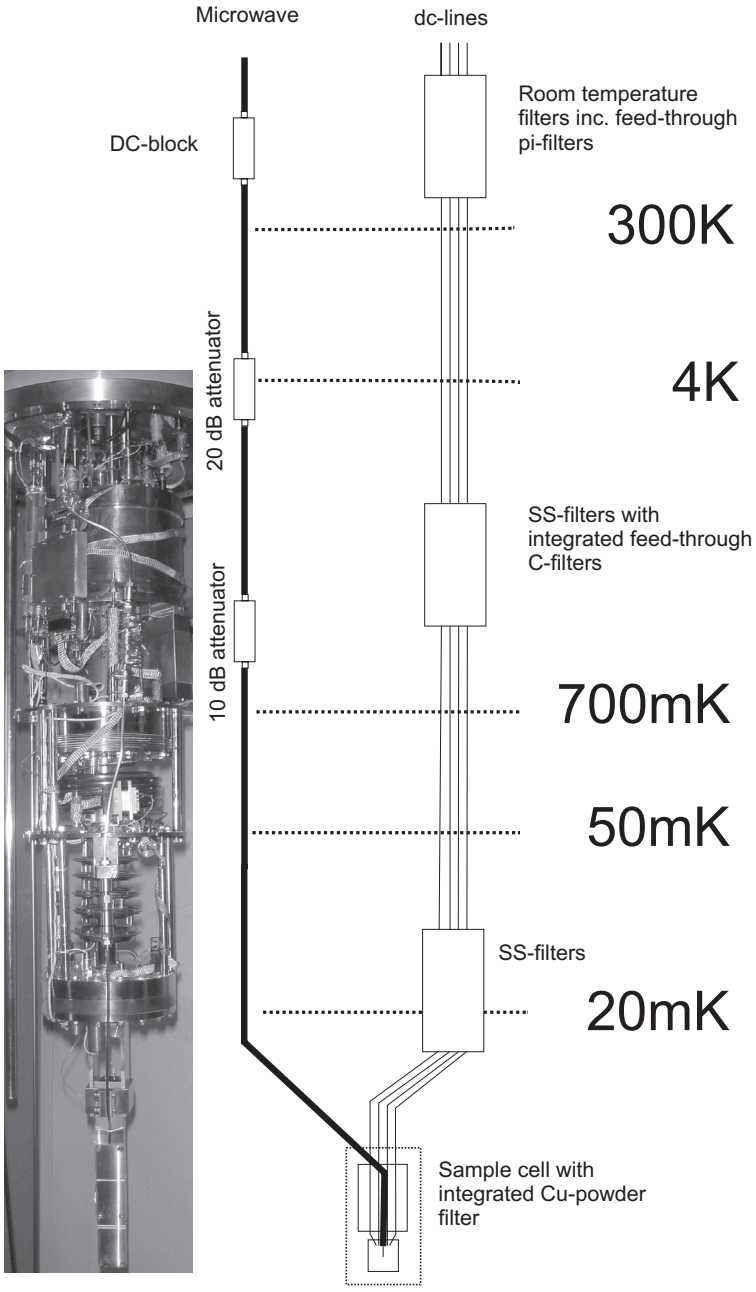

Figure 4.7: Picture and schematic of the insert showing the position of the various filters.

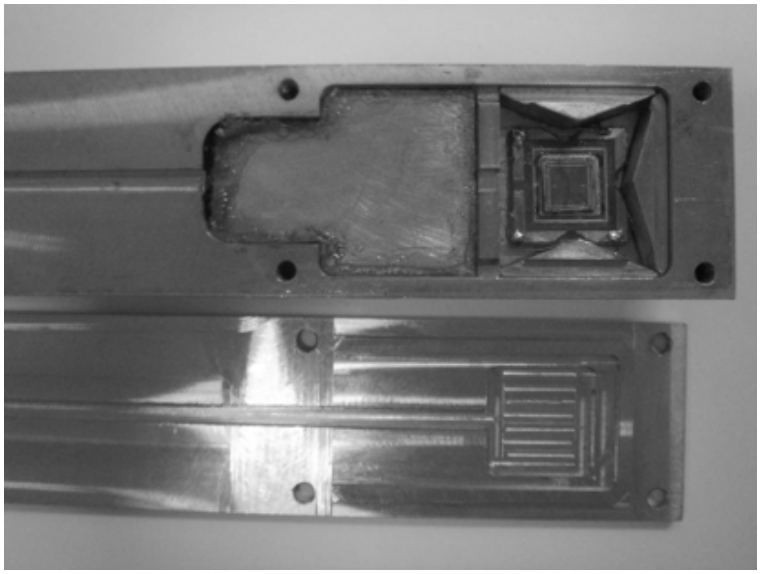

Figure 4.8: The sample cell used for the microwave spectroscopy. The whole cell is made from copper. The wiring comes from the left and goes through an integrated copper powder filter. The walls are arranged so that they are *not* parallel in order to avoid standing waves in the cell.

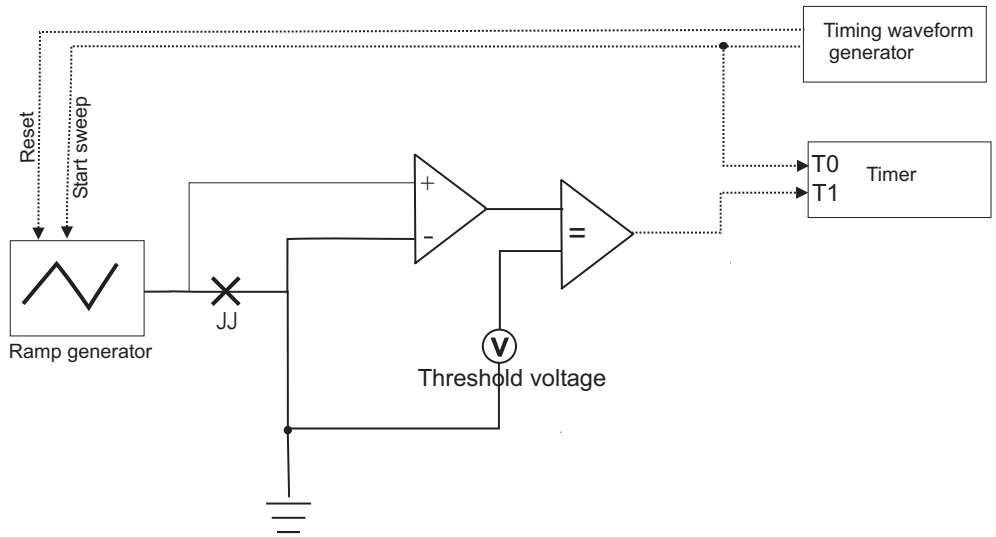

Figure 4.9: A schematic of the Time-of-flight measurement setup. The dotted line indicates logic level signals.

Chapter 5

Properties of High-Angle YBCO Josephson Junctions

This chapter deals with properties of d-wave junctions and in particular how the structure of the GB affects the transport properties. I will start by introducing conventional junction types and then a description of some of the phenomenon that occur in high-angle GB junction will be given: π-facets, excess current and midgap states. Thereafter I will describe a model of the dynamics of a d-wave junction in magnetic field. Finally, I will discuss our experimental results, in particular the scaling behavior of mesoscopic YBCO junctions.

Josephson junctions fabricated from conventional superconductors can be divided into categories depending on the type of electrodes and barrier used. The most common types, as well as an explanation of the nomenclature, can be found in table 5.1. Of these the SIS- and SNS-junctions are the most commonly used. These are well described by the BTK (after Blonder-Tinkham-Klapwijk)-theory [35]. In BTK-theory the barrier is characterized by a parameter T known as the transparency. If D=0 the junction is SIS-type (tunnel regime) and if D=1 it is SNS (ballistic regime). In reality all junctions have T-values somewhere in between and are neither SNS (which would require a perfectly clean interface) nor SIS (a perfect insulator). The current-phase relation in conventional junctions depends on the value of D [36] and for T close to 1 it is non-sinusoidal. In most real conventional junctions the transparency is however so low that the deviation from the simple $\sin\phi$ dependence is very small.

When the first HTS junctions were realized it was therefore natural to try to classify them according to the same scheme. The transparency can be calculated as [37]

$$D \approx \frac{\rho_{ab} l}{R_N A} \tag{5.1}$$

where ρ_{ab} is the resistivity in the ab-plane, l is the mean free path, A is the total area of the junction and R_N the normal resistance of the junction. The values calculated from this formula are usually fairly low, 10^{-2} and lower which would put HTS junctions in the SIS- (tunnelling) limit. The BTK-model of Josephson junctions is very useful and equations such as 5.1 are frequently used to estimate D in order to compare experimental data with theoretical predictions. Moreover, D (or other parameters with similar meaning) is frequently introduced even in very sophisticated models of junctions. The problem with this approach is that theoretical predictions of properties of HTS junctions often need to assume values of D that are several orders of magnitude from those predicted

Type	Name	Comment
Superconductor-Insulator-Superconductor	SIS	Superconducting tunnel junction
Superconductor-Normal Metal-Superconductor	SNS	
Superconductor-"weak Superconductor"-Superconductor	SS'S	The barrier is made of a material with lower T_c
Superconductor-Ferromagnet-Superconductor	SFS	Used to study pair-breaking and make so-called π-junctions
Superconductor-Constriction-Superconductor	ScS	A constriction is a very narrow, -quasi 1D- current channel

Table 5.1: The most common types of conventional Josephson Junctions

by eq. 5.1 in order to be consistent with experimental data (often a D of 1 is used). Hence, it seems to be very difficult to describe HTS interfaces using a single value. Moreover, HTS junctions in general -and those with high misorientation angles in particular- exhibit many properties very different from those found in conventional junctions. The reasons for these differences can be attributed both to the complicated structure of the interface and the d-wave symmetry of the pairing wavefunction in HTS superconductors. A model valid for HTS junctions therefore needs to take both these effects into account.

5.1 The interface of HTS GB Josephson Junctions

In order to understand the properties of d-wave Josephson junctions it is important to realize that when one talks of e.g. $0°$-$45\circ$ junctions one is referring to the *nominal* misorientaion angle; the meandering of the GB means that the transport takes place across a wide variety of angles as can be seen in figure 5.1. As we will see, transport properties, such as the critical current density, are

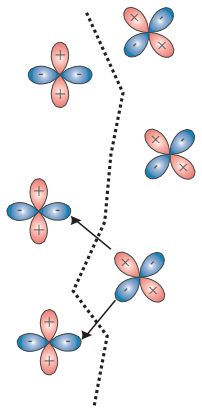

Figure 5.1: The $d_{x^2-y^2}$ symmetry means that meandering has a large influence on the transport properties of GB junctions and junctions with a large misorientation angle in particular. The meandering of this $0°$-$45°$ causes among other thing the formation of π-facets.

strongly dependent on the local angle. The meandering will cause the current distribution in a junction to be inhomogeneous. Moreover, since the CPR is also dependent on the angle we have in

reality a number of transport channels connected in parallel, each with its own CPR, current density and temperature dependence.
The meandering depends both on the nominal misorientaion angle and the method used to deposit the film. The latter is because the length of the facets depends on the growth mode during deposition. For PLD deposited films used in this work we usually assume an average facet length of 100 nm which means that we have tens of channels in our junctions.

5.1.1 π-loops and π-facets

In high-angle junctions the d-wave symmetry gives rise to π-facets. The mechanism for this is analogous to what happens in π-SQUIDs where one junction obtains a phase-shift of π relative to the other junction due to the symmetry of the wavefunction. π-loops in a GB essentially work in the same way; if two adjacent facets are oriented in such a way that there can be transport both between ,e.g, two "minus" lobes and between a "minus" and a "plus" lobe, one facet behaves as a π-junction (see the arrows in fig. 5.1). These facets are known as π-facets and carry a net *negative* current with respect to the ordinary 0-facets. As we will see the effects of π-facets are clearly seen in the way high-angle junctions modulate in magnetic fields.

5.1.2 $\mathbf{J}_c$ vs. angle for grain boundaries: d-wave effects

Even though this work is not concerned with power-applications it is interesting to note that it was when trying to understand why the critical current,J_c, [1] of polycrystalline samples were so much lower than one would have expected from measurement of the value of the gap-voltage that the concept of a d-wave order parameter was first established. In a famous work by Sigrist and Rice in 1992 [38] they showed that the critical current density of an all d-wave junction can be written

$$J_c = J_0(n_x^2 - n_y^2)_L(n_x^2 - n_y^2)_R \sin\varphi \tag{5.2}$$

where J_c is the maximum Josephson current density, φ is the difference in phase in the two electrodes, n_x and n_y are the projections of the unit vector $\mathbf{n}$ onto the crystallographic axes in the right(R) and left(L) electrodes respectively. This result of course has very important implications when trying to make for example cables that need to carry large currents. It tells us that in order to optimize the J_c of a polycrystalline sample we need to make sure that most of the GB are low-angle. It should however be pointed out that this result is not quite correct; according to eq. 5.2 the critical current should be zero in a $0°$-$45°$ junction (see figure 5.2) which is not the case (even though, as has already been mentioned, J_c is very low). As can be shown in a more detailed study[39], the reason for the discrepancy is that 5.2 does not consider transport through bound Andreev states. Even though eq. 5.2 is phenomenological, it agrees reasonably well with experiments on single GB. This has been tested using the biepitaxial technique where it is possible to fabricate many junctions with different orientations on the same chip [40].
The fact that eq. 5.2 seems to work quite well despite the meandering of the GB is in itself quite interesting, it tells us that the *average* properties of a junction are largely governed by the nominal misorientation angle; the actual shape of the GB on the microscopic scale is not as important for the average critical current density as one might think. Nevertheless, if we consider eq. 5.2 it *does* tell us

[1] The expression "critical current" is used in two different contexts. The critical current of a Josephson junction is the maximal supercurrent it can carry, the critical current of a film or bulk sample is the value of the current when the sample is starting to become resistive, either due to the self field becoming higher than the critical field or in a polycrystalline sample because the current carrying capabilities of the the grain boundaries have been exceeded

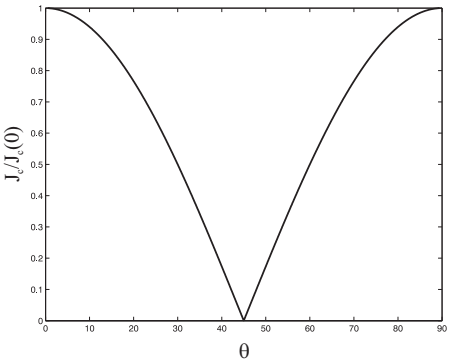

Figure 5.2: Critical current density as a function of angle for a 0-θ junction according to the Sigrist-Rice formula 5.2

that the meandering causes the current distribution in HTS junctions to be inhomogeneous; as will be seen a striking effect of this is an anomalous dependence of the critical current on the magnetic field.

5.1.3 Excess current

Excess current is always a problem for applications of HTS devices, and this is true also for bicrystal junctions. The physical mechanism behind excess current varies, it can be a consequence of a high-transparency barrier but also by ”defects” in the form of pin-holes and micro-shorts. There are several effects which are usually attributed to excess current, not being able to completely suppress the critical current using an external magnetic field or microwave radiation and the slope of the normal branch of the IV curve not going through zero being the most common. The excess current is usually attributed to for example pinholes or other defects in the barrier. When working with high-angle junctions one has to be careful when interpreting the data. As was shown in the simulations the presence of a 2^{nd} harmonic in a non-uniform barrier affects the modulation in magnetic field and R_N is not always well defined. That said some of the supercurrent in our devices, both narrow and wide, is probably carried by excess current. It is possible that a better control of the grain boundary could help to reduce this problem

5.2 Midgap states

In 1994 Hu[41] suggested a novel mechanism for the creation of bound states in a superconductor with $d_{x_a^2-y_b^2}$ symmetry. Hu made the important observation that since the order parameter changes sign as one crosses a nodal direction states with essentially zero energy relative to the Fermi surface will be created [42]. Several experiments reported enhanced conductivity near zero bias voltage (a so-called ”zero-bias conductance peak”, ZBCP) in symmetric junctions and often this was explained by scattering against magnetic impurities in the barrier. Hu was however able to show that the reason was more likely to be due to the existence of transport channels in which the current is carried by zero energy (with respect to the Fermi energy) Andreev bound states, known as midgap states (MGS). Andreev transport is a well known phenomenon which is not unique to HTS materials. The basic process is quite simple if the wavefunction has an s-wave symmetry. An electron coming from a normal metal electrode impinges on a NS-boundary. If the energy of the electron is lower than the

gap energy of the superconductor there are no available quasiparticle states on the S-side and the electron can not pass through the barrier, hence no current can flow. However, in an Andreev process the electron is reflected from the boundary as a *hole* which has an opposite momentum and charge. This means that a Cooper pair can be created in the superconducting electrode without violating charge- or energy conservation (since there is no restriction on the number of Cooper pairs that can exist below the gap). The net result of this process is therefore a charge transfer of 2e across the boundary, the whole process is illustrated in figure 5.3. The reason for the appearance of coherent Andreev states is that the electron- and hole-like wavefunctions, which have opposite electron momenta k_x (the momenta k_y parallel to the specular surface is conserved), can combine to form current carrying states. It can be shown that these states can form Andreev bands if phase dispersion is taken into account.
Andreev transport is not limited to NS or IS interfaces but can also exist in SIS structures. In fact, it turns out that if one calculates the current carried across such an interface by Andreev states the resulting equations will be identical to the Josephson equations 3.6 and 3.8; *Hence, all Josephson phenomena can be completely understood in terms of Andreev transport*. This picture is very useful when studying the Josephson effect in d-wave superconductors. The presence of bound states in Josephson junctions is often directly observed in symmetric junctions [43] but most systematic studies have used tunnelling spectroscopy where TRSB has also been observed[44].
In a high-angle HTS junction an Andreev process is much more complicated than in transport between two s-wave superconductors. The main difference stems from the fact that the wavefunction changes sign for certain quasiclassical trajectories. Figure 5.5 shows the orientation of the wavefunctions and the magnitude of the gap on both sides of the interface.
Here we will mainly limit the discussion to the 0-45° case and for a more general discussion see the review by Löfwander et al [45].
Referring to figure 5.5 we see that the junction can be described as a SIS-structure.
A quasiparticle -hole- or electron-like- coming from the left electrode can give rise to Andreev transport. However, since the phase changes by π when passing from one lobe to the next there will be *two* Andreev-levels, one with a effective phase $\tilde{\phi} = \phi$ ("zero-level") and another with $\tilde{\phi} = \phi + \pi$ ("π-level). The current carried by the π-level will be a 2π-periodic function of the the phase, but will be shifted by π with respect to the zero-level just as in so-called π-junctions which carry a *negative* Josephson current. The net resulting current from both of these processes is π-periodic in phase and from the Josephson relations we see that the Josephson frequency doubles.
The model described above does not take noise and effects of disorder into account. The temperature dependence of the 2^{nd} harmonic differs from that of the 1^{st} which means that there can be a transition temperature where the transport starts to be dominated by the 2^{nd} harmonic. Il'lichev et. al [46] found that this temperature is of the order of 20K. In realistic models of Andreev transport the roughness of the interface and scattering due to impurities and defects has to be taken into account. It can be shown [47] that this can drastically affect the transport properties of high-angle GBJJ. The main result of this analysis is that the Andreev processes giving rise to the 2^{nd} harmonic in the CPR can be suppressed if the quality of the interface is low.
Note that the physics of *symmetric* 45° junctions, i.e. devices with a 22.5°-22.5° orientation of the electrodes, is different from *asymmetric* 0°-45° case considered here and it is important not to confuse these two cases. But also in symmetric junctions one finds many interesting phenomena that can be attributed to midgap states, a recent example is the demonstration of a MGS-based π-junction [48].
The possibility of a strong 2^{nd}harmonic (or, equivalently, a π-periodic CPR) in d-wave junctions has been considered in [49] [50] [51].

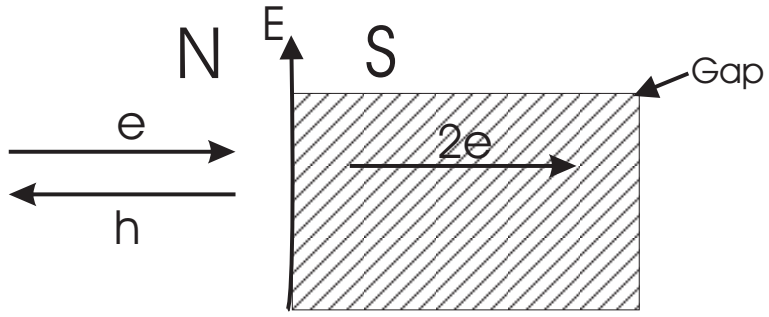

Figure 5.3: Conventional Andreev transport through a NS boundary when the superconducting wavefuntion has s-wave symmetry

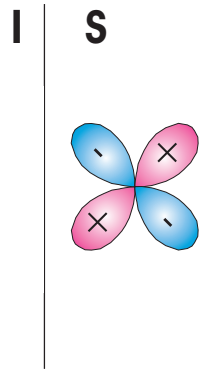

Figure 5.4: The formation of bound Andreev states at a specular interface between an insulator and a superconductor with $d_{x^2-y^2}$ symmetry, the superconducting electrode is rotated so that the node is normal to the interface.

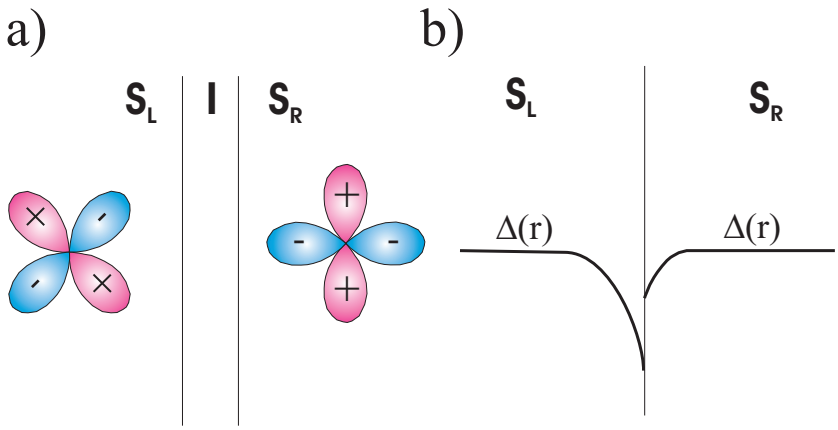

Figure 5.5: The formation of Andreev states in a specular 2-dimensional junction. a) The orientation of the wavefunction b) The magnitude of the gap

5.3 Some further properties of GBJJ

There are many other interesting phenomena that can take place in high angle grain boundaries, some of which are related to the phenomenon studied in this thesis.
One important effect is that the vortex dynamics can be significantly altered at high-angle GB. For example the so-called *splinter vortices* form [52]. These are unquantized flux which form pairs that sum to a flux of Φ_0. This is still an active area of research and it is not completely clear how these affect the dynamics. Their influence should however be insignificant as long as one is studying short junctions. Another effect related to this is the existence of spontaneous currents in grain boundaries [53], again this is an effect which is not that well understood experimentally even though it has been predicted in theoretical works.

5.4 Field suppression of the critical current in HTS junctions

As was mentioned above the meandering means that the current distribution in HTS junctions is not uniform (unless perhaps the junction is very narrow; ~ 100 nm). Furthermore, it is also likely that there exist a few narrow "channels" with high conductance (this is very likely explanation for the lack of correlation between junction transparency and normal resistance which will be discussed later). It is possible to account for these effects as well as other d-wave effects such as π-facets with the help of an extended version of the standard model of a distributed junction that can be found in e.g. [20]
If we assume that the junction is magnetically short we do not need to take self-field effects into consideration. We divide the junction into N pieces, each element being Δz long and w thick and having a critical current $\delta I_c^n = J_c^n w \Delta z$ where the superscript denotes the element number. The presence of a magnetic field B creates a phase difference between each adjacent pair of elements since they are separated by a distance δz, the area of each loop being equal to $(2\lambda + t)\delta z \approx 2\lambda \Delta z$ where t is the thickness of the barrier. When we move between two elements the phase will therefore change by an amount:

$$\delta\phi = \frac{2\pi(2\lambda + t)B}{\Phi_0}\Delta z \tag{5.3}$$

Hence, the total current through the junction is

$$I(\Phi) = \sum_{n=1}^{N}\sum_{k=1}^{\infty} \delta I_c^{n,k} \sin k(\delta\Phi + \theta) \tag{5.4}$$

where the inner sum is the CPR of the element and θ is the phase in the absence of a magnetic field. The critical current is equal to the maximum value of this sum with respect to θ. In order to model high-angle junctions we assume that the CPR can be written $I^n(\Phi) = I_c^{I,n} \sin\Phi - I_c^{II,n} \sin 2\Phi$ and we get

$$I_c(\Phi) = \max_{-\pi \le \theta < \pi} \left[\sum_{n=1}^{N} I_c^{I,n} \sin(\delta\Phi + \theta) - I_c^{II,n} \sin 2(\delta\Phi + \theta) \right] \tag{5.5}$$

If only a first harmonic is present this can be written in the more familiar form (in the limit $\Delta z \to 0$)

$$I_c(\Phi) \left| \int_0^l w J_c(z) e^{i\phi(z)} dz \right| \tag{5.6}$$

which of course reduces to the familiar formula $I_{c0}|\sin(\pi\Phi/\Phi_0)|/|\pi\Phi/\Phi_0|$ when J_c does not change as we move along the boundary, i.e. we get the expression for the well-known Fraunhofer pattern which was already mentioned in chapter 3.
A non-uniform J_c will change the shape of the pattern quite dramatically, this is especially true if π-facets are included as seen in figure 5.6. For a dominant 2^{nd} harmonic in the CPR the periodicity of the pattern is doubled as can be seen in 5.7.
Note that the pattern in figure 5.6 is asymmetric with respect to zero-field. Lack of symmetry is usually attributed to flux trapping but can also be due to an unconventional CPR.

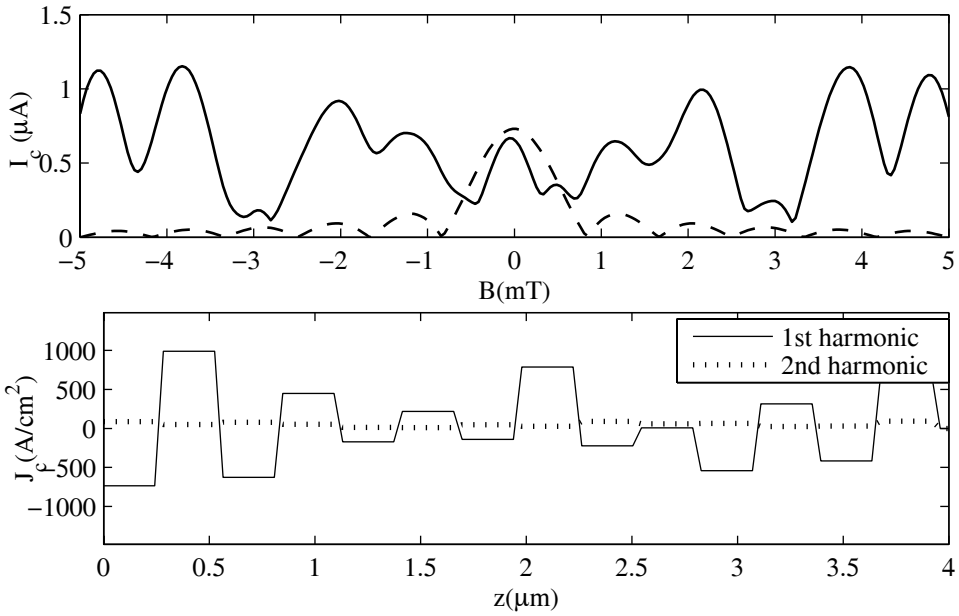

Figure 5.6: A so-called anomalous Fraunhofer pattern calculated using eq. 5.5. The current distribution of the 1^{st} and 2^{nd} harmonic components respectively can be seen in the lower plot. Note that the pattern is slightly asymmetric with respect to zero field. The "normal" Fraunhofer is calculated by assuming a J_c which is just the mean of the current distribution along the boundary.

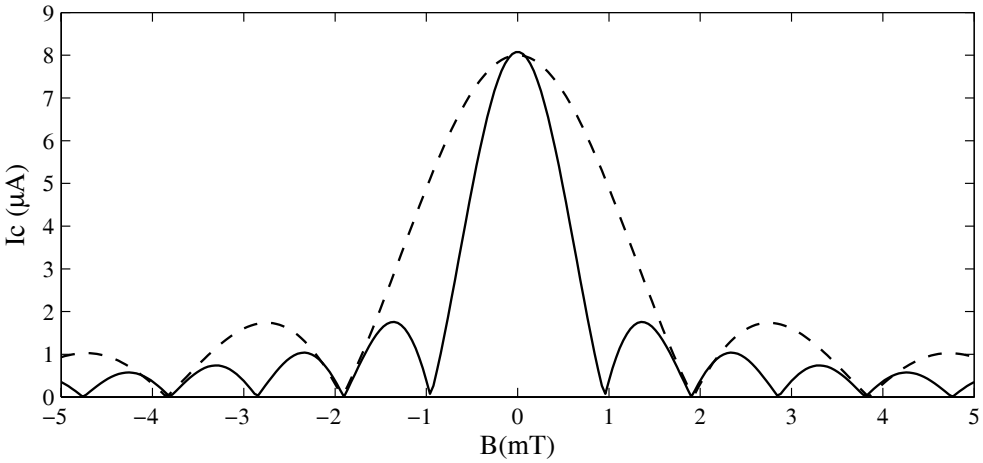

Figure 5.7: The anomalous Fraunhofer pattern when the junction is uniform and the CPR only contains a 2^{nd} harmonic.

5.5 Summary of Results

In this section I will summarize and comment on some of the results found in papers I and III. Whereas the papers are partly focused on the possible applications of the structures under consideration in quantum informatics, the discussion here will be limited to basic properties.
The main result of this work is that it demonstrates that the fabrication procedure outlined in chapter 4 is a reliable method for fabricating very narrow ,mesoscopic, Josephson junctions. This is important both because it allows for a great deal of freedom in the device design and because it has allowed us to investigate properties that are difficult to probe in wide junctions, e.g. the properties at high voltages. However, it also turned out that the properties of mesoscopic junctions scale in a non-trivial way as the width is reduced.

5.5.1 DC Properties of High-Angle Junctions

The most basic measurement one can perform on a Josephson junction is a dc current-voltage characterization or "IV-curve". One can obtain a lot of information from an IV-curve and its derivative, the dynamic resistance dV/dI. It can directly give information about the energy spectrum of the various transport processes when plotted versus the voltage. A transport channel with an energy of, for example, 3 meV will appear as a dip in the dynamic resistance at 3 mV.
High-angle junctions often exhibit an IV-characteristic rich with features. This is especially true in very narrow junctions. Because of their high resistance we can measure IV-curves extending up to voltages of the order of the gap voltage,Δ, which in the case of YBCO is about 25 meV. Hence, the BCS pair breaking voltage should be at $2\Delta \approx$50 meV in a YBCO junction. Indeed features in the spectra are often seen at these values.
Figure 5.8 illustrates some typical I-V and dV/dI vs. V characteristics. They refer to a 0.2 μm wide 0°-45° junction at around 20 mK. The critical current can be seen to be about 400 nA but the normal resistance is not well defined. In conventional junctions, R_N is defined as the resistance above the gap (which should be constant in a BCS superconductor) but here the dynamic resistance decreases up to about 50 mV (corresponding to 2Δ) and then it starts to increase. It varies between 150-250 Ω. There is no clear consensus on how to define R_N in HTS junctions. In most cases it is simply assumed that the dynamic resistance approaches some constant value at a current a few times I_c but this is not true in high-angle junctions.
There are also a number of peaks in the spectra shown in figure 5.8. These may be due to Multiple Andreev reflections (MAR) which occur at fractions of the gap voltage $2\Delta/n$[54]. MAR is not expected to be present in 0°-45° junctions (in theoretical models MAR occurs in *symmetric* high-angle junctions) so probably their appearance means that some other angles are also present in the GB due to faceting.

5.5.2 Scaling behavior

One would expects the dc-properties, I_c, C and R_N, of junctions fabricated on the same chip to scale with the junction area, or equivalently the width since the film thickness can be assumed to be uniform. As indicated in the graphs in papers I and III there is, however, no such simple dependence. At the same time we could observe the usual scaling law $I_cR_N = j_c\rho_N \propto \sqrt{jc}$ on a large number of junctions fabricated on two 0°-32° and two 0°-40° samples. There can be several reason for this nontrivial scaling

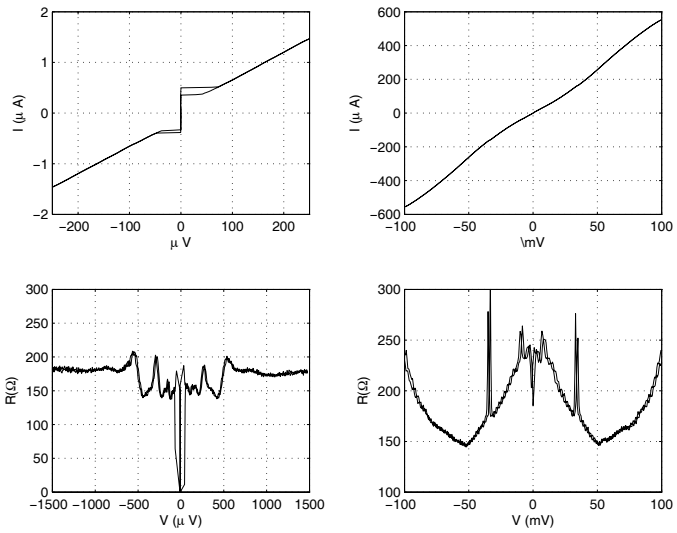

Figure 5.8: Current-Voltage characteristics and dynamic resistance for a 0.2 μm wide junction at 20 mK (the measurement was done using a dilution refrigerator).

- The real width is different from the nominal. This can for example happen if the etching process causes the junctions to become rounded with sloped sides. AFM studies have shown that the relative effect should be rather small unless the junction is extremely narrow. At sizes of 1 μm this effect should be negligible.

- Oxygen out-diffusion. It is not unreasonable to assume that there exists a thin "dead layer" on the sides where the junction is not superconducting due to oxygen out-diffusion and disorder in the film. The thickness of this layer should not be directly related to the size of the features but the relative importance will of course increase as the junctions become more narrow.

- Defects/disorder, both natural and fabrication induced. Again, the relative importance will increase when the junction size decreases, it is however difficult to see why that would give a scaling behavior, the effect should be random.

- Finally, the barrier of the smaller junctions may be free from 'shorts' - narrow channels of high transparency, which mainly govern the properties of the wider junctions. This possibility is supported by the fact that their I_c's extrapolate to zero as the width goes to zero.

It is interesting to note that even though there are some inconsistencies when comparing the parameters of wide and narrow junctions the behavior of junctions of equal width is relatively reproducible. A parameter spread of about 10% was observed on one chip.

Another, somewhat puzzling fact, is that the measurements on dc-SQUIDs mentioned in paper I seem to indicate that the CPR of mesoscopic 0°-45° junctions has a conventional $\sin\phi$ CPR dependence. The reason of this is not clear but it might be due to, e.g., increased disorder and oxygen out-diffusion which would suppress the d-wave order parameter.

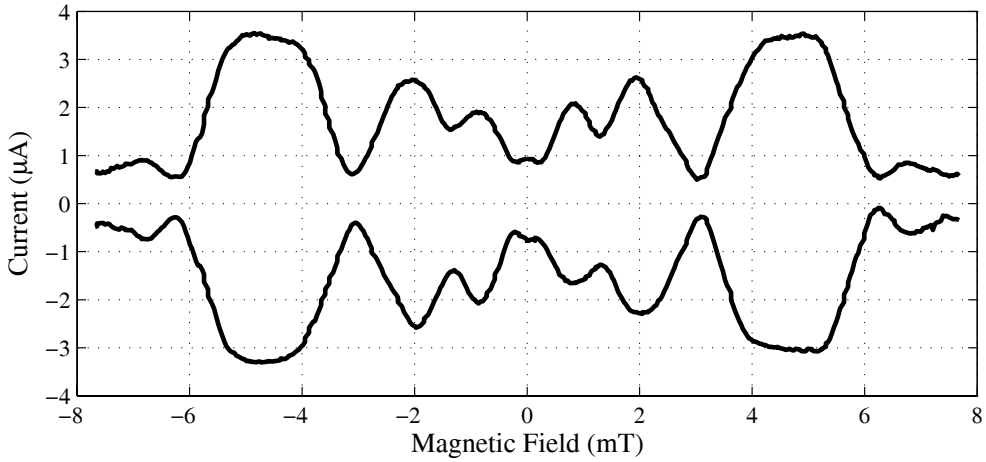

Figure 5.9: Anomalous Fraunhofer patter of a 2μ 0°-45° junction at 4.2K. The global minima in the center is an indication of the presence of π-facets.

5.5.3 Anomalous Fraunhofer patterns

Figure 5.9 shows the anomalous Fraunhofer pattern of a 2 μ wide junction. The presence of π-facets means that the current reaches its maximum value at around 5 mT. The expected quasi-period, $\Phi_0/2\lambda w$, of this junction is about 4 mT using a London penetration depth, λ of 130 nm.
The pattern depicted in figure 5.9 is that of the right arm of the dc-SQUID denoted SQ5 in paper V. In that experiment we first characterized a SQUID and then cut the loop so that the junctions could be measured individually (I will return to this in the next chapter). This allowed us to determine the parameters of each junction. For this junction $\alpha = 4$ meaning the 1^{st} harmonic component of the Josephson current is suppressed at low fields and the 2^{nd} harmonic dominates. Interesting is also that the other arm (the left) had a critical current of about 3.5 μA at zero field, i.e. close to the value this junction reaches at 5 mT.
It is often possible to increase the current carrying capability of a high-angle junction by redistributing the current using a magnetic field. One therefore need to be careful about drawing conclusions about the microscopic J_c of high-angle junctions just by studying the critical current of the junction at zero-field. What we measure is the *average* J_c, which can be close to zero in a junction with many π-facets. The real, microscopic, J_c can be several times higher than what a zero-field measurement would indicate.

Chapter 6

High-angle HTS dc-SQUIDs with Unconventional Current-Phase Relation – Comparison between Numerical and Experimental Results

The presence of midgap states in $0°$-$45°$ junctions can give rise to a strong 2^{nd} harmonic component in the CPR. From an experimental point of view, the presence of a 2^{nd} harmonic is difficult to detect when working with single junctions. This is because the junction will always strive to minimize its free energy with respect to the phase and will do so regardless of the exact shape of the current-phase relation. It is therefore difficult to directly see any effect on the dc-properties of a junction. Some parameters, such as the critical current of the junction, are affected, but in most cases these effects are quite small. A junction can, for example, switch to the running state earlier than it would do with a purely sinusoidal CPR, thus causing a reduction of the measured I_c but that can also happen due to many other reasons. The effects on the dependence on an applied magnetic field can be quite strong, but it is hard to separate the 2^{nd} harmonic influence from effects of inhomogeneous current distribution, π-facets and flux-trapping.
Hence, in order to be able to detect a 2^{nd} harmonic in the CPR with confidence, one has to use a method that avoids these problems. In the case of a single junction, the most common way is to study the microwave response. This can be an accurate way to detect the presence of a 2^{nd} harmonic since it will cause the appearance of subharmonic Shapiro steps at frequencies e/h. This technique has for example been used in [55]. But the most sensitive way of studying these effects is to use quantum interference, this is the technique employed in the work by Il'ichev *et al* where a RF-SQUID was used [46]. Here we will instead focus on dc-SQUIDs.

6.1 The Influence of a 2^{nd}-harmonic in the CPR on the dynamics of a dc-SQUID

Most of the matter discussed in section 3.5.2 is still valid if we retain higher order terms in (3.14). The dynamics are ,however, altered compared to conventional dc-SQUIDs and the current- and voltage response change.

Current modulation

When there is a significant contribution from a 2^{nd} harmonic , the equation for the CPR of a dc-SQUID in presence of an external magnetic field $\phi_x = 2\pi\Phi_x/\Phi$ can be written

$$I_s(\phi, \phi_x) \quad = \quad I_{c1}^{I} \sin\phi \; - \; I_{c1}^{II} \sin(2\phi) \; + \; I_{c2}^{I} \sin(\phi \; + \; \phi_x) \; - \; I_{c2}^{II} \sin 2(\phi \; + \; \phi_x) \quad (6.1)$$

where we have assumed that self-field effects can be neglected. The critical current is equal to the maximum supercurrent the SQUID can carry

$$I_c(\phi_x) = \max_{\phi} I_s(\phi, \phi_x). \quad (6.2)$$

It is straightforward to numerically calculate the I_c vs. ϕ_x dependence of the SQUID. Figure 6.1 shows the results for one of these calculations for a few values of the critical currents. The parameters used can be found in table 6.1.
One can make a few striking observations from these calculations

I. The modulation becomes quasi-π-periodic when the 2^{nd} harmonic is introduced (the true period being 2π unless the first harmonic is exactly zero).

II. The positive and negative curves become shifted with respect to each other, however inversion symmetry is still conserved. The maximum I_c is no longer at zero field.

III. The modulation depth becomes very small when the SQUID is highly asymmetric with respect to junction parameters.

Voltage modulation

Another common way of characterizing a SQUID is to measure its voltage modulation as a function of applied field. If we limit ourselves to the RSJ-model and introduce the necessary generalizations we can write the average voltage over the SQUID as

$$\bar{V}^{-1} \quad = \quad \frac{G_1 + G_2}{2\pi} \int_{-\pi}^{\pi} d\phi \left[I - (G_1 - G_2)\frac{\hbar}{2e}\frac{d\delta}{dt} \; - I_1\left(\phi + \frac{\delta}{2}\right) - I_2\left(\phi - \frac{\delta}{2}\right)\right]^{-1} \quad (6.3)$$

Here $G_{1,2}$ are the normal conductances of the junctions, and

$$\delta + \phi_x + \frac{\pi L}{\Phi_0}(I_2(\phi - \delta/2) - I_1(\phi + \delta/2)) = 0, \quad (6.4)$$

gives the difference, δ, in phase drops across each junction.
Expression 6.3 can easily be integrated numerically to yield a family of curves which show the modulation for a few values of the bias current; the result can be seen in figure 6.2. Again, one can make a few interesting observations

I. The positive and negative curves are shifted, inversion symmetry is conserved.

II. The curves become less distorted at high values of the bias, the effects of the 2^{nd} harmonic is ”washed out”.

III. The modulation depth is again very small.

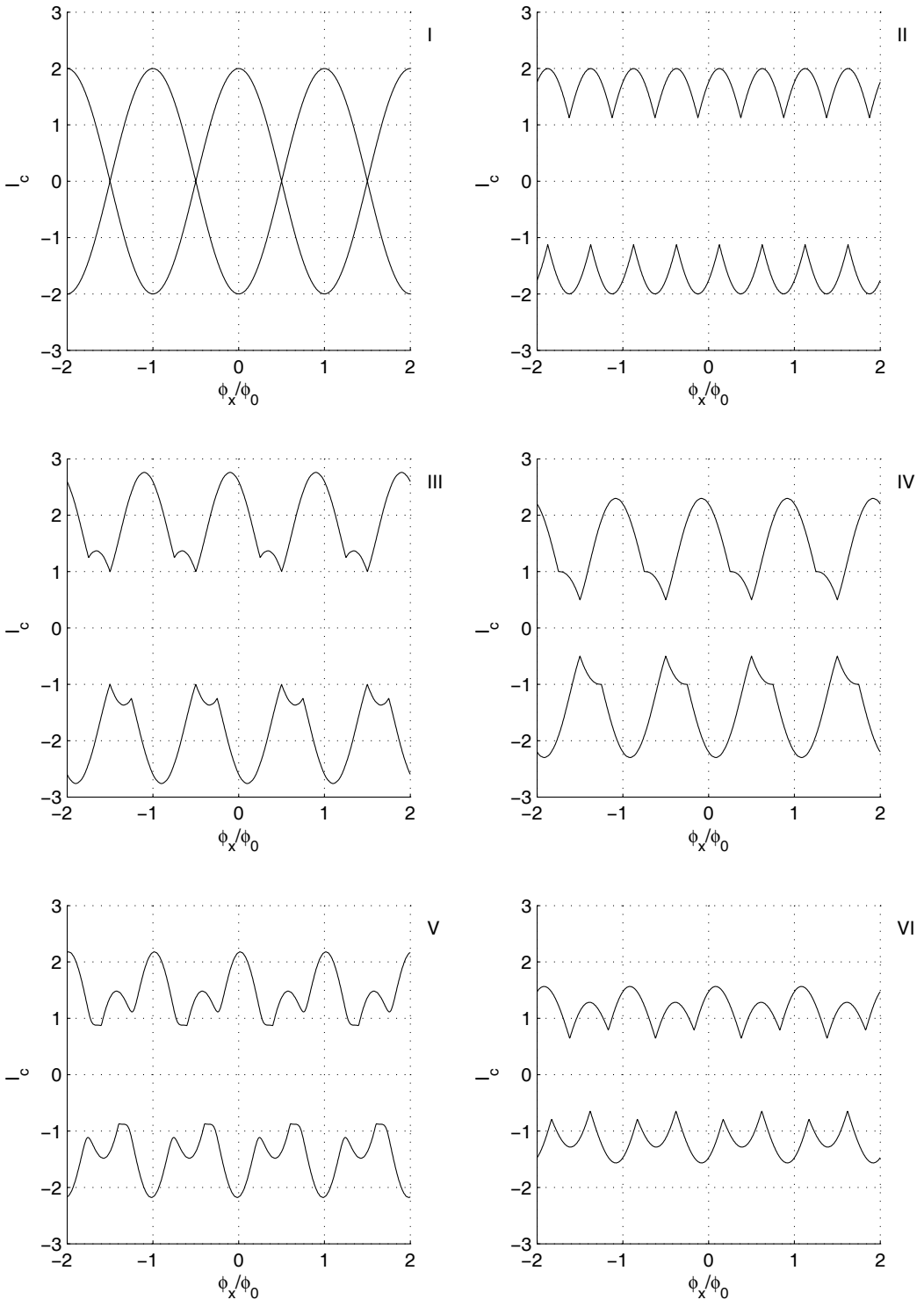

Figure 6.1: A few examples of I_c vs. ϕ patterns for dc-SQUIDs with different ratios of the 1^{st} and 2^{nd} harmonic. I_c has been normalized to I_{c1}^1. Table 6.1 lists the parameters values

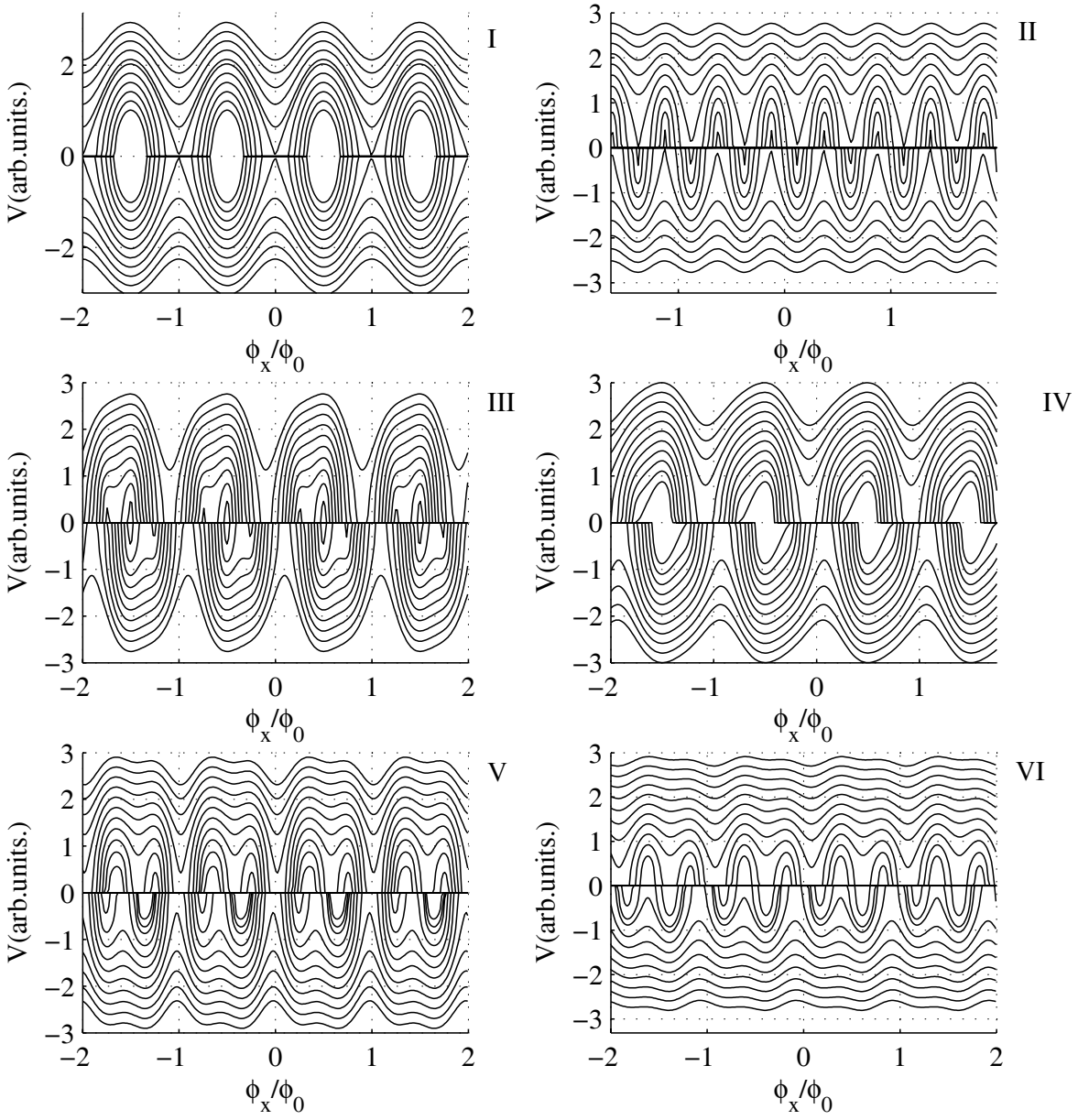

Figure 6.2: V vs. ϕ patterns. The parameters are the same as in figure 6.1, the patterns are plotted for $i = I/I_c = 1$ to $i = I/I_c = 3$ in steps of 0.2I$_c$.

Figure	I_{c1}^{I}	I_{c1}^{II}	I_{c2}^{I}	I_{c2}^{II}
I	1.0	0	1.0	0
II	1.0	0	0	1.0
III	1.0	1.0	1.0	0
IV	1.0	0.5	1.0	0
V	1.0	0.5	0.5	0.5
VI	1.0	0.1	0.2	0.4

Table 6.1: Parameters used to plot figures 6.1 and6.2.

From these simulations it should be clear that the presence of a 2^{nd} harmonic can affect the dynamics of dc-SQUIDs quite dramatically. Note, however, that the effects are most striking in asymmetric SQUIDs. In the limit of a symmetric SQUID where all the current is carried by a 2^{nd} harmonic the only effect on the dynamics is that the periodicity doubles. This can be difficult to detect experimentally unless the exact field threading the SQUID-loop is known and it is possible to accurately calculate the expected period of the SQUID (including any flux-focusing effects).

Calculation of the Free energy It is instructive to plot the free energy of these systems. In the case of a single junction in the overdamped limit the calculation is straightforward. The relation between the current, energy and phase difference, $I_c(\phi) = (2e/\hbar)\partial E_J/\partial\phi$ follows from gauge invariance (and the Cooper pair charge being 2e) and does not depend on the exact form of E_J. Therefore the Josephson energy of the *n*th harmonic must be equal to $\hbar I_n \cos(n\phi)/(2en)$. We need to calculate

$$U = \frac{\hbar}{2e}\int_0^{\phi} I(\theta)d\theta \tag{6.5}$$

and, keeping only the first two harmonics

$$E_J(\phi) = -E_J^I\left[\cos(\phi) - \frac{\alpha}{2}\cos(2\phi)\right] \tag{6.6}$$

where the energy scale is set by E_{1J}. The potential will take the shape of a double well if $\alpha = I_2/I_1 > 0.5$.
In the slightly more complicated case of a dc-SQUID the phase differences across the junctions will be related to the external flux. Neglecting the self-inductance of the loop, the Gibbs free energy of a current-biased dc SQUIDs can then be written [56] [1] as a function of the external phase $\phi_x = \phi_1 + \phi_2$ and a new variable $\gamma = (\phi_1 - \phi_2)/2$ which corresponds to the total phase difference across the SQUID.

$$U(\gamma, \phi_x) = \frac{(\phi - \phi_x)^2}{2\beta_L} - \varepsilon_\phi\left[\cos\gamma - \frac{\tilde{\alpha_\phi}}{4}\cos(2\gamma)\right] + \tilde{U}(\gamma, \phi_x) \tag{6.7}$$

where

$$\varepsilon_\phi = (1+\eta)\cos(\phi/2) \tag{6.8a}$$

$$\tilde{\alpha_\phi} = [2(\alpha_1 + \eta\alpha_2)\cos\phi]/[(1+\eta)\cos(\phi/2)] \tag{6.8b}$$

$$\eta = E_2^I/E_1^I \tag{6.8c}$$

$$\tilde{U} = -\left[\eta - 1 + 2(\alpha_1 - \eta\alpha_2)\cos\tfrac{\phi}{2}\cos\gamma\right]\sin\tfrac{\phi}{2}\sin\gamma \tag{6.8d}$$

[1] Note that the definition of α differs from that in [56].

The first term in eq. 6.7 drops out in the case of negligible self-inductance. Just as in the case of the individual Josephson junctions, the total potential shows a double well behavior as can be seen in figure 6.4. We still have something which reminds us of a "tilted washboard" but now there are extra features. If α is small, the dynamics will look similar to that of an ordinary junction in the running state. However, if α is large,enough, the "phase particle" can get trapped *twice* as the phase changes by 2π, this will naturally affect the dynamics of the SQUID.

6.2 Distributed SQUIDs

It is straightforward to extend the model for a distributed single junction eq. 5.5 to the case of a dc-SQUID. However, the dynamics becomes much more complicated than in the single junction case since the resulting patterns are the result of *both* junction- *and* SQUID modulations.
Following the usual method of deriving the equation that governs the behavior of a magnetically short junction, we introduce

$$\delta\Phi = 2\pi\frac{2\lambda B}{\Phi_0}\delta z \tag{6.9}$$

The amplitudes of the critical current components of junction i for facet n can be written

$$I^I_{c,k}(n) = f_i(n)\overline{J_c}w\Delta z \tag{6.10}$$

$$I^{II}_{c,k}(n) = g_i(n)\overline{J_c}w\Delta z \tag{6.11}$$

where w is the thickness of the film, $\overline{J_c}$ the total average (measured) critical current density of the junction; $f(n)$ and $g(n)$ are functions that are piecewise constant over some typical distance l and tells us how the current density varies as we move along the GB. This is a simplification since f and g are of course continuous in a real junction, but nevertheless this captures the essential physics.
Using this we can write the field dependent critical current of a dc-SQUID as

$$I_s(\phi_x) = \overline{J_c}w\delta z \cdot \max_{-\pi<\theta<\pi}\Big\{\sum f_1(n)\sin(\delta\Phi+\theta) - g_1(n)\sin 2(\delta\Phi+\theta) + f_2(n)\sin(\delta\Phi+\theta+\phi_x) - g_2(n)\sin 2(\delta\Phi+\theta+\phi_x)\Big\} \tag{6.12}$$

where ϕ_x is the normalized external flux $2\pi BA/\Phi_0$, A being the area of the SQUID-loop. Note that the function has been written in a form suitable for numerical simulations.
In SQUIDs with distributed junctions, the $I_c - \phi$ is a combination of the SQUID- and junction responses to the applied field resulting in complex dynamics, the simplest case being that of the SQUID modulating within the junction envelope. The general result is however more complicated. Figure 6.3 shows some results of numerical simulations using this formula.
Several sets of parameters have been used but in all cases the facet length of 100 nm has been kept. The parameters are listed in table 6.2. Note that the pattern in figure II comes from a zig-zag junction with a non-zero mean J_c due the currents from facets at the edge of the junction not cancelling each other perfectly. Figure IV is interesting because it shows that the response of a symmetric SQUID can look almost conventional,except for a very small modulation depth, despite the presence of both π-facets and a 2^{nd} harmonic current component.
This model and its consequences are discussed to some length in paper V.

Figure	Type
I	π-SQUID
II	Junctions with alternating 0- and π-facets
III	Symmetric SQUID with $\alpha_1 = \alpha_2$
IV	Symmetric SQUID with π-facets and 2^{nd} harmonic, $\alpha_1 = \alpha_2$
V	SQUID with randomized facets
VI	SQUID with randomized facets: Larger field range

Table 6.2: Parameters used to plot fig. 6.3.

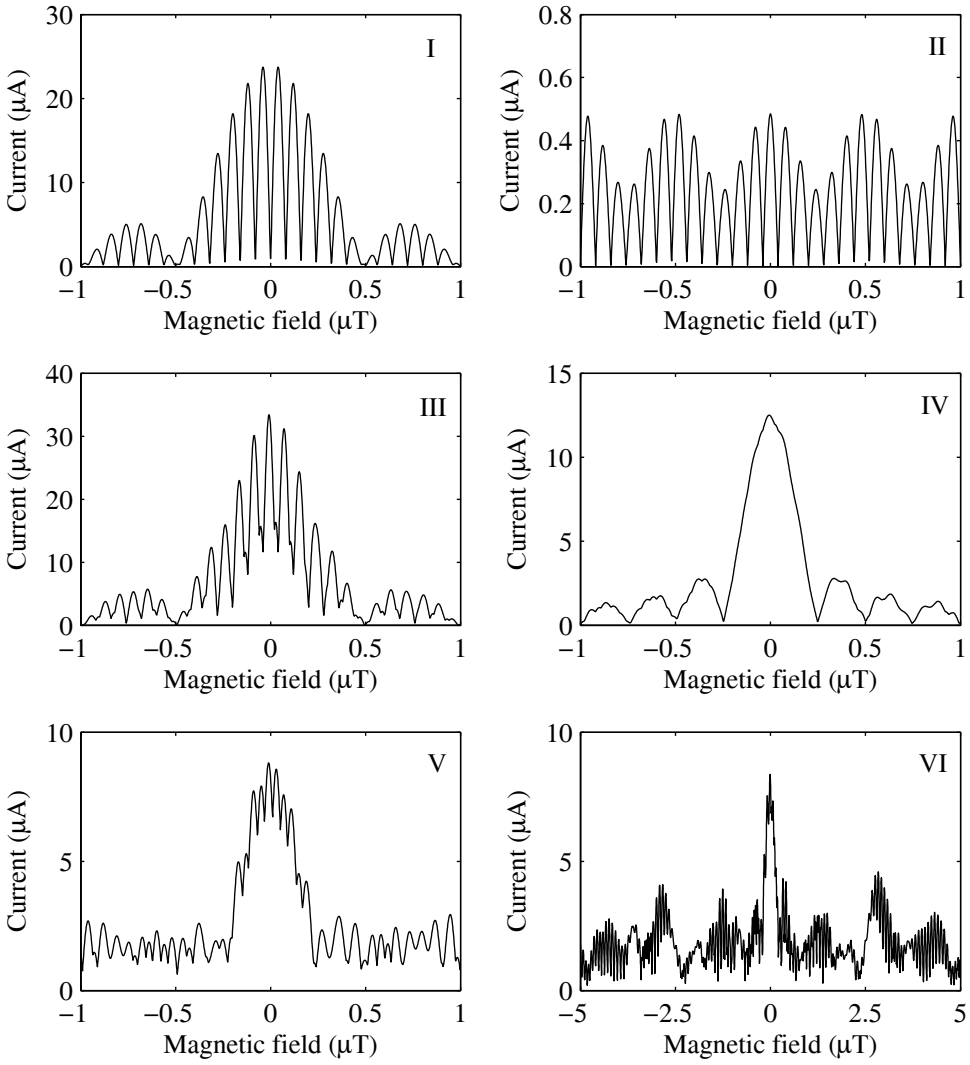

Figure 6.3: Examples of results from numerical simulations of SQUIDs with both π-facets and 2^{nd} harmonic. The parameters can be found in table 6.2.

6.3 Comparison between numerical and experimental results

The most important conclusions contained in papers II and V is that the presence of a 2^{nd} harmonic in the CPR of 0°-45° junctions indeeds affect the dynamics of dc-SQUID. Moreover, we can understand both the behavior at low fields ("pure" SQUID modulation) and high-field (which includes the effect of the anomalous Fraunhofer pattern) if the meandering of the GB is taken into consideration.
Figure 6.5 shows the effect of a 2^{nd} harmonic on the voltage modulation of a dc-SQUID. The similarities between this experimental pattern and the numerical simulations are striking. There is a clear π-periodic structure in the pattern which disappears at higher bias current. As expected the positive and negative curves are shifted but field inversion symmetry is retained. In paper II we were able to fit the critical current modulation of this SQUID using eq. 6.1. Unfortunately, we needed to assume the presence of excess current in the junctions in order to fit the data. This introduced two more variables into the problem which made the fitting procedure complicated. The latter is an example of a general problem with this type of experiments; the behavior is very non-linear meaning that e.g. a Fourier transform of the response does not give any information.
In order to reduce the number of unknown parameters we therefore repeated the same experiment on SQUIDs with three electrodes. The results is discussed in paper V. This geometry allowed us to first characterize the SQUID and then cut the loop making it possible to measure each junction individually. This reduces the problem to 3 variables (α_L,α_R and background field) making the fitting procedure much more accurate and reliable. We also did not need to assume the presence of excess current, consistent with the fact that it was possible to reduce the critical current of the junctions to zero using microwaves. The α-values extracted from this experiment were 0.72 and 4.2 meaning the relative magnitude of the harmonics differ by a factor of g between the junctions. These alpha values correspond to 2^{nd} harmonic current components of 0.5 μA and 3.1 μA, respectively. The critical current values differ by a factor of 3. The large difference in α in our samples is of course striking. However, as has already been stated, the effects of the 2^{nd} harmonic are much more visible if the samples are asymmetric. This means that we purposely pick samples for measurements (and the subsequent fitting) that are very asymmetric both with respect to α and I_c.
The usage of numerical simulations has helped us understand the behavior of SQUIDs in the high-field regime. The non uniform current distribution (of both the 1^{st}- and 2^{nd} harmonic) combined with the presence of π-facets lead to highly complex patterns that are in general asymmetric with respect to zero field (but still field inversion symmetric). Figure 6.7 shows a pattern where these effects are visible. Shown is also another effect consistent with numerical simulations; whether or not the effects of the 2^{nd} harmonic are visible depend on the magnitude of the field. There are field regions where only conventional modulation is seen and all π periodic features are absent.
Finally, the tilt-tilt bicrystals are promising candidates for application in the quantum regime. Whereas bicrystal SQUIDs fabricated on ordinary [001]-bicrystals usually have a $\beta_c \approx 1$ the tilt-tilt SQUIDs are usually hysteretic but at the same time they exhibit a strong 2^{nd} harmonic component in the CPR. This means that they should be suitable for the same type of switching current experiments that are discussed in the next chapter.

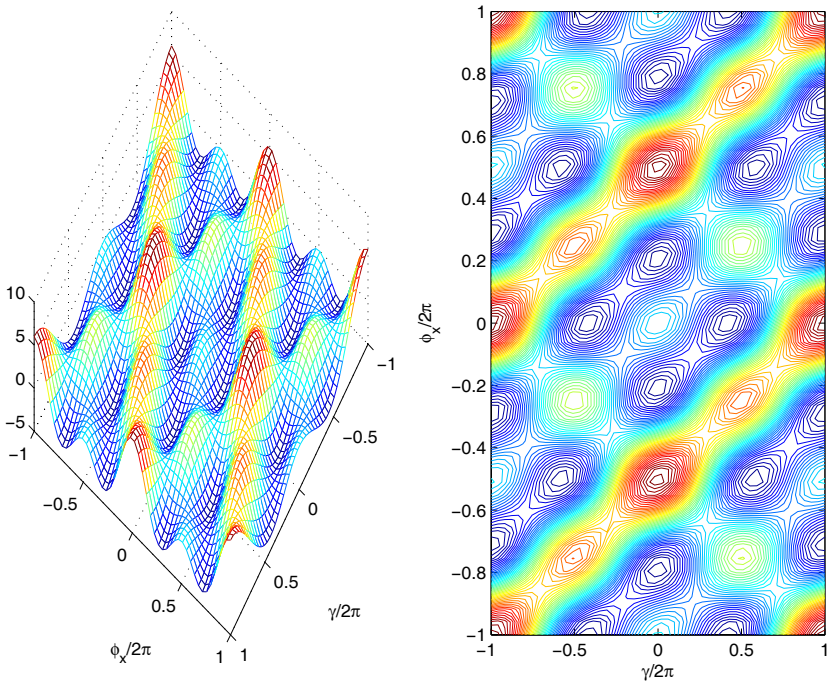

Figure 6.4: Free Energy of a dc-SQUID with $\alpha_1 = \alpha_2 = 2$ and $\eta = 2$. *Left:*3D-plot and *Right:*Contour Plot.

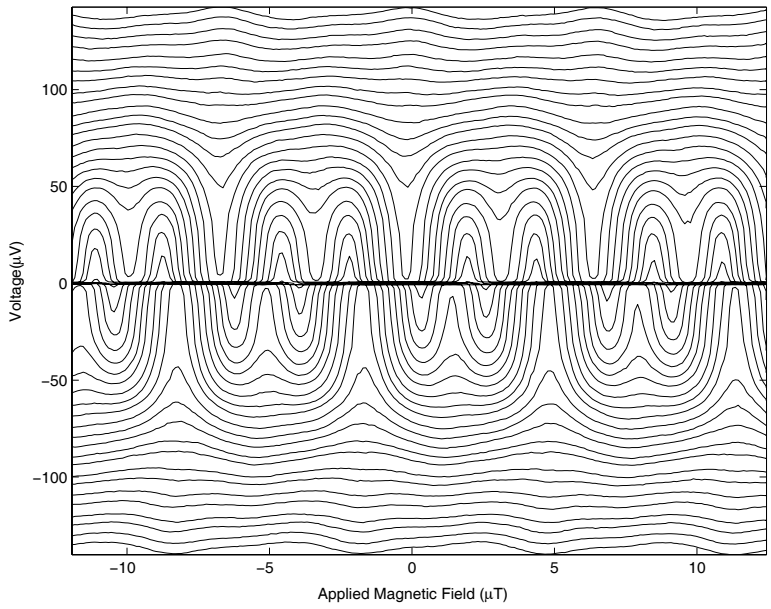

Figure 6.5: Voltage modulation of as a function of applied field for a 15x5 μm^2 dc-SQUID with 2 μm junctions. I_c was 43 μA and the geometric inductance was estimated to be 25 pH. In paper II we showed that the $I_c - B$ dependence of this SQUID can be fitted using $I_{c1}^I = 9$ μA, $I_{c2}^I = 0.3$ μA, $I_{c1}^{II} = 3.7$ μA and $I_{c2}^{II} = 22.7$ μA .

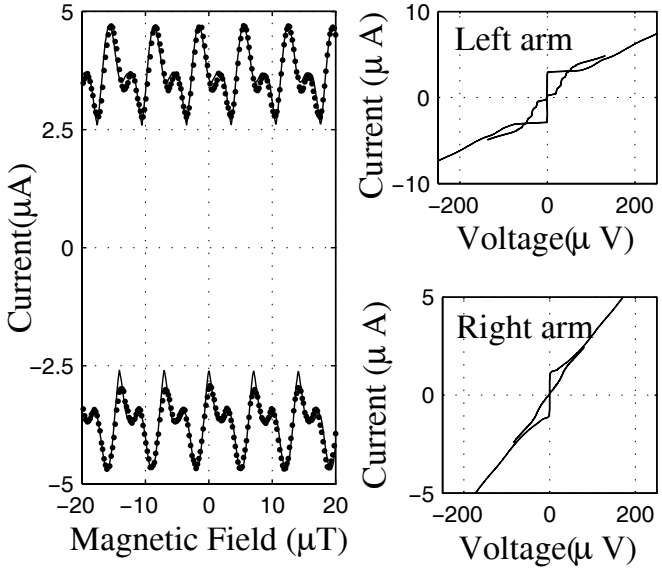

Figure 6.6: Current modulation of dc-SQUID and the IV curves of the individual junctions at 4.2K. The dots are experimental data. The fitting parameters were I_{cR}=3.5 μA, I_{cL}=1.1 μA, α_R=4.2 and α_L=0.72. Shown is also the IV curves under 5 GHz microwave radiation. This graph was taken from paper V.

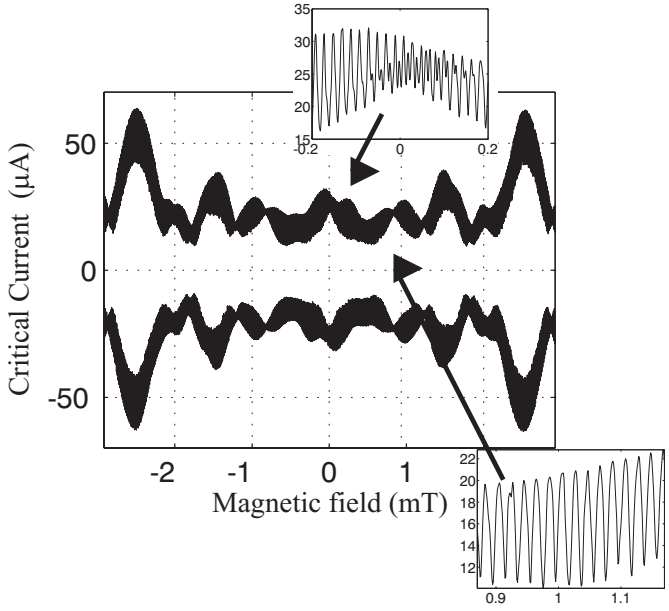

Figure 6.7: Current modulation at high fields for a 10x10 μm^2 tilt-tilt SQUID with 4μm wide junctions at 4.2K. The insets show regions in field with and without signs of a π-periodic component of the CPR This graph was taken from paper V.

Chapter 7

Macroscopic Quantum Tunnelling and Resonant activation in HTS Devices

Even though Josephson junctions are inherently quantum mechanical devices it is in most cases enough to describe them in the classical framework used so far in this thesis. However, if temperature and dissipation are low enough a number of effects arise that can only be understood using a fully quantum mechanical description. I have already touched on this topic in chapter 3, here a more complete description will be given along with experimental results on resonant activation in biepitaxial YBCO junctions.

The concept of *Macroscopic quantum tunnelling* (MQT) was first discussed by A.J. Leggett in 1980 in conjunction with the ”quantum measurement problem”. Detection of MQT demonstrates that a given macrosystem[1] can exhibit a quantum-mechanical behavior without classical analogue. Superconductivity is of course in itself a macroscopic quantum phenomena but is the result of ”collective” *microscopic* quantum effects, there are no interference effects of *macroscopically distinct* states.

Several systems can exhibit MQT but the Josephson junction has turned out to be a perfect oject for the study of this effect. Much of the theory that will be used here can also be applied to other systems, e.g. MQT of magnetic moments [57]; whence there is no explicit reference to superconductivity in the theory.

This chapter covers several topics. I will start by discussing MQT, energy levels and resonant activation in Josephson junction and how these phenomenon can be described using a Master equation approach. I will then describe how this approach can be used in numerical modelling of these phenomena and show that the results are in qualitative agreement with experiments. This is followed by a description of methods for analyzing experimental switching current data. Finally I discuss our experimental results concerning resonant activation in a HTS junction; in particular the high quality factor and why our results can *not* be understood if one assumes a cubic junction potential. A modified RCSJ-model of the junction is described which is shown to agree with experimental data.

[1] By macroscopic we here mean that the number of dynamical degrees of freedom is large

7.1 Theory of MQT

Quite generally we can write the total Hamiltonian that describes the dynamics of a Josephson junction initially in the superconducting state as

$$H = H_J + H_i \tag{7.1}$$

where I have divided the Hamiltonian into two parts; H_J describes the dynamics of the junction whereas H_i describes the interaction with the continuum. H_J can be written in the usual form

$$H_J = \frac{1}{2m_\phi}p^2 + U(\phi) \tag{7.2}$$

where m_ϕ is the "mass" $(\hbar/2e)^2C$ of the junction and $p = (\hbar/2e)^2C\dot{\phi}$. The potential $U(\phi)$; in the case of a tunnel junction described by eq. 3.40. This equation is valid as long as the Josephson energy E_J is much larger than the *charging energy* E_c

$$E_c = \frac{e^2}{2C} \tag{7.3}$$

If $E_J \gg E_c$ the phase ϕ is a well-defined quasi-classical variable.
From now on the following *assumptions* will be used in the model

- The junction is interacting weakly with the environment, i.e. the coupling to the continuum only perturbs the system slightly. Essentially this means that we are modelling the junction as an isolated well.
- Any change of the bias γ is so slow that the system changes adiabatically.

Using these two assumptions the problem reduces to a standard time-independent eigenvalue-problem

$$H_J\Psi = E\Psi \tag{7.4}$$

The eigenfunctions of this equation are of course not true energy eigenstates of the complete Hamiltonian (if they were the system would be static); the interaction with the environment will cause the states to decay meaning they are in fact *metastable* (the eigenstates of H_J are said to be *virtual ground states*).
Note that all eigenvalues of eq. 7.4 are real, a semiclassical calculation with the full Hamiltonian would result in complex eigenvalues $\epsilon = E - i\Gamma\bar{/}2$ corresponding to quasistationary energies and decay rates which would fully describe the dynamics of the system. Hence, it is in principle possible to solve this problem "exactly" using numerical methods but in reality even that proves to be difficult. In the case of a tunnel junction this problem can be somewhat simplified by approximating the potential of the junction with a cubic potential [58] $U(q)$ where q is the position of the "phase particle" in the potential. We can therefore write

$$U(q) = 3U_0\left[\frac{q}{q_0}\right]^2\left[1 - \frac{2}{3}\frac{q}{q_0}\right] \tag{7.5}$$

where the height of the barrier U_0 and the position of the maximum, q_0 ,are given by

$$U_0 = 2E_J[(1-\gamma^2)^{1/2} - \gamma\arccos i] \approx E_J\frac{4\sqrt{2}}{3}(1-\gamma)^{3/2} \tag{7.6}$$

$$q_0 = 2\sqrt{3}\left[1 - \frac{\gamma \arccos\gamma}{(1-\gamma^2)^{1/2}}\right]^{1/2} \tag{7.7}$$

These expressions are very useful and agree well with experimental data for e.g. Nb junctions and are therefore almost universally used in literature [58][59].

7.2 Energy Levels in Josephson Junctions

To find the position of the energy levels in the potential we need to solve eq. 7.4, which, in the case of a single junction, amounts to solving a 1-D Schrödinger equation, Unfortunately there are no analytical solutions for this problem even for simplified potentials like eq. 7.5 and in general numerical methods need to be used. However, for deep lying levels with an energy $E \ll U_0$ we can simplify the problem even further by using an harmonic approximation. Setting U(bottom of well)=0 we get the well-known result for an harmonic oscillator

$$E_n = \left(n + \frac{1}{2}\right)\hbar\omega_p \tag{7.8}$$

which means the interlevel energy spacing is just $\hbar\omega_p$, Plancks's constant times the classical plasma frequency. This turns out to be a surprisingly good approximation which is useful in many situations. Using numerical methods it is of course straightforward[2] to solve the problem for any potential. Fig. 7.1 shows the position of the levels in the well, the normalized bias is $\gamma = 0.9$ and there is room for 7 levels in the well.

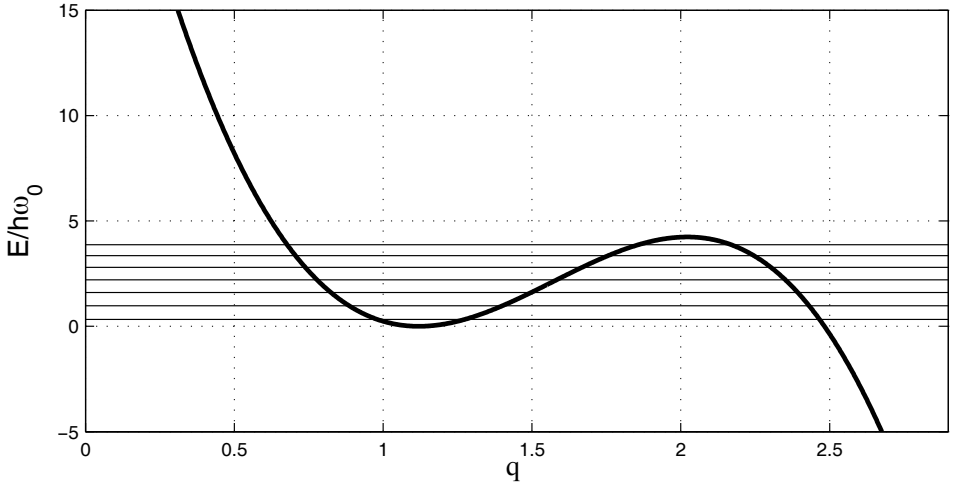

Figure 7.1: Solving eq. 7.4 for a standard junction potential (here with $\gamma = 0.9$) results in a spectrum of almost equidistant levels. The figure has been plotted in units of of the zero-bias plasma energy $\hbar\omega_0$.

In fig. 7.2 the interlevel spacing has been plotted for the tunnel junction potential for the first three levels. For low bias the levels are almost equidistant $\Delta E = \hbar\omega_p$ but as the bias is increased the distances start to differ slightly. As the bias is increased the height of the barrier is reduced and the levels drop out of the well. The fact that we can "tune" the interlevel energy spacing by simply

[2]The only problem is that one needs to make sure that the states are localized to the well, in practical calculations this is done by forcing the wavefunctions to be zero at the top of the right barrier $\Psi(q_0) = 0$; this is an approximation but it has very little effect on the position of the levels.

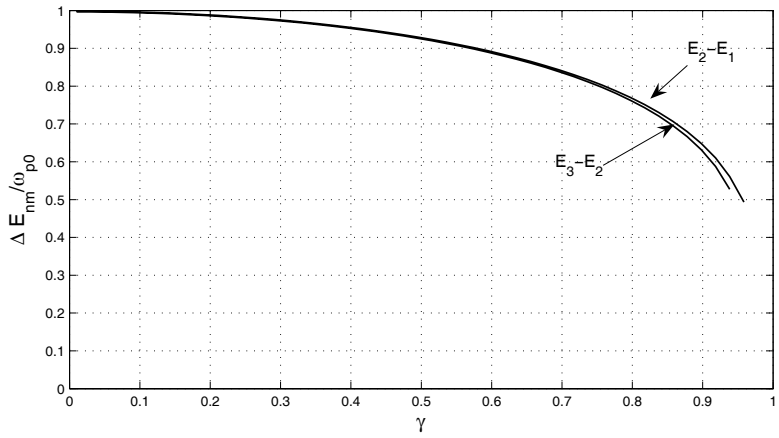

Figure 7.2: The interlevel $\Delta E_{mn} = E_n - E_m$ spacing for the first three levels as function of the normalized bias current for a tunnel junction. The energy has been normalized to $\hbar\omega_0$

changing the bias current is what makes the Josephson junctions such a good tool for studying quantum mechanical effects. In essence the junction behaves like an artificial atom.
The picture given above is somewhat simplified. As was stated in the introduction of this section we have assumed that the junction can be treated as an isolated well. In a real junction there are always dissipation mechanisms which broadens the levels. However, the model outlined above works surprisingly well as long as the temperature is much smaller than the interlevel distance $k_B T \ll \hbar\omega_p$ and the dissipation is low (meaning that the junction has a $Q \gg 1$).
In most models we use an effective resistance R to describe the dissipation of the system. Nominally R is just inversely proportional to the real part of the admittance the junction sees $R = 1/Re(Y(\omega))$ [60]. Note that R is frequency dependent but generally only the value around $\omega = \omega_p$ is important since this is the characteristic frequency of the system; hence what is important is *not*, e.g., the normal resistance of the junction or the dc-resistance of the leads. Since the plasma frequency is of the order of GHz for most junctions, determination of the impedance the junction sees is very difficult. Usually it is assumed that R is of the order of the impedance of free space (377Ω) since the leads work as antennas and couple electromagnetically to the environment. However, the coupling (and therefore the impedance) is determined by e.g. the geometry, sample design etc. so in principle there is nothing preventing R from being much larger than 377 Ω. By careful sample design and the use of protective circuitry it is possible to increase R to very high values [61].

7.2.1 The effect of an unconventional CPR

As we will see in the next chapter the presence of a 2^{nd} harmonic in the CPR can significantly modify the dynamics of junctions and SQUIDs in the quantum regime. However, for the moderate magnitude of the 2^{nd} harmonic component we have seen so far in junctions used in the resonant activation experiments the effect is much less pronounced.
As was shown in [62] the main effect of a small 2^{nd} harmonic is to effectively suppress the barrier of the junction. Unless $\alpha > 2$ the junction will always switch from the lower well and the only effect that can be detected is that the histogram of the switching current distribution is slightly wider than expected because of the reduced barrier height; since α is temperature dependent, the effect can be

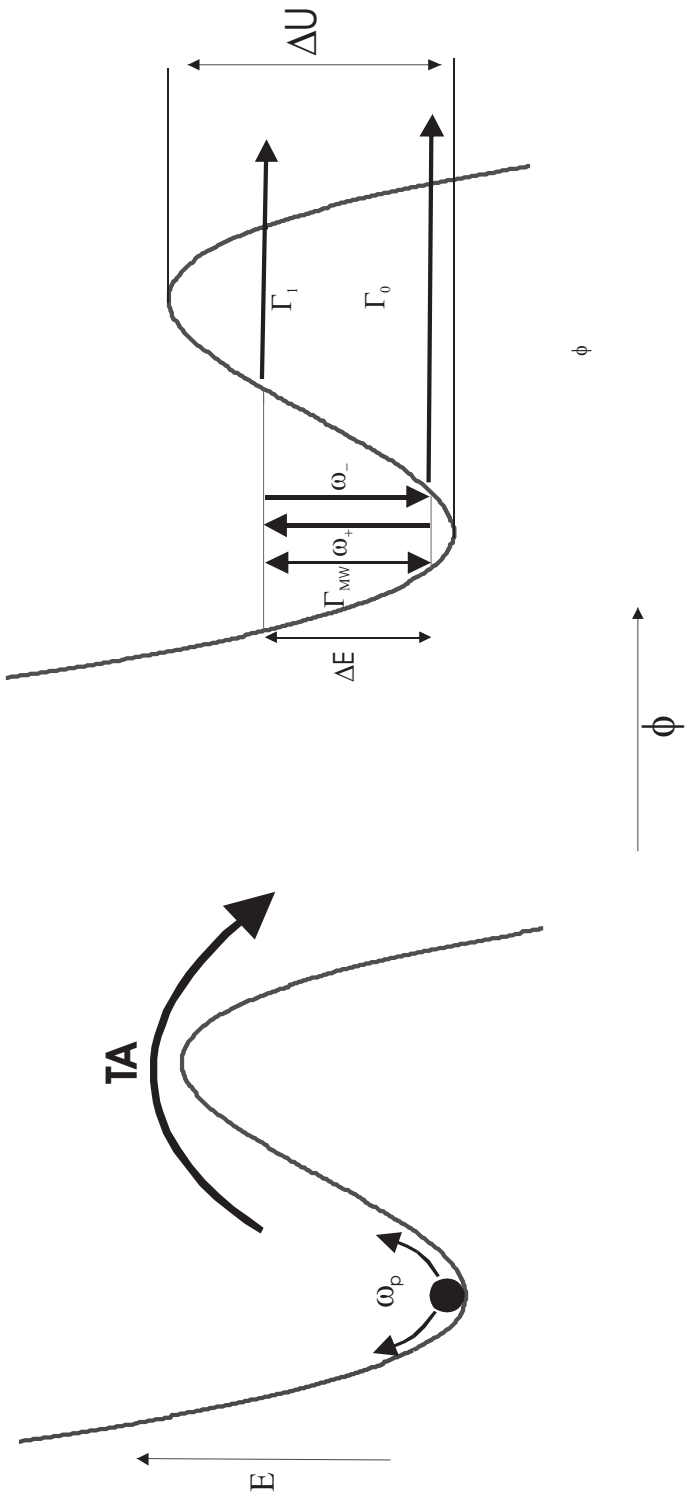

Figure 7.3: A "bumpy slope" which is the archetypical shape of a potential suitable for MQT-experiments [23]. The potential of Josephson junction closely reassembles this shape. In the well there are a number of meta-stable states which can escape to the continuum via either thermal activation *over* the barrier or via tunnelling *through* the barrier, which mechanism that dominates depends on the temperature. At high temperatures the system can be modelled as a classical particle which undergoes plasma oscillations at the bottom of the well. At low temperatures where macroscopic quantum tunnelling dominates the escape a number of discrete levels are present in the well, by applying microwave radiation is it possible to pump the system between these states.

seen as a change of slope in a plot of the width of the histogram vs. temperature as the α becomes larger. Essentially, for $\alpha < 2$ the well nearly has the shape given by eq. 7.5 for values of γ close to 1 which is what is relevant for a switching current experiment.

7.3 Modelling Using a Master Equation

Experimentally we gain information about the quantum dynamics of a junction or SQUID by measuring the voltage over the device. In a switching current measurement, we measure the value of the bias current at which the junction switches into the running state; it can be detected by the sudden appearance of a finite voltage.
As will be shown in section 7.7 we are primarily interested in statistical properties such as the escape rate Γ. An approach originally developed by Larkin and Ovchinnikov [63] makes it possible to calculate Γ taking into account both thermal interlevel transitions as well as the effect of transitions induced by external microwave irradiation.
Central to the Larkin and Ovchinnikov theory is a Master equation

$$\frac{\partial \rho_j(t)}{\partial t} = \sum_{k=0}^{n} [\omega_{k\to j}\rho_k(t) - \omega_{j\to k}\rho_j(t) - \Gamma_j \rho_j(t)] \tag{7.9}$$

which takes into account all transition rates and tells us how the system evolves in time. Here $\rho_j(t)$ is the probability of finding the system in the jth level at time t, $\omega_{k\to j}$ is the total transition rate from level k to level j and Γ_j is the tunnelling rate through the barrier from level j. The probability of finding the system in the superconducting state at time t is therefore

$$\rho(t) = \sum_j \rho_j(t) \tag{7.10}$$

Usually we are only interested in steady-state solutions of 7.9 and once such a solution has been reached we can calculate the *total* escape rate from the system -which is what me measure experimentally- by summing over the probability of finding the junction in level j multiplied by Γ_j

$$\Gamma = \sum_j \Gamma_j \rho_j \tag{7.11}$$

In order to solve these equations we will need expressions for all rates, both interlevel transitions and escape rates from the quantum well.

7.3.1 Interlevel transition rates

It can be shown[64] that if a well weakly coupled to an environment is modelled as discrete levels coupled to a broad continuum; the probability density of the discrete state $|\varphi>$ can be written

$$\frac{dN_\varphi}{dE} = \frac{\hbar\Gamma/2\pi}{(\frac{\hbar\Gamma}{2})^2 + (E - E_0)^2} \tag{7.12}$$

which is a Lorentzian curve centered at E_0 of width $\hbar\Gamma$ where Γ is the sum of the transition rates in and out of the level.

We can use Fermi's Golden rule [65] to calculate the thermal transition rate $j \rightarrow k$ [60]

$$\omega^t_{j\rightarrow k} = \frac{\Delta E}{2R^2} \frac{| < j|\phi|k > |^2}{e^{\Delta E/k_B T} - 1} \tag{7.13}$$

which gives the transition rate from level j to any level k with $E(k) > E(j)$. From detailed balancing we immediately get the rate in the opposite direction $k \rightarrow j$

$$\omega^t_{k\rightarrow j} = \omega^t_{j\rightarrow k} e^{\Delta E/k_B T} \tag{7.14}$$

A useful approximation for the two lowest transitions in the system is [66]

$$\omega^t_{0\rightarrow 1} = \frac{1}{RC(e^{\Delta E/k_B T} - 1)} \tag{7.15}$$

$$\omega^t_{1\rightarrow 0} = \frac{1}{RC(1 - e^{\Delta E/k_B T})} \tag{7.16}$$

which explicitly show the dependence of the rates on the RC time constant of the junction [3]. Looking at these expressions we see that the rates depend on the dissipation resistance, the energy difference, the overlap integral of the wavefunctions and the temperature. Using these results as well as eq. 7.12 we can now understand the importance of the dissipation resistance. A low value for R means that the interlevel transition rates are high and that the levels become wide, if R is too low the levels will start to overlap.
When the junction is irradiated by microwaves transitions $k \rightarrow j$ or $j \rightarrow k$ -corresponding to the absorbtion or emission of a photon - can be induced if the frequency corresponds to the difference in energy between the levels $\hbar\omega_\mu = E_k - E_j$. This occurs at a rate [67]

$$\Gamma^{MW}_{j\rightarrow k} = \Gamma^{MW}_{k\rightarrow j} = \frac{I^2_\mu}{16e^2} | < j|\phi|k > |^2 \cdot \frac{\chi_{jk}}{(\omega_\mu - \Delta E/\hbar)^2 + \chi^2_{jk}/4} \tag{7.17}$$

where

$$\chi_{jk} = \sum_i \omega^t_{j\rightarrow i} + \sum_i \omega^t_{k\rightarrow i} + \Gamma_j + \Gamma_k \tag{7.18}$$

is the sum of the transition rates in and out of the levels. Note that the Lorentzian shape of the levels is explicitly taken into account in this expression, i.e. the levels are not infinitely sharp but have a width $\hbar\chi$ just as in eq. 7.12.

7.3.2 Calculation of escape rates

There are two ways for the junction to switch into the running state. As was mentioned in section 3.6 the escape rate in the thermal regime can be written

$$\Gamma^{TA} = a_t \frac{\omega_p}{2\pi} \exp\left[-\frac{\Delta U}{k_B T}\right] \tag{7.19}$$

Strictly speaking this is just the limiting case of a more general theory[68]. However, for the range of parameters usually found in experiments eq. 7.19 is a very good approximation.

[3] Note that $R = Re(Z)$ is the *effective* dissipation resistance that the junction sees, not the resistance of the junction itself

The second case is quantum escape which dominates in the MQT-regime. For levels sufficiently deep inside the well we can use the WKB formula for the tunnelling rate

$$\Gamma_j = \frac{\omega_p}{2\pi} \exp\left[-\frac{2S_j(E)}{\hbar}\right] \tag{7.20}$$

Where S_j is the Euclidian action functional which in the 1D case can be written [58]

$$S(E) = \int_{q3}^{q2} dq\sqrt{2m[E - U(q)]} \tag{7.21}$$

where $q3$ and $q2$ are the classical turning points at energy E, i.e. the roots to $V(q) = E$ such that $0 < q3 < q2$. Note that while this is still an approximation -the result of a "naive" application of the WKB-approach[23]- it is good enough for practical applications (i.e. comparison with experiments). Note also the similarities between eqs. 7.19 and 7.20; in both formulas there is a pre-factor $\sim \omega_p$ of the junction multiplied by an exponential function which is related to the height of the barrier. This is of course not surprising since there is no clear "limit" where eq. 7.20 is no longer valid; ideally 7.20 will smoothly merge with eq. 7.19 at a temperature $\sim T^*$.
Eq. 7.21 is not valid for levels near the top of the well. Instead the following expression can be used[58]

$$y \ln\left[6q0\frac{\sqrt{2m\hbar\omega_p}}{\hbar}\right] - \frac{\pi}{2}x - \ln(\sqrt{2\pi}) + \mathbf{Re}\left[\ln\Gamma\left[\frac{1}{2} - \frac{y}{2} - ix\right]\right] = 0 \tag{7.22}$$

where $y = \Gamma_j/\omega_p$, Γ is the gamma function and

$$x = \frac{E - U_0}{\hbar\omega_p} \tag{7.23}$$

The solution should merge smoothly with eq. 7.20 at an energy $U_0 - 0.5\hbar\omega_p$.

7.4 Resonant Activation

The term resonant activation refers to experiments where a "premature" switching event is induced by irradiating the junction with microwaves. From eqs. 7.9 and 7.17 we see that the effect of the microwaves is to "pump" states between levels which will tend to enhance the population [4] of the excited states. In theory this can lead to almost a 50%-50% distribution of the population of $|0>$ and $|1>$ if the radiation is resonant with the level splitting $E_1 - E_0$ and the power is high enough. Note that although the rates up and down are always equal (the junction is equally likely to absorb and emit a photon) the net effect of the microwaves is to increase the population of the excited states since the probability of an interlevel transition is proportional to the population of the starting level; and at low enough temperatures $\rho_0 = 1$ before the microwaves are turned on.
Hence, in order to explain the effect of the microwaves we can imagine the following scenario at low temperatures[5]: At times $t < 0$ the probability ρ_0 of finding the system in the ground state $|0>$ is 1. At a time $t = 0$ the microwave radiation is turned on which causes the interlevel transition rates to be changed according to 7.17. Assuming the radiation is resonant with the transition $|0> \rightarrow |1>$, the

[4]The word "population" is here often used instead of "probability", the reason is simply that since we are mainly interested in statistical properties of the system the former is more convenient to use.

[5]by "low" we here mean temperatures such that the thermal rates up are negligible

state of the system is pumped into level $|1>$ where the probability of escaping from the well is exponentially higher compared to what it was in the ground state. During the time $0 < t < t_1$ the system evolves according to eq. 7.9. Schematically some of the possible transitions in this two-level scenario are

$$|0> \overset{\omega_+^t}{\longrightarrow} |1> \overset{\Gamma_1}{\longrightarrow} \mathbf{continuum} \tag{7.24}$$

$$|0> \overset{\Gamma_{mw}}{\longrightarrow} |1> \overset{\Gamma_1}{\longrightarrow} \mathbf{continuum} \tag{7.25}$$

$$|0> \overset{\omega_+^t}{\longrightarrow} |1> \overset{\omega_-^t}{\longrightarrow} |0> \tag{7.26}$$

$$|0> \overset{\omega_+^t}{\longrightarrow} |1> \overset{\Gamma_{mw}}{\longrightarrow} |0> \tag{7.27}$$

$$|0> \overset{\Gamma_{mw}}{\longrightarrow} |1> \overset{\Gamma_{mw}}{\longrightarrow} |0> \tag{7.28}$$

These processes are shown schematically in figure 7.3. For $t > t_1$ the system has presumably reached a steady-state where the long-time averaged probability of finding the system in a certain level does not change. As will be seen in the next section the resulting escape rate of the system has a value $\Gamma_0 < \Gamma < \Gamma_1$. Since Γ_1 is about two order of magnitude larger than Γ_0 the system will mainly escape from state $|1>$ even though the probability of finding the system there at any given time is small, from simulations we know that the escape from $|1>$ will dominate if ρ_1 is about 1%.
Whence, the microwave power needed to induce a significant change in the population is small. From numerical calculations we know that a microwave current of the order of $0.001 I_{c0}$ should be enough to observe a resonance.
Experimentally the resonant condition can be seen as a sudden drop in the measured I_c. When the current is ramped up the junction will reach a current $I_r < I_c$ where the radiation is resonant, $|1>$ will be populated and since $\Gamma_1 \gg \Gamma_0$ the junction escapes "prematurely". By tuning the microwave power it is actually possible to have a situation where *two* critical currents are observed, this corresponds to the condition $\rho_0\Gamma_0 = \rho_1\Gamma_1$.
Hence, even in a two-level system the dynamics are very complicated. Generally speaking any number of levels can be involved. At high temperatures the system will have a non-negligible population of all levels, meaning it will always escape from excited states. Moreover, since the difference in energy level splitting is small, one often also has a situation where the radiation is resonant with two (or more) transitions at once. This happens because of the finite width of the energy levels; transitions are possible for a continuous range of energies $\hbar\omega$ and not just for a single frequency. The system can therefore be pumped to high levels by absorbing several photons in a "ladder-process" of the type $|k> \rightarrow |k+1> \rightarrow |k+2>$ etc. Furthermore, it is also possible for the radiation to be resonant with a process of the type $|k> \rightarrow |k+2>$, i.e $\hbar\omega = E_{k+2} - E_k$; but usually the probability for this process is small.
The most obvious way of performing this type of experiment -to sweep the frequency and observe the histogram- does not work very well. The reason is that in any real experiment the coupling strength between the Josephson junction and the microwave generator is strongly frequency dependent; hence changing the frequency also means changing the power. Instead we keep the frequency fixed and sweep the microwave *power*.
What happens as we increase the power depends on the selected frequency

- If the frequency corresponds to a resonance close to I_c we will almost immediately see a decrease of the current and a broadening of the histogram as the excited levels start to become populated. Eventually all escape will be from an excited state and the histogram becomes narrow again. This is the regime used to to determine quality factor of the system.

- If the chosen frequency corresponds to a resonance current $I_r$further away from I_c, the resonance will not be visible in the measurement since the escape rate Γ at I_r is too low. However, if we continue to increase the power we will start to effectively *suppress* the effective height of the barrier[69]. This will increase Γ at I_r and eventually the resonance becomes visible. As long as the power is not too high this process will not change the level splitting, meaning the value of I_r is not affected

- At even higher powers a number of higher-order processes will start to occur. The barrier is suppressed even further and higher excited states will become populated leading to further reduction of I_c. It is also possible to observe resonances that correspond to *fractional* values, m/n, of $\hbar\omega_p$. This is probably due to many-photon absorbtion processes of the type $E_j + n\hbar\omega \rightarrow E_{j+m}$. One example would be a 3-photon absorbtion leading to a transition from the ground state $|0>$ to the second excited state $|2>$. Since the levels are nearly equidistant this will be seen as a 3/2-photon resonance.

By repeating many sweeps and recording at which current we hit the resonance condition we can still map out the frequency dependence. One caveat is that if high powers are used we are not probing the unperturbed system. For measurements of the Q-value of the system it is therefore important to choose resonances that appear very close to the unperturbed I_c.

7.5 Numerical Calculations

By combining all the theory outlined so far it is possible to quite accurately model the dynamics of a Josephson junction in the quantum regime. By using numerical methods one can also use an arbitrary shape of the junction potential which is especially useful when working with HTS devices.

7.5.1 Numerical method

In order to solve the problem we note that if n levels are to be included in the calculation eq. 7.9 can be written as

$$A\dot{\rho} = 0 \tag{7.29}$$

where A is a $n \times n$ matrix with elements A_{jk} which couple levels j and k. In general we are interested in finding the escape rate of the junction as a function of applied bias current. In order to generate such a plot with m points we therefore go through the following steps m times

I. Solve eq. 7.4 to find the position of the levels and the eigenvectors.

II. Calculate the classical plasma frequency of the well

III. For each level solve eq. 7.21 or eq. 7.22 to find the escape rates Γ_j.

IV. Use eq. 7.12, 7.13 and 7.17 to calculate the interlevel transition rates resulting from thermal effects and microwave induced transitions.

V. Use the calculated values for Γ_j and the interlevel rates to construct A.

VI. Solve eq. 7.29. After normalization this gives us the population of each level.

VII. Calculate the total escape rate from the well Γ using eq. 7.11.

Unfortunately this is a pretty slow process. Mainly because we need to solve the eigenvalue problem 7.4 for each value of the bias current which takes a significant amount of time for typical grid sizes ($\sim$5000 grid points). Usually it is enough to include 5-10 levels in the problem (depending on temperature and microwave power) but it can still take several hours to solve.
I should point out that two effects that occur when the levels are very close to the top of the well have been neglected in my simulations. Firstly, the possibility of transitions to the resonance level (a level which is permanently positioned just at the top of the well) and secondly, the enhancement of the thermal interlevel transition rate which occur because the lifetime is so short that two levels become broad enough to almost overlap. These two effects are generally not important for low lying levels and can therefore be neglected.
As has already been mentioned the methods outlined here can also be used to study the effects of an unconventional CPR, dynamics of SQUIDs etc; making this technique much more versatile than the usual analytical formulas.

7.5.2 Numerical results

Figure 7.4 shows a typical result of the calculations. The solution can be interpreted with the help of the "levels" that can be seen as dashed lines in figure 7.4. Each line correspond to the escape rate Γ_j from level j in the well. The interlevel dynamics will transfer probability between these "levels" resulting in an escape rate lying in between the Γ_j lines. A Γ_J line end when the corresponding level can no longer fit in the well and drops out.
The effects of the microwave radiation can be seen as a "hump" in the escape rate at the resonance current where $\hbar\omega = \Delta E = E_{k+1} - E_k$. Note that this "hump" can appear at a current I_r where even the enhanced Γ is lower than the escape rate closer to I_{c0}. Hence, in an experiment the resonance would not be visible because the junction will still escape at a current $I_c > I_r$. Moreover, since the microwave induced transition rate is related both to the overlap of the states and the lifetime of the levels the exact shape of the "hump" will depend on where in current it occurs.
The range of microwave currents used in this simulation is 0.5-5 nA, i.e. less than 0.1% of $Ic0$ and still the effect is rather dramatic. It is also obvious from figure 7.4 that multi-level dynamics plays a large role even at relatively moderate powers. Despite the fact that $\Gamma < \Gamma_1$ for all powers a "dent" in the curve is clearly visible when the third level (Γ_2) drops out of the well.
The effect on Γ from levels dropping out of the well are slightly exaggerated in this calculation. In reality levels that are about to drop out become very wide due to their short lifetime meaning this effect is often "washed out" . However. the effect can be seen experimentally if the highest levels are thermally populated, see e.g. [58].
At zero temperature and no microwave radiation Γ will just coincide with Γ_0 but as the temperature is increased the higher levels will also be populated (see figure 7.5). As long as the levels are discrete the population is nearly Boltzmann distributed; but at higher temperatures the levels become broad due to the increase in the thermal interlevel transition rate. The overlap increases resulting in an enhanced population of the excited levels. This results in a population which is not Boltzmann distributed.

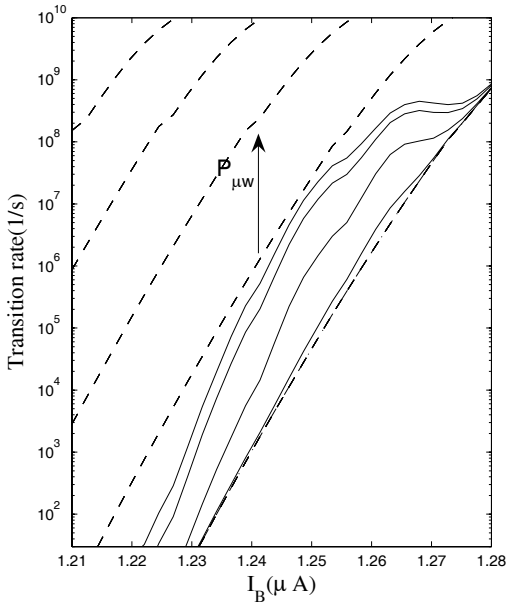

Figure 7.4: Numerically calculated escape rate under 4.5 GHz microwave radiation at 15 mK for increasing microwave power $P_{\mu w}$. The junction parameters are $I_{c0} = 1.3$ μA, C=1.6 pF and Q=40. The curves corresponds to microwave currents of 0, 0.5 nA, 2 nA, 4 nA and 5 nA, respectively. The dashed lines represent the escape rates from the first five levels.

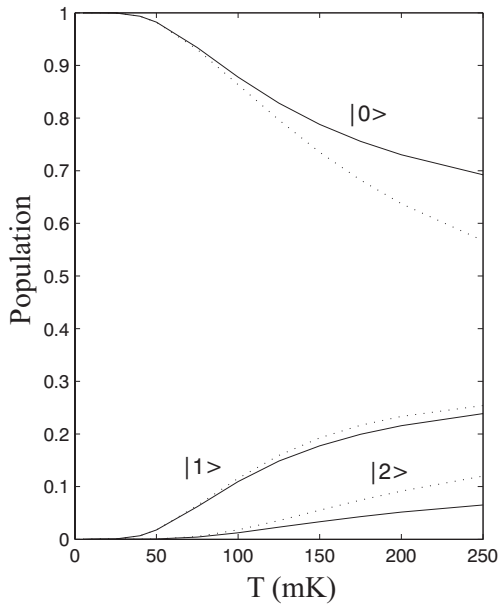

Figure 7.5: At low temperatures where the levels are truly discrete, the population follows a Boltzmann distribution. Here the population has been plotted for $\gamma = 0.93$. The parameters of the junction are the same as in 7.4. The plot shows the population of the ground state and the first two excited states. *Solid line:* Solution of the Master equation. *Dotted Line:* Boltzmann distribution.

7.6 Multi-Photon Transitions

Multi-photon transitions between levels in a Josephson junction have previously been studied in Nb junctions [59]. However, many aspects are still poorly understood. To the best of my knowledge no theory has been developed that can be used to calculate the transition probability between two levels due to a multi-photon absorbtion process.
Formally the process considered can be written as

$$E_j + n\hbar\omega = E_{j+1} \tag{7.30}$$

where E_j and E_{j+1} are the energies of two adjacent levels. It is generally assumed that the probability for a n-photon process can be written

$$P_{j\to k} = \frac{\sigma_n}{n} I^n \tag{7.31}$$

where I is the intensity and σ_n is the cross-section of the process. Hence, the probability for a multi-photon even increases sharply with intensity. Lets consider the example of laser spectroscopy of molecules. Here the cross-section of a two-photon process at typical power levels is often 20 orders of magnitude lower than that of a single photon process(the probability increases dramatically if there are one or more real levels in between, e.g. $E_j \to E_{j+2}$ but that is not considered here); even with extremely high powers, 3- and more photon events are rare.
Hence, at first sight is seems the probability of seeing, e.g., a 10 photon transition in a Josephson junction would be very remote. There are, however, two effects that can increase the probability significantly. First of all the Josephson junction is an extremely anharmonic system and results obtained using e.g. a harmonic approximation (i.e. modelling the junction as a harmonic well) has only limited applicability. (multi-photon transitions between two adjacent levels are in fact explicitly forbidden in an harmonic well). Secondly, at high powers the absorbtion/emission of photons become a highly non-linear process, meaning results obtained by first order perturbation theory are no longer valid [6].
Attempts have been made to develop a more general theory. In [69] the case of a strongly driven junction is considered using perturbation theory, it is shown that in the limit

$$\left(\frac{\omega}{\omega_p}\right)^5 \geq \frac{\hbar\omega_p}{E_J} \tag{7.32}$$

the presence of microwaves leads to an effective suppression of the potential barrier. However, this theory is still only valid for single-photon processes.

7.6.1 An outline of a theory of multi-photon transitions in Josephson junctions

In atomic physics multi-photon transitions in tunable non-linear systems have been experimentally studied using Rydberg atoms[70]. The theory for atoms is well developed and can be used to explain the dynamics of very complex systems. This theory has never been applied to Josephson junctions but the arguments are very general and should hold regardless of the exact shape of the potential. Furthermore using the same arguments as in the case of Rydberg atoms we might be able to get a qualitative (and possible a quantitative) understanding for why we do see e.g. 10 photon transitions

[6] It is interesting to note that in most earlier works, see [2], the experiments were explicitly designed to be in the low-power, approximately linear, regime

in Josephson junctions. I would like to emphasis that this is a hypothesis, more work is needed before one can say if this approach is valid or not. In essence the idea is to use systems like the Rydberg atom as an analogue to a Josephson junction assuming that the only difference from a modelling point of view is the shape of the potential.
If the power of the microwave radiation is so high that it can no longer be treated as a small perturbation, the states of the system are modified and are no longer stationary. The addition of the microwaves causes the total potential to become time dependent $U + U_{MW}\cos\omega t$. This modulates the energy of the wavefunction, breaking it into a carrier and sidebands. Presumably the new wavefunctions can be expressed as a Fourier series of the form

$$\Psi(\mathbf{r},t) = e^{-iWt}\Psi(\mathbf{r})\sum_m J_m\left(\frac{\eta}{2e\omega}\right)e^{-im\omega} \tag{7.33}$$

where $J_m(x)$ is the *m*th order Bessel function and η is the microwave current. [7] The physical interpretation of this is that the appearance of the side-bands in between the unperturbed states causes a "ladder-effect"; the junction can effectively "climb" from state $|j>$ to $|k>$ by successive absorbtion of n photons, each with energy E_{jk}/n. The final result of this approach is a Hamiltonian periodic in time

$$H(t+T) = H(t) \tag{7.34}$$

where $T = 2\pi/\omega$. A general non-perturbative approach known as Floquet theory [72] can be used to reduce this to a time-independent *quasi*energy eigenvalue problem; the solution of which can be used to calculate the long-time average probability of the transition.
Whether or not this is a valid approach and if it can be used to explain the large probabilities of n-photon transitions in Josephson junctions remains to be seen. However, I believe that at least part of the answer lies in the non-harmonicity of the potential coupled to non-linear effects of high powers. Using Floquet theory it should be possible to use efficient numerical methods to solve the problem even for a large number of photons.

7.7 Methods for Analyzing Switching Current Experiments

The output of a switching-current experiment is typically a record of e.g. 20 000 values of the current. In the analysis of the data we consider this to be an ensemble and use statistical tools to extract information.
The most convenient way to analyze the data is to plot it as a histogram showing the number of counts as a function of the critical current. Once we have the histogram we can also calculate the escape rate

$$\Gamma(I) = \frac{1}{\Delta I}\frac{dI}{dt}\ln\left[\frac{\sum_{i>I}P(i)}{\sum_{i>I+\Delta I}P(i)}\right] \tag{7.35}$$

where dI/dt is the current ramp rate, ΔI the bin-width and $P(i)$ is the number of counts of current i. Figure 7.6 shows a typical example of data from a switching current experiment.
The probability that a junction switches at a current I can be written[73]

$$P(I) = \left(\frac{dI}{dt}\right)^{-1}\Gamma(I)\exp\left(-\int_0^I\Gamma(I')\left[\frac{dI}{dt}\right]^{-1}dI'\right) \tag{7.36}$$

[7] This argument has also been used to explain photon-assisted tunnelling in Josephson junctions [71], Ψ is then the BCS-wavefunction.

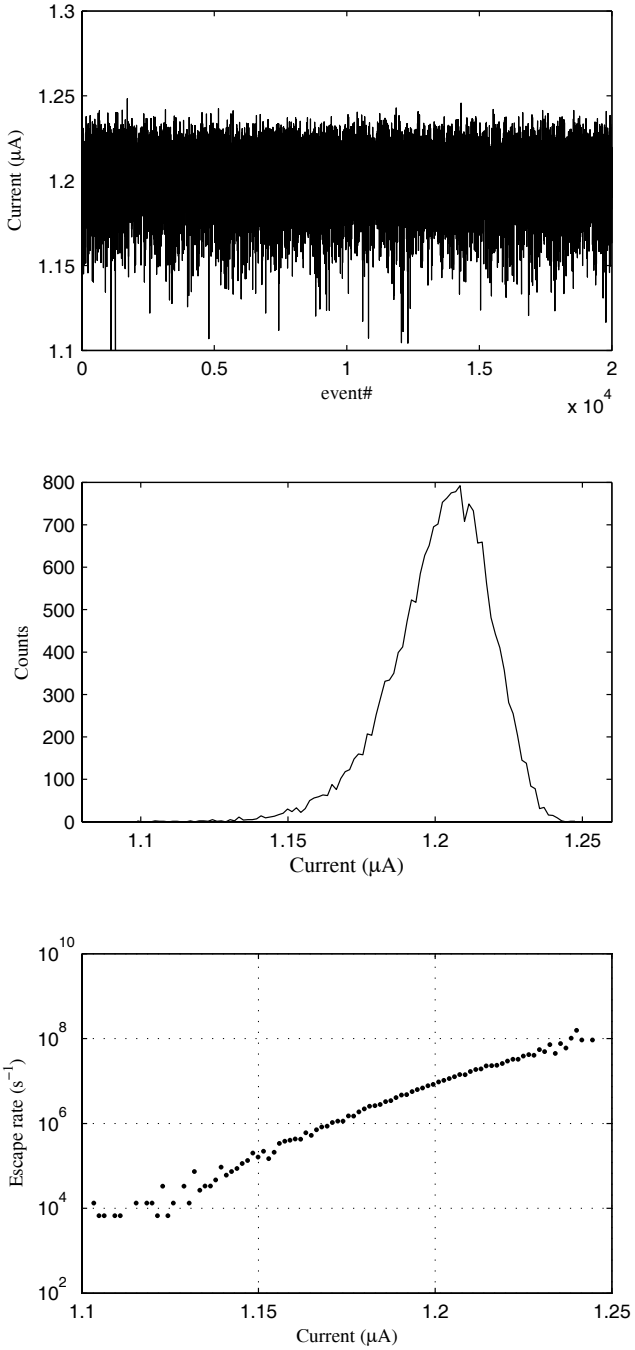

Figure 7.6: An example of how the data analysis of a switching current experiment is done. If the data are plotted as it is(*top*) it just look like noise. However, when the same data is plotted in the form of a histogram (*middle*) a well defined shape which is determined by junction parameters and the escape temperature can be seen. Using eq. 7.35 the data can also be plotted in terms of escape rate. In this example, which is the result of a simulation, T=300mK and I_{c0}=1.30 μA.

.

This expression can be used to calculate the theoretical shape of a histogram given an expression of Γ.
The ramp rate dI/dt in eqs. 7.35 and 7.36 does not change the *value* of $\Gamma(I)$. It does,however, affect the *range* of Γ-values we are sampling. The reason is that there is always a finite probability for the junction to switch. If we are ramping up the current slowly the junction is likely to switch at a low current, at high ramp rate the junction is more likely to switch at a current close to I_{c0}. Hence, we can "move" the switching current histogram up and down along the current axis by changing the ramp rate. In order to sample values very close to I_{c0} we need to use high ramp rates. Note that if the rate is too high we will start to induce non-equilibrium effects in the junction and the theory outlined here is no longer valid. The advantage of representing the data as a plot of Γ is therefore that there is no direct dependence of experimental parameters such as sweep rate (despite the factor dI/dt) making a comparison with theoretical predictions easier.

7.7.1 Determination of T_{esc} and I_{c0}

The conventional way of measuring the effective escape temperature T_{esc} and the noiseless critical current is to fit the data to the expression for the thermal escape

$$\left(\ln\frac{\omega_p(I)}{2\pi\Gamma_{meas}(I)}\right)^{2/3} = \left(\frac{E_j 4\sqrt{2}}{k_B T_{esc}}\right)^{2/3}\frac{I}{I_{c0}}(I_{c0}-I) \tag{7.37}$$

which works well for tunnel junctions where the potential can be approximated by eq. 7.5. In many cases it is however better to directly fit the data to the histogram using eq. 7.36 since one is then able to choose an arbitrary form of the potential.
From a physical point of view there is no difference between thermal- and electrical noise as long as the latter is reasonably white. If there is additional noise in the system due to e.g insufficient filtering of the bias leads one would therefore expect $T_{esc} > T_{bath}$ in the thermal regime. The presence of noise can also have the same effect as MQT, i.e. a "flat" dependence on the bath temperature below a certain temperature; it is therefore important to check that one is indeed in the MQT-regime and is not limited by the noise of the system. The simplest way to check this is to reduce the critical current of the device by applying a magnetic field and verify that the crossover temperature is reduced.

7.7.2 Determination of the Q-value

The quality factor (Q-value) of the system can be directly determined using microwave spectroscopy without any *a priori* assumptions or models of the system.
As the microwave power is increased the Γ-curves are shifted upwards (meaning the escape rate increases) and a "bump" appears which is approximately centered around the value of the current which corresponds to a level splitting equal to the microwave frequency $\hbar\omega$. An example can be seen in figure 7.7.
The microwave *enhancement* is defined as

$$\frac{\Gamma(P)-\Gamma(0)}{\Gamma(0)} \tag{7.38}$$

where $\Gamma(P)$ is the escape rate with- and $\Gamma(0)$ the rate without microwaves. Similar to the shape of the levels given by eq. 7.12 the enhancement has a Lorentizan shape as can be seen in figure 7.13.

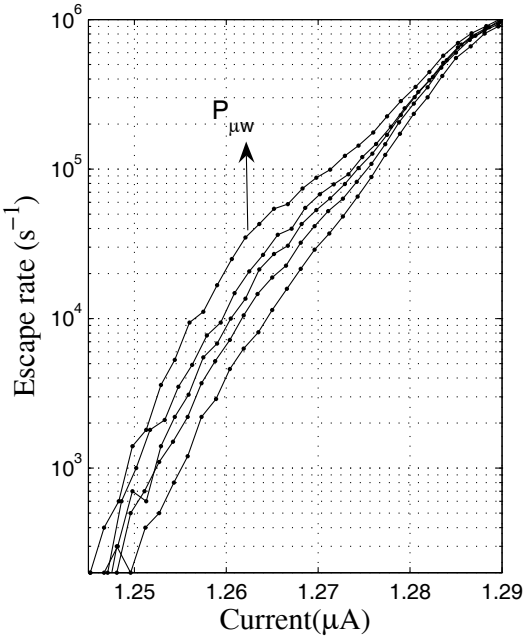

Figure 7.7: The escape rate at 15 mK showing the effect of increasing microwave powers. The applied power varies from -20 dBm to -14 dBm.

The Q-value can then be determined by the usual formula

$$Q = \frac{f}{\Delta f} \tag{7.39}$$

where Δf is the full width at half maximum of the enhancement peak. In order the use this equation we somehow need to convert current into frequency. In the low power regime this can be done by measuring the resonance currents of two nearby frequencies and then interpolating between those values.

Note that in order to use this procedure two conditions need to be fulfilled: First of all the resonance current needs to be close to I_{c0} since eq. 7.38 can only be used if $\Gamma(P)$ and $\Gamma(0)$ are in the same current range (experimentally this means that the resonance peak should appear "inside" the unperturbed histogram). [8] Secondly, the applied microwave power should be so small that the dissipation in the junction is still dominated by intrinsic sources and not by microwave induced effects, otherwise the level lifetime will decrease resulting in a lower Q-value.

[8] In principle the same procedure can be used even if the microwave radiation has already suppressed the critical current somewhat before the appearance of the histogram, it is however not straightforward to interpret the result since the very fact that the current has decreased means that it is not the properties of the unperturbed system which are probed. However, presumably the resulting Q-value will never be higher than for the unperturbed system. In the data presented we here we made sure that I_c was *not* affected by the microwaves when the Q-value was determined.

7.8 Experimental Results

Experimental results on resonant activation in HTS Josephson junctions will be presented in this section. Some experimental data from Nb junction similar to what has been obtained earlier (see ref [2] and [59]) will also be shown. The reason for showing these data is that they serve as a good reference since the properties of Nb junctions are quite well understood and -with the exception of multi-photon transitions- experiment and theory agrees quite well. Moreover, our measurements on Nb junctions have also been a good way to test equipment and experimental procedures.

All the measurements presented here were done using the same biepitaxial junction which was selected after measuring several samples. The first step was to characterize the junction and confirm that a transition into the MQT-regime could be observed. The junction had a critical current of 1.3 μA, a normal resistance of $R_N = 500\ \Omega$ and the capacitance was 1.6 pF. Using conventional theory this would give a plasma frequency ω_0 of 7.9 GHz but as we will see in the next section that turns out *not* to be correct. The temperature dependence of the width of the histogram can be seen in figure 7.8. The junction enters the MQT regime at $T^* \approx 30 - 40$ mK. Note the change of slope as the 2^{nd} harmonic component starts to increase. This effectively suppresses the barrier. From these measurements we expect $\alpha \approx 0.7$ which is too low to qualitatively change the dynamics of the junction.

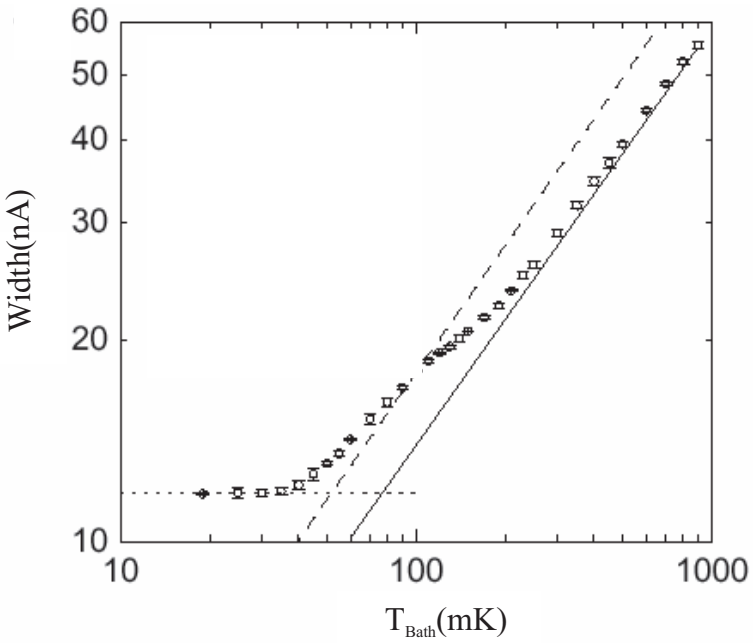

Figure 7.8: Width of the current distribution as a function of temperature for the sample used in our experiments, clearly showing the transitions into the MQT-regime at $T^* \approx 30$ mK.

7.8.1 Experimental demonstration of resonant activation in a HTS junction

Figure 7.8.1 is a plot showing how the histogram evolves as the microwave power is increased [9]. The behavior follows essentially the scenario outlined in section 7.4. At low power the histogram does not change but as the power is increased there is a small decrease in critical current which eventually drives the system into resonance with the applied frequency resulting in a sudden suppression of I_c. In figure 7.8.1 we see this happening at a microwave power of around -20 dBm [10]. The frequency is 850 MHz which corresponds to a 3-photon transition.

Figure 7.10 shows four of the histograms in more detail. Note how the shape of the histogram changes and becomes broader as the power is increased. This is due to more and more of the escape events taking place from the first excised state. At -14 dBm the induced microwave current is so high that escape from the first excited state totally dominates. Note that in this case the resonance current is so close to I_{c0} that the two histograms overlap.

Generally it is somewhat difficult to interpret data of this type. After the resonance condition is met the current can be suppressed even further if the power is increased. This is in part due to the finite width of the resonance which at high power increases the escape rate in the left "tail" of the resonance peak to a point where the junction can switch at currents much smaller than I_r. At even higher powers non-perturbative effects come into play which can not be described by the simple model outlined above.

7.8.2 Mapping of the interlevel spacing

By making many power-sweep plots it is possible to map out the resonance current as a function of applied frequency in plots similar to figure 7.2. Two such plots are shown in figure 7.11 and 7.12.

Figure 7.11 show data from one of our test samples: A standard tri-layer Nb junction fabricated on silicon with a critical current of 21.65 μA and a capacitance 1.6 pF. The plot for the Nb-junction shows the expected behavior for the single- as well as the multi-photon resonances: The dependence follows that of the plasma frequency of the junction since the level splitting is approximately $\hbar\omega_p$ However, looking at figure 7.12 we see that the HTS junction has a much "flatter" -more harmonic- dependence than the NB junction. This was the first indication that the dynamics of the HTS jnction is different from that of the Nb junction, I will return to this in section 7.9

Note that only the 2- and 3-photon resonances are visible in figure 7.12. We were not able to observe a single photon resonance in the experiments on the HTS junction. There could be several reasons for this. One obvious difficulty when performing microwave experiments on samples made on substrates with high dielectric constants is that it is often the case that one can not couple radiation into the junction at certain frequencies. However, that can not be the whole explanation since we were able to observe Shapiro steps up to frequencies of about 10 GHz (albeit at power levels much higher than the ones used to induce the resonances). One explanation could be that the power levels that would have been needed to induce a single photon resonance (which should appear at frequencies around 2.7 GHz) were also high enough to locally heat up the sample, this would have completely smear out the levels making it impossible to observe any clear resonance.

[9] Note that the power is given in logarithmic units, 1 dBm=1 mW

[10] Note that these values refer to the power sent out from the microwave source, only an extremely small part of that power actually reaches the sample.

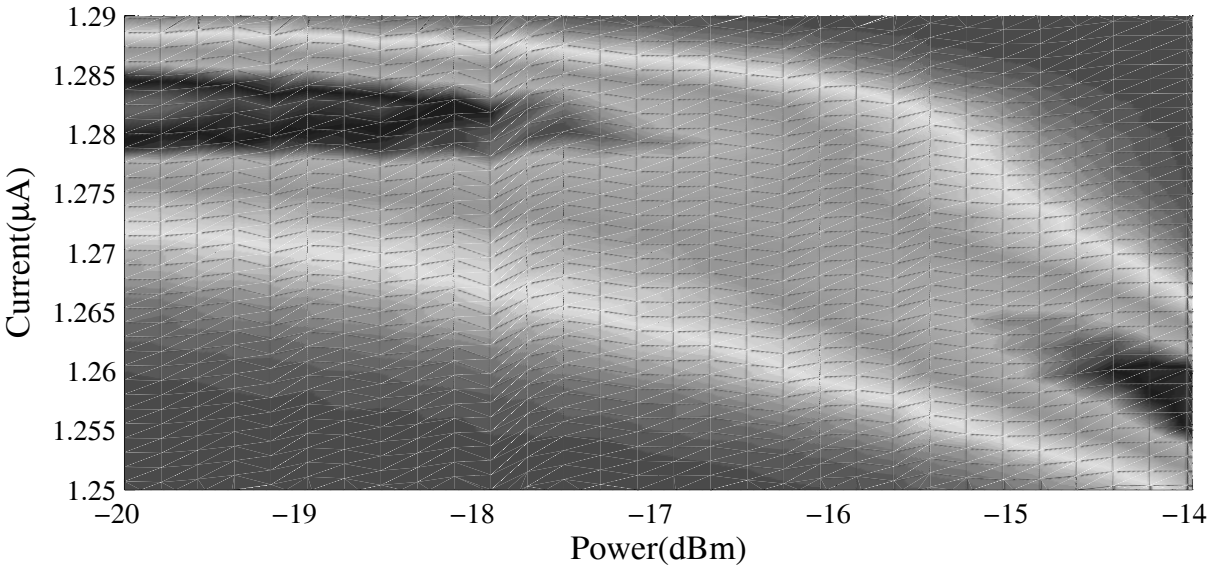

Figure 7.9: The current distribution as a function of applied microwave power at 15 mK. The microwave frequency is 850 MHz corresponding to a 3-photon transition..

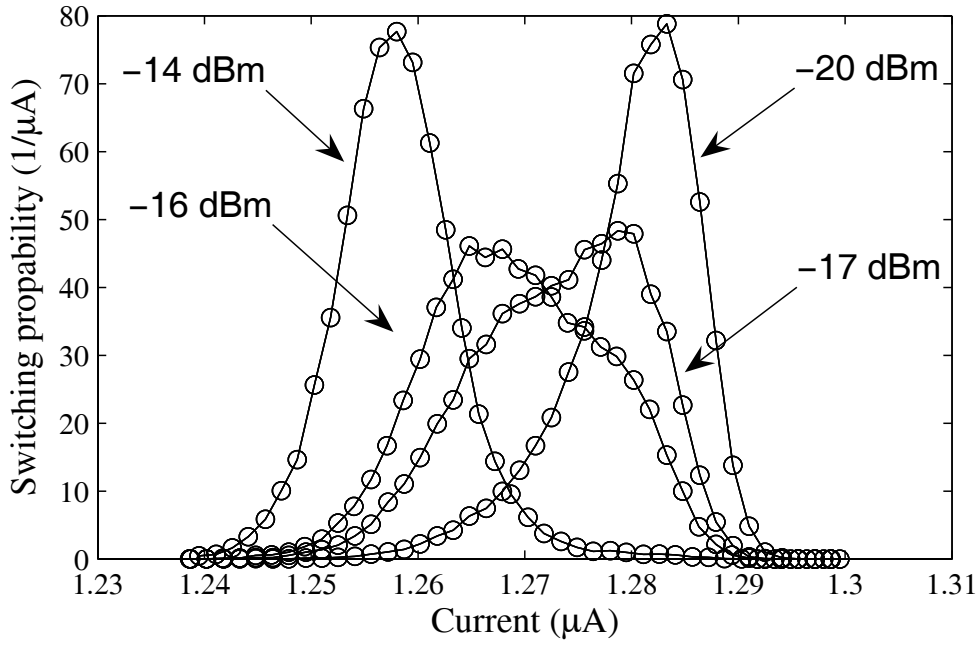

Figure 7.10: The evolution of the histogram as under the power is changed from -20 dBm to -14 dBm at 15 mK. Here is is easy to see how the unperturbed histogram gradually changes as the power is increased . The microwave frequency is 850 MHz. Note that this is the same data as is shown in figure 7.8.1.

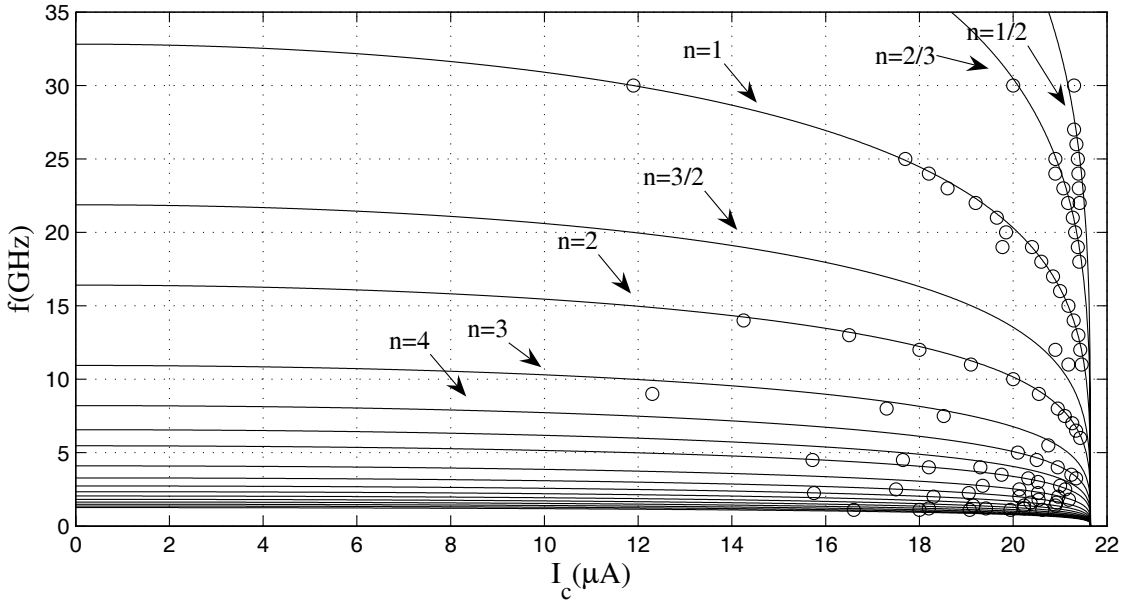

Figure 7.11: Resonance current as a function of applied microwave frequency at 20 mK for a Nb junction. Each "band" corresponds to a n-photon transitions. I_{c0} for this junction was 21.65 μA.

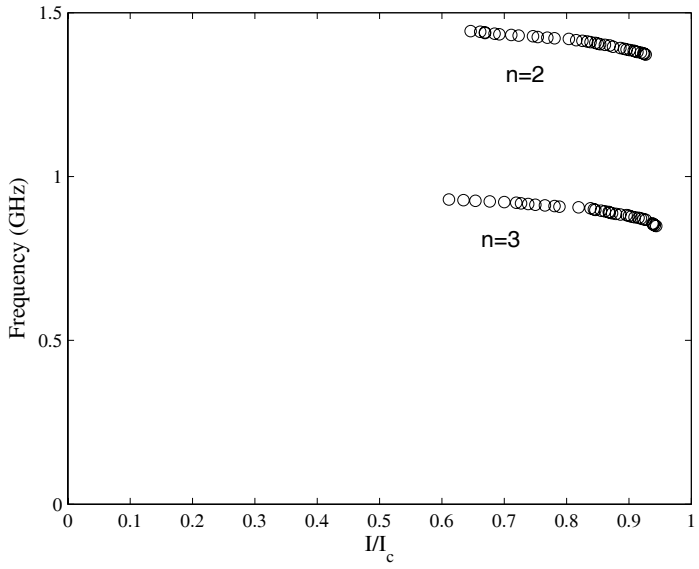

Figure 7.12: Resonance current as a function of applied microwave frequency for the HTS junction showing the 2- and 3-photon transitions at 15 mK.

7.8.3 Q-value of the HTS junction

In order to determine the Q-value of the junction we first calculated the escape rates. The result can be seen in figure 7.7) which is a 3-photon resonance. In order for the aforementioned procedure to be valid the enhancement should be fairly small, in the range 1-5 meaning that the enhanced curve should deviate only slightly from the unperturbed one. In this case we used the curve corresponding to -17 dBm to calculate the enhancement (figure 7.13). Using the enhancement curve we then determined the Q-value of the junction. The result was Q=40$\pm$10 for the 3-photon transition induced by a microwave frequency of 850 MHz. much higher than expected (from the dc-measurements one would have expected a Q of the order of 3-4). This Q-value is of the same order of magnitude as what is usually measured for e.g. Nb junctions where the dissipation is dominated by the impedance of the leads. This clearly demonstrates that the intrinsic dissipation mechanisms in HTS junctions are much less detrimental than many have previously thought; a somewhat naive assumption has been that the presence of nodal quasiparticles in the high-T_c superconductors would ruin any chance of observing discrete levels in HTS junctions.

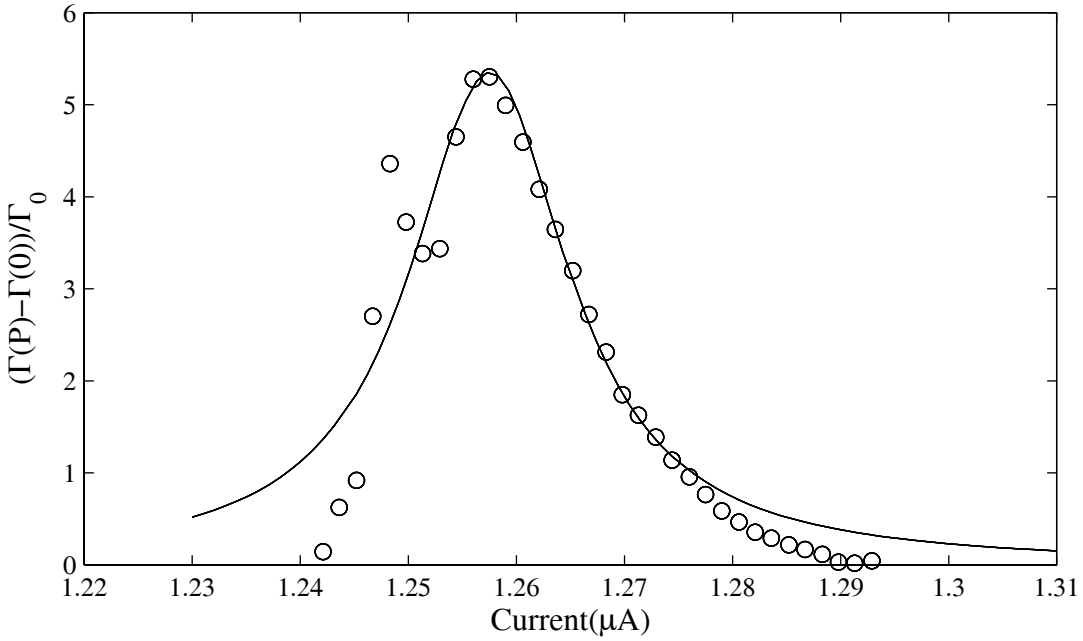

Figure 7.13: A plot of the enhancement for the 3-photon transition. The microwave power was -17 dBm. The increased scattering at low currents is due to the reduced probability of escape. Low probability means fewer events and therefore less reliable statistics. .

Note also that Q=40 is a *lower bound*, the intrinsic Q-value of the junction might be much higher; in our experiment there is no ”protective” circuitry close to the junction meaning that the impedance of the leads is probably the main source of dissipation just as in experiments on Nb junctions.
Using the Q-value it is also possible to calculate the effective dissipation resistance R using eq. 3.34. This gives a value of $R \approx 1.6$ kΩ. Moreover, this is for the *3-photon resonance*. In conventional junctions it is often assumed that the Q-value of an n-photon resonance is $1/n$ times the Q value of the junction. In our case that would mean that the Q value of the junction is at least $3x40 = 120$

rendering a R-value of $\approx 4.7\ \Omega$. However, since we do not have a theory for multi-photon processes we can not say for sure that this is correct. What we can say is that the real Q-value -and therefore R- of this junction is definitely *higher* than Q. The fact that R is significantly higher than 377 Ω also suggests that the junction is somehow "protected" from the environment due to sample geometry and the use of a substrate with a very high dielectric constant

7.9 Modelling of Resonant Activation in Biepitaxial Junctions with Large Kinetic Inductance

As has already been mentioned, the dependence seen in fig. 7.12 the measured dependence of the resonance frequency on the bias current deviates significantly from what one expects in a conventional tunnel junction. The plasma frequency is approximately 2.7 GHz, a factor of two less than what one would expect from the values of I_{c0} and C.
The biepitaxial junctions differ from bicrystal junctions in that the film in one of the electrodes leading to- and from the junction is oriented in such a way that the electric transport takes place in the c-axis direction. Since the London penetration depth in the c-axis direction can be very large the kinetic inductance L_K of the c-axis oriented electrode can be significant. The inductance can be estimated from

$$L_K = \mu_0 \frac{\lambda^2 l}{wt} \tag{7.40}$$

where w is the width and t the thickness of the electrode. L is the length of the electrode. The kinetic inductance is of no great importance for the dc-properties of the junction but it does affect high-frequency properties such as, e.g., the plasma frequency.
Another effect which has already been discussed and is readily observed in the resonant activation experiments is the effect of the stray capacitance of the substrate. In these experiments $SrTiO_3$-substrates were used which have a dielectric constant of about 25000 below 4K. Hence a large part of the measured capacitance is not due to the junction interface but to a distributed stray capacitance C_S which in effect shunts the junction.
We can account for C_S and L_K by using the modified RCSJ-circuit model shown in fig. 7.14 which includes a "shell-circuit" with a capacitor and an inductor [11]. In reality these are of course not discrete elements but the use of this model simplifies the analysis significantly. Moreover, since we are interested in frequencies of the order of 1 GHz the relevant wavelength is of the order of millimeters even in the substrate; this justifies the use of a lumped circuit element analysis.
The addition of the "shell-circuit" to the model of the JJ results in a 2D-potential $U(\varphi, \varphi_s)$ with the phase across the junction φ and the total phase across the whole system φ_s as free variables.
In the superconducting state the potential can be written

$$U(\varphi, \varphi_s) = E_J \left[\frac{1}{2\beta}(\varphi - \varphi_s)^2 - \gamma\varphi_s + 1 - \cos\varphi \right] \tag{7.41}$$

where $\beta = L_K/L_{J0}$, L_{J0} being the zero-bias Josephson inductance $\Phi_0/2\pi I_{c0}$. This is a 2-dimensional potential which makes the dynamics much more complex than for an ordinary junction. This can be seen in figures 7.15 and 7.16. We can also imagine a "nominal" escape trajectory which follows an almost straight line from the minima to ' the saddle point.

[11] One obvious question is if these effects can instead be attributed to the unconventional CPR? From extensive simulation we know that the answer is no. An $\alpha \approx 0.7$ will only re-normalize the height of the barrier and the plasma frequency, it can not account for a deviation from the conventional behavior as large as this.

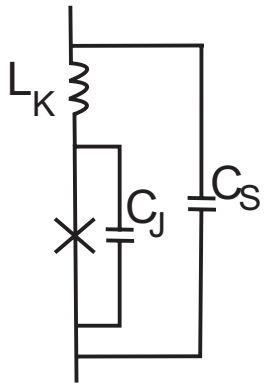

Figure 7.14: Schematic of the model used to explain the results in the resonant activation experiments on biepitaxial junctions. C_J is the junction capacitance, C_S the shell capacitance due to the substrate and L_K the kinetic inductance. .

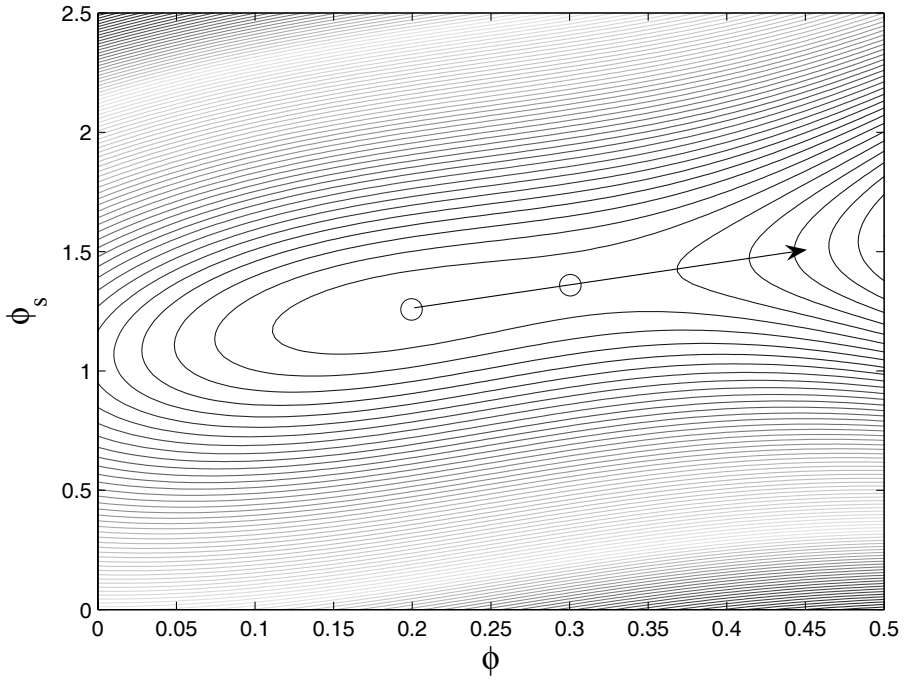

Figure 7.15: A plot of eq. 7.41 for $\gamma = 0.95$ and $\beta = 7$. Initially the junction will oscillate around the minima at $(\arcsin\gamma, \beta\gamma + \arcsin\gamma)$ but eventually γ will have increased so much that the junction will switch by escaping either thermally or via MQT through the saddle point at $(\pi - \arcsin\gamma, \pi - \arcsin\gamma + \beta\gamma)$. A 3D version of this figure can be seen in figure 7.16.

For the circuit depicted in figure 7.14 we expect the plasma frequency to be

$$\omega_p = \frac{1}{\sqrt{(L_J + L_K)C_S}} \tag{7.42}$$

assuming $C_S \gg C_J$, i.e. that the stray capacitance dominates. In order to verify that this model could describe our experimental data a magnetic field was applied to reduce the critical current. This changes L_J whereas L_K is field-independent. Figure 7.17 shows that it is possible to fit all curves using the same value of the kinetic inductance (eq. 7.40) $L_K = 1.7$ nH. Assuming λ_J= 6 μm [74]in the c-axis direction this implies an effective electrode length of 10 μm which is reasonable.
Using this model we can calculate the height of the barrier as a function of bias.

$$\Delta U = E_J[2\gamma \arcsin\gamma - \gamma\pi + 2\sqrt{1-\gamma^2}] \tag{7.43}$$

Hence, there is no dependence on β which explains why the junction behaves like an ordinary device: Unless the level splitting (and thereby the plasma frequency) is measured directly the effects of the high kinetic inductance are invisible.
Now, let us redefine our energy scale so that $U(bottomofwell) = U(a,b) = 0$ (we measure all energies relative to the minima) and all energies are measured in units of E_J. Then we can expand the potential to the second order around the minimum

$$U(a+h, b+k) = h^2\left(\frac{1}{2\beta} + \frac{\sqrt{1-\gamma^2}}{2}\right) + k^2\frac{1}{2\beta} - 2hk\frac{1}{2\beta} \tag{7.44}$$

where we have used that $\cos(\arcsin(\gamma)) = \sqrt{1-\gamma^2}$. By introducing two new coordinates (χ, ξ) we can write this in the canonical form

$$U(\chi,\xi) = \lambda_+\chi^2 + \lambda_-\xi^2 \tag{7.45}$$

where $\lambda_{+,-}$ are eigenvalues of the coefficient matrix to eq. 7.44. $\lambda_{+,-}$ can be written

$$\lambda_{+,-} = \frac{2 + \beta\sqrt{1-\gamma^2} \pm \sqrt{(1-\gamma^2)\beta^2 + 4}}{4\beta} \tag{7.46}$$

Finally, if we write the potential as

$$U(\chi,\xi) = \frac{2\lambda_+}{2}\chi^2 + \frac{2\lambda_-}{2}\xi^2 \tag{7.47}$$

which is just a (separable) equation for the potential of a harmonic oscillator in 2 dimensions. Hence, we know that we will get a spectrum of eigenfrequencies given by

$$\epsilon(n,m) = n\sqrt{\frac{2\lambda_+}{M}} + m\sqrt{\frac{2\lambda_-}{M}} \tag{7.48}$$

where M is the usual mass of the phase particle and n, m are integers. This expression shows yet another reason why the potential behaves "almost" 1D; the solutions that corresponds to eigenvectors perpendicular to the nominal escape trajectory have much higher energies than the parallel solutions. For the first 3-4 eigenfrequencies the 1D expression eq. 7.42 and eq. 7.48 will give the same result. It is possible to numerically solve for the eigenvalue spectrum of the 2D potential 7.41. This was done using the software Femlab. The difference between the numerically calculated values and

eq. 7.48 were found to be insignificant as long as $\beta = L_K/L_J > 1$ (for small β the harmonic approximation does not work).
Unfortunately, the fact that the potential is 2D makes the modelling extremely complex. However, as has been demonstrated the junction behaves ”almost” as a conventional junction. The fact that there is a single saddle point probably means that the junction will always escape along approximately the same trajectory both in the MQT- and thermal regime. The only way to truly verify this is to perform numerical simulations of the full dynamics of the system.

7.9.1 Is the junction intrinsically protected from dissipation?

It is of course interesting to speculate about whether or not the high kinetic inductance and the use of a substrate with a high dielectric constant is helping to protect the junction from the environment. It is clearly a possibility that there is a ”comb-filter effect”. The same effect that make it possible to couple to the junction only at certain frequencies would then be protecting the junction so that the impedance it sees is very high.
A way to check this statement would be to perform similar experiments on samples fabricated on substrates with a low dielectric constant.

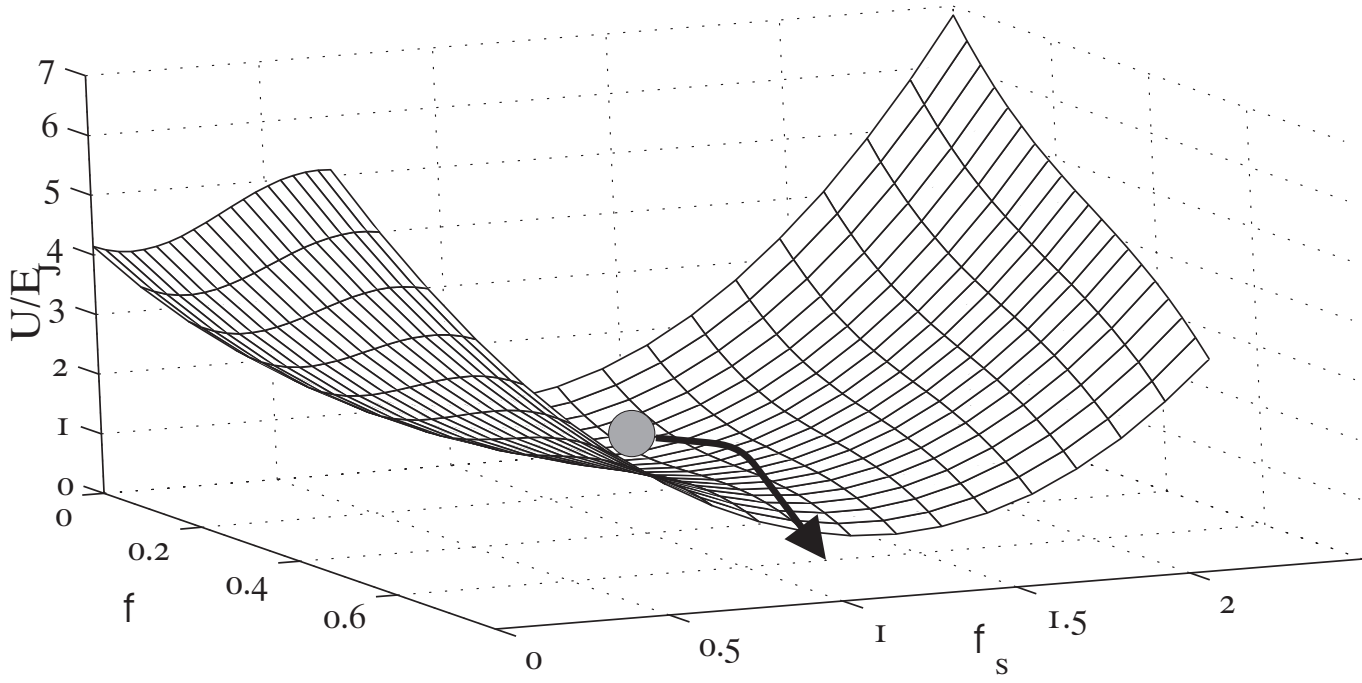

Figure 7.16: A 3D-plot of figure 7.15.

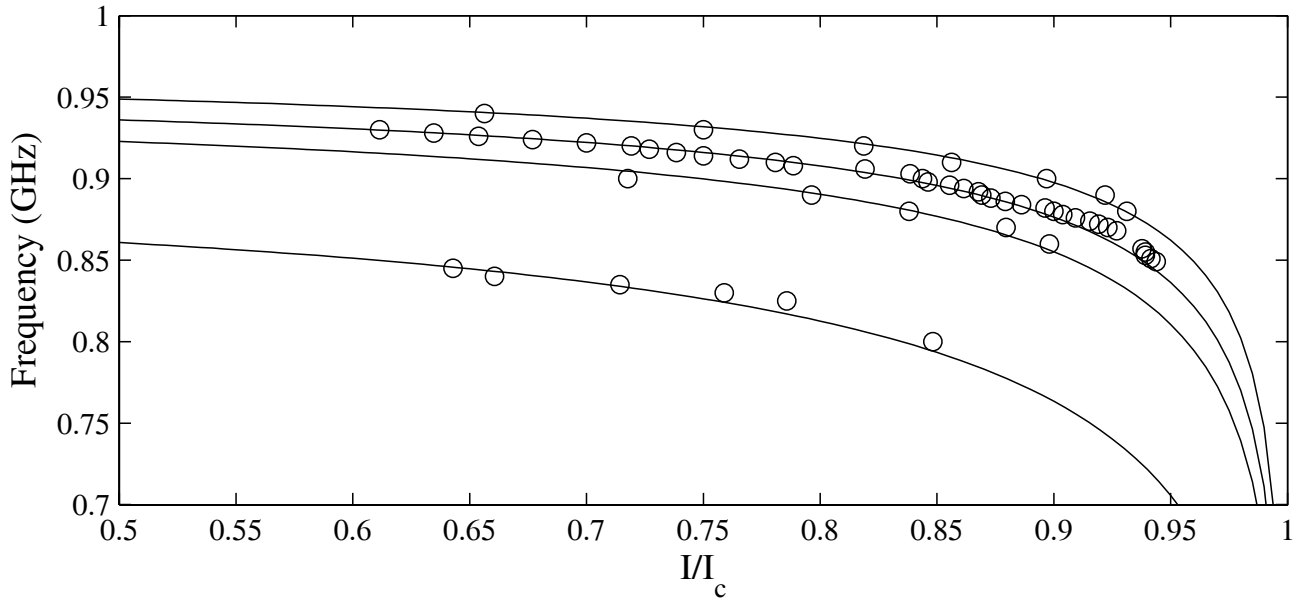

Figure 7.17: Resonance current as a function of applied microwave frequency at 20 mK for 4 values of the Josephson inductance L_{J0}. L_{J0} was changed by applying an external magnetic field. *From top to bottom:* 0.20 nH, 0.25 nH, 0.30 nH and 0.57 nH. .

Chapter 8

The d-wave Qubit

The past few years have seen a huge increase in the amount of work going into the realization of qubits; much of the effort have been focused on ideas that involve Josephson junctions. There are many ways to use the Josephson effect to build qubits and Rabi-oscillations have already been demonstrated in several implementations: Ordinary tunnel junctions [61], the single Cooper-pair box [15] and dc-SQUIDs [75].
Designing and fabricating solid state qubits is very challenging even when working with well known materials such as aluminium. A very high degree of precision is necessary and it is well known that e.g. fluctuators present in the barrier can cause decoherence. Hence, it does not make sense to simply replace e.g. Al by YBCO in a qubit design [1]. Since all qubits presently need to be operated at mK temperatures in order to avoid decoherence due to thermal excitations the higher critical temperature of YBCO is not relevant. As has been discussed in this thesis we still do not have precise control over junction properties and the interface. Reproducibility is still an issue; as are sub-gap excitations, two-level fluctuators due to charge traps in the interface etc. Hence, it is only if we somehow utilize the one property not found in LTS that a HTS qubit makes sense: Namely the d-wave symmetry.
A "d-wave qubit" was first suggested by Ioffe et al. [76] and was based on networks of 0- and π-junctions, the idea being that a network of this type can be "topologically protected" from decoherence. However, no one has successfully implemented this idea, at least in part because of the complexity of the design. Some preliminary work has been done using low-T_c SFS-junctions [77] to create the π-junctions.
The unconventional CPR found in high-angle YBCO junctions is another consequence of the d-wave symmetry that can potentially be used to implement novel qubit designs with great advantages when compared to their LTS counterparts.

8.1 Qubits based on a 2^{nd} harmonic in the CPR

Consider eq. 6.7, the potential of a dc-SQUID where the junctions have a 2^{nd} harmonic component in their CPR, in the case of negligible self-inductance

$$U(\gamma, \phi_x) = -\varepsilon_\phi \left[\cos\gamma - \frac{\tilde{\alpha_\phi}}{4} \cos(2\gamma) \right] + \tilde{U}(\gamma, \phi_x) \tag{8.1}$$

[1] At least not if the purpose is primarily to build a qubit with good properties. Demonstration of coherent phenomena in a single YBCO junction would be very interesting from a fundamental point of view though.

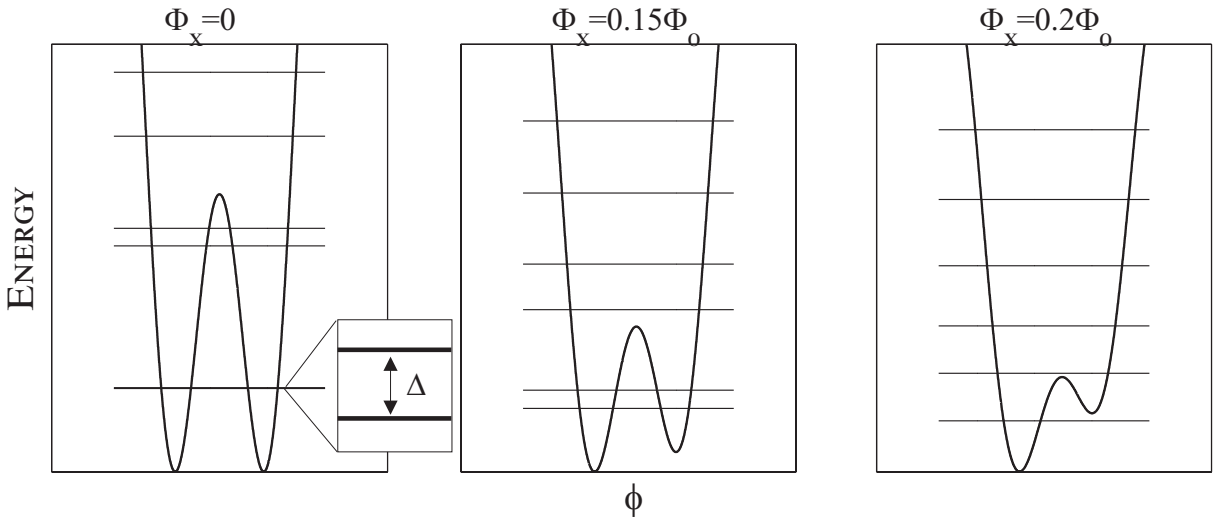

Figure 8.1: The evolution of the shape of the potential of an asymmetric dc-SQUID with $\eta = E_2^I/E_1^I = 1.5$ and $\alpha_1 = I_1^{II}/I_1^I = \alpha_2 = 2$. As the field is increased, the barrier tend to disappear and the well is tilted, making it possible to prepare the system in a known state. The horizontal lines indicate the position of the energy levels.

where

$$\tilde{\alpha_\phi} = [2(\alpha_1 + \eta\alpha_2)\cos\phi]/[(1+\eta)\cos(\phi/2)] \tag{8.2}$$

and the rest of the definitions are as given in section 6. The shape of the potential depends both on the asymmetry $\eta = E_2^I/E_1^I$ and the relative magnitude of the second harmonic α in each junction. A single qubit is essentially a controllable two-state system and as shown in figure 8.1, the potential 8.1 meets this criteria. At zero external flux the potential has the familiar double-well shape which is exactly what we want in order to make a qubit. By increasing the field we can reduce the height of the barrier and "tilt" the well meaning that we can prepare the system in a known initial state. The potential has been plotted for the case $\eta = 1.5$ and $\alpha_1 = \alpha_2 = 1.5$ but there are many possible sets of parameters that fulfill the conditions. It is however important that the SQUID is asymmetric with respect to I_c (i.e. $\eta \neq 1$). Otherwise it is impossible to "tilt" the well.
The two states of the qubit -which classically would correspond to a clockwise- or anti-clockwise circulating persistent current- are separated by a flux-dependent energy barrier

$$W(\phi_x) = \cos(\phi_x/2)(\tilde{\alpha}_\phi + \tilde{\alpha}_\phi^{-1} - 2) \tag{8.3}$$

Tunnelling occurs between the two minima due to the uncertainty relation between charge Q and superconducting phase θ on the island. The tunnelling matrix element is approximately given by ($\hbar = k_{\mathrm{B}} = 1$)

$$\Delta \approx \omega_p(\phi_x) e^{-\sqrt{\zeta W(\phi_x) E_J/E_c}}, \tag{8.4}$$

where ζ is a constant of the order of 1, E_J is the Josephson energy and E_c the charging energy. The coefficient $\omega_p(\phi_x) \equiv \sqrt{\omega_p^+ \omega_p^-}$ is determined by the plasma frequencies $\omega_p^\pm$ of the right and left minima, respectively. Figure 8.1 also shows the positions of the energy levels in the well. The energy spacing Δ separating the working levels from the next excited state is almost independent of $\tilde{\alpha_\phi}$. This

means that it is possible to tune Δ using $\tilde{\alpha_\phi}$ while at the same time keeping the system effectively decoupled from the other levels of the well. Hence, despite there being many levels in the well only the two lowest are involved in the qubit operation meaning it is effectively a two-state system.
This qubit is in many ways similar to the flux-qubit first implemented by the Delft group in 2000 [78] which was later shown to exhibit Rabi-oscillations. There are, however, two key differences. First of all there is no need to flux-bias the SQUID in order for the potential to have a double well shape. Secondly, this qubit is "silent" in the sense that at the operating point it is almost completely decoupled from any fluctuations generated by the controlling circuitry. This, very important argument, is discussed in more detail in paper IV.

8.2 Decoherence in d-wave Josephson Devices

The concept of decoherence and dissipation in HTS materials is an often somewhat misunderstood subject. In order to understand why, we need to remember the usual argument for why s-wave low-T_c superconductors are ideal candidates for e.g. qubit applications: The presence of a gap in the quasiparticle spectrum means that superconducting qubits are intrinsically protected from decoherence since the quasiparticle transport is suppressed. If we try to apply the same argument to pure d-wave superconductors we see why they may appear to be unsuitable for qubit-applications. Here the gap disappears in the nodes which means low-lying quasiparticles will be present. Ergo, according to this simple argument there is no intrinsic protection from dissipation in a d-wave junction. In the case of $0^o - 45^o$ junctions there is yet another source of dissipation due to the midgap states (MGS). In this case node-to-MGS tunnelling is possible which contributes to the dissipation of the junction; this effect can lead to strong dissipation in asymmetric junctions.
A number of theoretical works, both pertaining directly to d-wave qubits [79][80][81] and MQT [82][83] in c-axis (e.g. Bi2212 intrinsic junctions) and ab-plane junctions have,however, shown that none of these effects needs to spell doom for the high-T_c qubit. Obviously the high quality factor we observed in the experiments presented in this thesis is further proof of this.
Unfortunately, even in the case of "simple" systems like s-wave Josephson junctions the theoretical machinery for describing the effects of dissipation is quite complicated(see e.g. [23] and [60]). In the case of d-wave superconductors, the theories become even more complex and are well beyond the scope of this thesis. I therefore refer the interested reader to the relevant references.
The lesson we do learn from existing theoretical work is that the presence of nodal quasiparticles does,indeed, increase the dissipation. However, it turns out that the effect is weak. The decrease in the MQT escape rate is less than one order of magnitude and is therefore negligible in a real experiment. The situation with MGS is much the same. Again there is an effect but the difference in dissipation between a $0^\circ - 0^\circ$ (where there are no MGS) and a 0°-45° junction is relatively small. Hence, if these two effects were the only sources of dissipation in the system we would therefore expect to measure very large quality factors. However, just as in the case of Nb tunnel junctions we have to take account dissipation due to coupling to the environment via the electrodes, background charge-fluctuations etc. In a real device, these effects are likely to be far more important than the dissipation due to node-to-MGS tunnelling and nodal quasiparticles. Therefore, it seems the main sources of dissipation are not directly related to the type of superconductor used and are more or less the same regardless if low- or high-T_c superconductors are used. Naturally there are still major issues with, e.g., the quality of the barrier in real high-T_c junctions, but this problem is also shared with many low-T_c materials and can not be said to be an intrinsic problem directly related to the d-wave symmetry.

Sometimes, another argument is used to show that HTS junctions can not be operated in the quantum regime. The line of reasoning is that the normal resistance R_N of HTS junctions is fairly low even for submicron junctions and therefore the dissipation should always be large since the junction is shunted by R_N. However, this line of reasoning is simply not valid. While it is true that in the case of a tunnel junction one can draw some conclusions about the dissipation of the system by studying the IV-curve, it is the *subgap* resistance which is the relevant parameter (which acts as a shunting resistance in the S-state), not R_N, since this is the resistance the junction sees in the *running state*. As our experiments have shown, the effective dissipation resistance in an HTS junction can be much larger than R_N and there is, in fact, no reason to expect any direct correlation between R and R_N. An attentive reader will notice that the issue of dephasing has been absent from the discussion so far. Moreover, no reference has been made to any specific qubit-implementation. The reason is that the main issue so far in the development of HTS qubits has been whether it is at all possible to use HTS Josephson junctions in a macroscopic quantum system; if the intrinsic dissipation in the junctions had turned out to be large the very idea of a qubit would have been dead, no matter what the actual implementation. The issue of decoherence (both due to dissipation and dephasing) is, of course, central in any discussion of a real qubit such as the one discussed above.

8.3 Outlook

The most obvious question one must ask is how to design a practical qubit that utilizes the unconventional CPR found in 0°-45° junctions. The issue is not so much the qubit itself -which is as has been shown here just a suitable dc-SQUID- but the readout scheme. The most obvious approach is to surround the qubit with a read-out SQUID which can detect the flux state. From a design point of view this is straightforward and we have fabricated demonstrators (figure 4.5 is in fact one example of such a demonstrator). The problem is that if we are using the bicrystal technique the read-out SQUID will also be made from 0°-45° junctions. Hence the outermost SQUID will also potentially exhibit very complex dynamics. It would therefore be desirable to use a "simpler" well-known system for the read-out scheme such as a dc-SQUID made from Nb or Al. There are two ways to implement this. One way would be to fabricate an Al dc-SQUID directly on the same substrate which has the advantage of making it possible to align the read-out SQUID very precisely using lithography. The main issue here is being able to fabricate high-quality Al junctions on a substrate which has already gone through extensive processing (including etching). The second way would be to us a flip-chip technique. In this approach the read-out circuitry and the qubit are on separate substrates and are glued together. This would make it possible to characterize the read-out circuit and the dc-SQUID independently and avoids all issues with mixing high- and low-T_c devices on the same substrate. The open question is if it is possible to align the devices precisely enough and how strong the coupling will be. Note that the flip-chip technique could also be used with the indirect read-out scheme discussed in paper IV, where the read-out consists of a high-quality LC-resonator[84].

Chapter 9

Conclusions

Using HTS grain boundary Josephson junctions for "quantum engineering" might seem a hopeless enterprise. Despite many years of research HTS devices have properties that can not be precisely controlled.

Nevertheless a lot of progress has been made over the past years. Well developed lithographic methods allow us to design and fabricate virtually any kind of device; we have demonstrated working devices with typical sizes similar to what is used in the semiconductor industry.

We now also believe we have a fairly good understanding of the basic physics of HTS grain boundaries. There is an abundance of coexisting phenomena that all play a role for the transport properties. However, we have reached a stage where we believe we can deal with the problems, to the extent that despite not being able to *predict* the exact properties of a given device, we can at least say we understand what comes out of the measurements. For someone working with semiconductors this might not seem like much; but considering just how complex the grain boundaries in high-T_c materials are, it is still a considerable achievement.

Obviously it would be desirable -in this application and others- to have a more reproducible junction fabrication technique, bicrystal- and biepitaxial junctions are very versatile tools but it seems clear that neither technology can come close to for example aluminium-based junction technology in terms of reproducibility. This is especially true for 0°-45° junctions where the meandering of the GB plays such a large role.

So what is the situation for the "silent high-T_c qubit"?

We have overcome two major obstacles: First we have demonstrated of the presence of strong 2^{nd} harmonic component in the CPR of 0°-45° dc-SQUIDs. At least in some devices we believe we have a CPR that should give rise to a double-well potential.

Secondly, we have shown that not only can a HTS junction exhibit macroscopic quantum tunnelling and discrete energy levels; the measured quality factor is comparable with what is measured in unprotected Nb junctions.

Despite the fact that there is still no experimental demonstration of a coherent phenomena (i.e. Rabi-oscillations) in a HTS device, the evidence we have today show that it should not only be *possible* to measure such an effect but that a well designed experiment is also *likely* to succeed. This situation is dramatically different from five years ago when most thought this to be impossible due to fundamental issues such as dissipation from nodal quasiparticles and midgap states.

More experimental data is needed before we can know for sure if a high-T_c qubit can be indeed realized. One also need to keep in mind that even if one succeeds in measuring Rabi-oscillations

there is no guarantee that the measured parameters will be able to rival those of ”conventional” qubits made from low-T_c materials.
My conclusion from these past five years is that in spite of all unsolved problems there are now enough evidence that points to the possibility of observing Rabi-oscillations in a 0°-45° YBCO dc-SQUID, that such an experiment is worth a try.

Chapter 10

Summary of Appended Papers

The papers in appendix B are commented on. I also specify my contribution in each case.

Paper I: Feasibility studies of ultra-small Josephson junctions for qubits

A.Ya. Tzalenchuk, T. Lindström, S.A. Charlebois, E.A. Stepantsov, A.M. Zagoskin, Z. Ivanov and T. Claeson(2003)
This paper describes fabrication and characterization of sub-micrometer sized Josephson junctions intended for qubit applications. Sub-micrometer processing of high temperature superconductors is non-trivial and a number of steps had to be developed and tested. This paper also introduces the idea of a d-wave qubit based on an unconventional current-phase relation. The fabrication technique outlined here has been used to make all samples for the measurements presented in this thesis.
In this work I was involved in characterizing the samples.

Paper II: Dynamical Effect of an Unconventional Current-Phase Relation in YBCO dc SQUIDs

T. Lindström, S.A. Charlebois, A.Ya. Tzalenchuk, Z. Ivanov, M.H.S Amin and A.M. Zagoskin(2003)
In this letter we presented measurements of dc-SQUID modulations showing a clear contribution of a 2^{nd} harmonic current component in the current-phase relation.
For this work I performed all the measurements together with Serge Charlebois and analyzed the data. I also performed the numerical simulations and the data fitting. Good fits could be obtained with reasonable parameters. This work has been extended in paper V. I am the main author of this paper.

Paper III: Mesoscopic Josephson Junctions of high-T_c Superconductors

A.Ya. Tzalenchuk, T. Lindström, S.A. Charlebois, E.A. Stepantsov, Z. Ivanov and A.M. Zagoskin(2003)
In this paper we discussed properties of mesoscopic Josephson junctions and presented data for 0°-32°, 0°-40° junctions. There is also a discussion of the possibility of a d-wave qubit based on a *single* Josephson junction.
In this work I was mainly involved in the measurements and the subsequent analysis of data.

Paper IV: Silent Phase Qubit Based on d-wave Josephson junctions

M.H.S. Amin, A.Y. Smirnov, A.M. Zagoskin, T. Lindström, S.A. Charlebois, T. Claeson, and A.Ya. Tzalenchuk (2003)
This is mainly a theoretical paper describing how a dc-SQUID with both 1^{st} and 2^{nd} harmonic components in CPR can be used as a ”silent” qubit.
My contribution to this work concerns some suggestions for the discussion óf the implementation of the qubit.

Paper V: Josephson Dynamics of Bicrystal d-Wave YBCO dc-SQUIDs

T. Lindström, J. Johansson, T. Bauch, F.Lombardi and S.A. Charlebois (2005)
The manuscript contains a fairly extensive discussion about properties of 0°-45° bicrystal grain boundary SQUIDs. In particular, there is a treatment of the 2^{nd} harmonic contribution in the current-phase relation. Comparisons are made between numerical and experimental results - an extension of paper II. A model of the grain boundary is discussed. I am the main author of this work and have performed measurements as well as numerical simulations together with Jesper Johansson. This is also the only work where I have actively contributed to the sample fabrication (SQ5). This manuscript will be somewhat revised before being submitted to a journal. We plan on replacing the data in figure 5 with data from new measurements. The conclusions, however, will not be affected.

Paper VI:Quantum Dynamics of a d-wave YBCO Josephson Junction

T. Bauch, F. Lombardi, T. Lindström, F. Tafuri, G.Rotoli, T. Claeson and P. Delsing (2005)
In this manuscript we show experimental evidence for resonant activation in an HTS Josephson junction. My contribution was in in the design and construction of the measurement setup as well as performing a substantial part of the measurements. Thilo Bauch was the responsible person for the measurements. I have actively participated in the interpretaion of the results.

Chapter 11

Acknowledgements

I would like to start by thanking my supervisor Doc. Floriana Lombardi and my examiner Prof. Tord Claeson. Their help, encouragement and insight into physics have been invaluable during my time as a PhD student.
Over the past five years I have had the pleasure and privilege to work with many talented, creative and supportive individuals without whom none of this work would have been possible.
Alexander Tzalenchuck who initiated this work. Our discussions in the lab has taught me a lot about physics.
Serge Charlebois, who fabricated most of the samples and participated in many of the measurements presented in this work. We have spent countless hours together building experimental setups, measuring and discussing physics.
Jesper Johansson who fabricated the tilt-tilt samples and with whom I have collaborated on the work on the effects of the 2^{nd} harmonic.
The work on resonant activation was done together with Thilo Bauch who performed most of the actual measurements and taught me a lot about how to perform these types of experiments
Alexandre Zagoskin at the University of British Colombia and Mohammad Amin at D-Wave who did most of theory for the d-wave qubit.
Evgueni Stepantsov who deposited the YBCO films and fabricated the tilt-tilt bicrystal substrates used in this work.
Mikael Fogelström for providing theoretical insight and input
Staffan Pehrson, our technician. Without his skills it would have been impossible to build and maintain our measurement setups.
Past and present PhD student in the QuOx group. In particular Robert Gunnarson who had to put up with sharing an office with me.
Prof. Zdravko Ivanov who accepted me as his PhD student and was my supervisor until his untimely decease on May 20th, 2003. He will always be a source of inspiration for me.
Finally I would like to thank all the people at the Quantum Device Physics Laboratory at Chalmers who have helped me in my work countless times and made these five years very enjoyable.

Bibliography

[1] J.G. Bednorz and K.A. Muller. Possible high-T_c superconductivity in the Ba-La-Cu-O system. *Zeitschrift fur Physik B (Condensed Matter)*, 64(2):189–93, 1986.

[2] J.M. Martinis, M.H. Devoret, and J. Clarke. Experimental tests for the quantum behavior of a macroscopic degree of freedom: the phase difference across a josephson junction. *Physical Review B (Condensed Matter)*, 35(10):4682–98, 1987.

[3] R.F. Voss and R.A. Webb. Macroscopic quantum tunneling in 1-μm nb josephson junctions. *Physical Review Letters*, 47(4):265–8, 1981.

[4] J Bardeen, J.N Cooper, and J.R. Schrieffer. *Phys. Rev*, 108:1175, 1957.

[5] M. Tinkham. *Introduction to Superconductivity*. McGraw-Hill, 1996.

[6] S.E. Barrett, J.A. Martindale, D.J. Durand, C.H. Pennington, C.P. Slichter, T.A. Friedmann, J.P. Rice, and D.M. Ginsberg. Anomalous behavior of nuclear spin-lattice relaxation rates in $YBa_2Cu_3O_7$ below T_c. *Physical Review Letters*, 66(1):108–11, 1991.

[7] D.A. Wollman, D.J. Van Harlingen, W.C. Lee, D.M. Ginsberg, and A.J. Leggett. Experimental determination of the superconducting pairing state in YBCO from the phase coherence of YBCO-Pb DC SQUIDs. *Physical Review Letters*, 71(13):2134–7, 1993.

[8] C.C. Tsuei and J.R. Kirtley. Pairing symmetry in cuprate superconductors. *Reviews of Modern Physics*, 72(4):969–1016, 2000.

[9] J. Mannhart and H. Hilgenkamp. Wave function symmetry and its influence on superconducting devices. In D.H.A. Rogalla, H.; Blank, editor, *Applied Superconductivity 1997. Proceedings of EUCAS 1997 Third European Conference on Applied Superconductivity*, pages 1–6 vol.1, Bristol, UK, 1997. Institute of Physics Publishing.

[10] B.D Josephson. Possible new effects in superconductive tunneling. *Physics Letters*, 1(7):251–253, 1962.

[11] J. Moreland, L.F. Goodrich, J.W. Ekin, T.E. Capobianco, A.F. Clark, A.I. Braginski, and A.J. Panson. Josephson effect above 77 K in a YBaCuO break junction. *Applied Physics Letters*, 51(7):540–1, 1987.

[12] D. Winkler. Superconducting analogue electronics for research and industry. *Superconductor Science & Technology*, 16(12):1583–90, 2003.

[13] P.W. Shor. Algorithms for quantum computation: discrete logarithms and factoring. In *Proceedings 35th Annual Symposium on Foundations of Computer Science, 20-22 Nov. 1994*, Proceedings. 35th Annual Symposium on Foundations of Computer Science (Cat. No.94CH35717), pages 124–34, Santa Fe, NM, USA, 1994. IEEE Comput. Soc. Press.

[14] L.M.K. Vandersypen, M. Steffen, G. Breyta, C.S. Yannoni, M.H. Sherwood, and I.L. Chuang. Experimental realization of shor's quantum factoring algorithm using nuclear magnetic resonance. *Nature*, 414(6866):883–7, 2001.

[15] Y. Nakamura, Yu.A. Pashkin, and J.S. Tsai. Coherent control of macroscopic quantum states in a single-cooper-pair box. *Nature*, 398(6730):786–8, 1999.

[16] M. Sigrist and T.M. Rice. Unusual paramagnetic phenomena in granular high-temperature superconductors-a consequence of d-wave pairing? *Reviews of Modern Physics*, 67(2):503–13, 1995.

[17] T Löfwander, V. S. Shumeiko, and G. Wendin. Time-reversal symmetry breaking at josephson tunnel junctions of purely d-wave superconductors. *manuscript*, 2000.

[18] M.H.S. Amin, A.N. Omelyanchouk, and A.M. Zagoskin. Mechanisms of spontaneous current generation in an inhomogeneous d-wave superconductor. *Physical Review B (Condensed Matter and Materials Physics)*, 63(21):212502–1, 2001.

[19] S.K. Tolpygo and M. Gurvitch. Critical currents and josephson penetration depth in planar thin-film high-T_c josephson junctions. *Applied Physics Letters*, 69(25):3914–16, 1996.

[20] Alan M Kadin. *Introduction to Superconducting Circuits*. John Wiley & Sons, 1999.

[21] J R Waldram. *Superconductivity of Metals and Cuprates*. IOP Publishing, 1996.

[22] J.C. Gallop. *SQUIDs, the Josephson Effects and Superconducting Electronics*. IOP Publishing, 1991.

[23] Shin Takagi. *Macroscopic Quantum Tunnelling*. Cambridge University Press, 1997.

[24] M. Buttiker, E.P. Harris, and R. Landauer. Thermal activation in extremely underdamped josephson-junction circuits. *Physical Review B (Condensed Matter)*, 28(3), 1983.

[25] H. Grabert, P. Olschowski, and U. Weiss. Quantum decay rates for dissipative systems at finite temperatures. *Physical Review B (Condensed Matter)*, 36(4):1931–51, 1987.

[26] K.K. Likharev. *Dynamics of Josephson Junctions and Circuits*. Gordon an Breach Science Publishers, 1986.

[27] J.M. Martinis, M.H. Devoret, and J. Clarke. Experimental tests for the quantum behavior of a macroscopic degree of freedom: the phase difference across a josephson junction. *Physical Review B (Condensed Matter)*, 35(10):4682–98, 1987.

[28] P.E. Flewitt and R.K. Wild. *Grain Boundaries-Their Microstructure and Chemistry*. Wiley, 2001.

[29] José A. Alarco. *Grain Boundary Structure of YBCO High-Tc Superconductors*. PhD thesis, Göteborg University, 1994.

[30] H. Hilgenkamp and J. Mannhart. Grain boundaries in high-T_c superconductors. *Reviews of Modern Physics*, 74(2):297–659, 2002.

[31] Y.Y. Divin, U. Poppe, C.L. Jia, P.M. Shadrin, and K. Urban. Structural and electrical properties of $YBa_2Cu_3O_7$ [100]-tilt grain boundary josephson junctions with large I_cR_N-products on $SrTiO_3$ bicrystals. *Physica C 5th European Conference on Applied Superconductivity. EUCAS 2001, 26-30 Aug. 2001*, 372-376(pt.1):115–18, 2002.

[32] E.J. Tarte, P.F. McBrien, J.H.T. Ransley, R.H. Hadfield, E. Inglessi, W.E. Booij, G. Burnell, M.G. Blamire, and J.E. Evetts. Capacitance as a probe of high angle grain boundary transport in oxide superconductors. *IEEE Transactions on Applied Superconductivity 2000 Applied Superconductivity Conference, 17-22 Sept. 2000*, 11(1, pt.1):418–21, 2001.

[33] M.M. Khapaev, A.Yu. Kidiyarova-Shevchenko, P. Magnelind, and M.Yu. Kupriyanov. 3d-mlsi: software package for inductance calculation in multilayer superconducting integrated circuits. *IEEE Transactions on Applied Superconductivity*, 11(1):1090–3, 2001.

[34] K. Bladh, D. Gunnarsson, E. Hurfeld, S. Devi, C. Kristoffersson, B. Smalander, S. Pehrson, T. Claeson, P. Delsing, and M. Taslakov. Comparison of cryogenic filters for use in single electronics experiments. *Review of Scientific Instruments*, 74(3):1323–7, 2003.

[35] G.E. Blonder, M. Tinkham, and T.M. Klapwijk. Transition from metallic to tunneling regimes in superconducting microconstrictions: excess current, charge imbalance, and supercurrent conversion. *Physical Review B (Condensed Matter)*, 25, 1982.

[36] A.A. Golubov, M.Yu. Kupriyanov, and E. Il'ichev. The current-phase relation in josephson junctions. *Reviews of Modern Physics*, 76(2):411–69, 2004.

[37] G.E. Blonder, M. Tinkham, and T.M. Klapwijk. Transition from metallic to tunneling regimes in superconducting microconstrictions: excess current, charge imbalance, and supercurrent conversion. *Physical Review B*, 25, 1982.

[38] M. Sigrist and T.M. Rice. Paramagnetic effect in high-T_c superconductors-a hint for d-wave superconductivity. *Journal of the Physical Society of Japan*, 61(12):4283–6, 1992.

[39] M.B. Walker and J. Luettmer-Strathmann. Josephson tunneling in high-T_c superconductors. *Physical Review B (Condensed Matter)*, 54(1):588–601, 1996.

[40] F. Lombardi, E. Tafuri, F. Ricci, F.M. Granozio, A. Barone, G. Testa, E. Sarnelli, J.R. Kirtley, and C.C. Tsuei. Intrinsic d-wave effects in $YBa_2Cu_3O_{7-\delta}$ grain boundary josephson junctions. *Physical Review Letters*, 89(20):207001–1, 2002.

[41] Chia-Ren Hu. Midgap surface states as a novel signature for $d_{x_a^2-x_b^2}$-wave superconductivity. *Physical Review Letters*, 72(10):1526–9, 1994.

[42] M. Fogelström, D. Rainer, and J.A. Sauls. Tunneling into current-carrying surface states of high-T_c superconductors. *Physical Review Letters*, 79(2):281–4, 1997.

[43] L. Alff, A. Beck, R. Gross, A. Marx, S. Kleefisch, Th Bauch, H. Sato, M. Naito, and G. Koren. Observation of bound surface states in grain-boundary junctions of high-temperature superconductors. *Physical Review B (Condensed Matter)*, 58(17):11197–200, 1998.

[44] L. H. Greene, M. Covington, M. Aprili, E. Badica, and D. E. Pugel. Observation of broken time-reversal symmetry with andreev bound state tunneling spectroscopy. *Physica B*, 280(1-4):159–64, 2000.

[45] T. Löfwander, V.S. Shumeiko, and G. Wendin. Andreev bound states in high-T_c superconducting junctions. *Superconductor Science and Technology*, 14(5):R53–77, 2001.

[46] E. Il'ichev et al. Degenerate ground state in a mesoscopic $YBa_2Cu_3O_{7-x}$ grain boundary josephson junction. *Physical Review Letters*, 86(23):5369–72, 2001.

[47] Yu.S. Barash. Quasiparticle interface states in junctions involving d-wave superconductors. *Physical Review B (Condensed Matter)*, 61(1):678–88, 2000.

[48] G. Testa, A. Monaco, E. Esposito, E. Sarnelli, D.-J. Kang, S.H. Mennema, E.J. Tarte, and M.G. Blamire. Midgap state-based pi-junctions for digital applications. *Applied Physics Letters*, 85(7):1202–1204, 2004.

[49] S.-K. Yip, O.F. De Alcantara Bonfim, and P. Kumar. Supercurrent tunneling between conventional and unconventional superconductors: a ginzburg-landau approach. *Physical Review B (Condensed Matter)*, 41(16):11214–28, 1990.

[50] Sungkit Yip. Josephson current-phase relationships with unconventional superconductors. *Physical Review B (Condensed Matter)*, 52(5):3087–90, 1995.

[51] A.M. Zagoskin. The half-periodic josephson effect in an s-wave superconductor-normal-metal-d-wave superconductor junction. *Journal of Physics: Condensed Matter*, 9(31):419–26, 1997.

[52] R.G. Mints, I. Papiashvili, J.R. Kirtley, H. Hilgenkamp, G. Hammerl, and J. Mannhart. Observation of splintered josephson vortices at grain boundaries in $YBa_2Cu_3O_{7-\delta}$. *Physical Review Letters*, 89(6):067004–1, 2002.

[53] F. Tafuri, J.R. Kirtley, F. Lombardi, and F.M. Granozio. Intrinsic and extrinsic d-wave effects in $YBa_2Cu_3O_{7-\delta}$ grain boundary josephson junctions: implications for pi circuitry. *Physical Review B (Condensed Matter and Materials Physics)*, 67(17):174516–1, 2003.

[54] O. Nesher and G. Koren. Measurements of delta and v_F from andreev reflections and mcmillan-rowell oscillations in edge junctions of $YBa_2Cu_3O_{6.6}$/$YBa_2Cu_{2.55}Fe_{0.45}O_y$/$YBa_2Cu_3O_{6.6}$. *Physical Review B (Condensed Matter)*, 60(13):9287–90, 1999.

[55] H. Arie, K. Yasuda, H. Kobayashi, I. Iguchi, Y. Tanaka, and S. Kashiwaya. Josephson tunneling of anisotropic high-T_c d-wave junctions with tilted ab-plane $YBa_2Cu_3O_{7-y}$ electrodes. *Physical Review B (Condensed Matter)*, 62(17):11864–71, 2000.

[56] M.H.S. Amin, A.Yu. Smirnov, A.M. Zagoskin, T. Lindstrom, S.A. Charlebois, T Claeson, and A.Y. Tzalenchuk. Silent phase qubit based on d-wave josephson junctions. *Cond-Mat/0310224*, 2003.

[57] E Chudnovsky and J Tejada. *Macroscopic Quantum Tunnelling of the Magnetic Moment*. Cambridge Studies in Magnetism. University Press, Cambridge, 1998.

[58] P. Kopietz and S. Chakravarty. Lifetime of metastable voltage states of superconducting tunnel junctions. *Physical Review B (Condensed Matter)*, 38(1):97–110, 1988.

[59] A. Wallraff, T. Duty, A. Lukashenko, and A.V. Ustinov. Multiphoton transitions between energy levels in a current-biased josephson tunnel junction. *Physical Review Letters*, 90(3):037003–1, 2003.

[60] K.S. Chow, D.A. Browne, and V. Ambegaokar. Quantum kinetics of a superconducting tunnel junction: theory and comparison with experiment. *Physical Review B (Condensed Matter)*, 37(4):1624–46, 1988.

[61] J.M. Martinis, S. Nam, J. Aumentado, and C. Urbina. Rabi oscillations in a large josephson-junction qubit. *Physical Review Letters*, 89(11):117901–1, 2003.

[62] T. Bauch, F. Lombardi, F. Tafuri, A. Barone, G. Rotoli, P. Delsing, and T. Claeson. Macroscopic quantum tunneling in d-wave $YBa_2Cu_3O_{7-\delta}$ josephson junctions. *Physical Review Letters*, 94(8):087003–1, 2005.

[63] A.I. Larkin and Y.N. Ovchinnikov. *Sov. Phys.-JETP*, 64:185, 1986.

[64] C. Cohen-Tannoudji, J. Dupont-Roc, and G. Grynberg. *Atom-Photon Interaction*. John Wiley&Sons Inc., 1992.

[65] J.J. Sakurai. *Modern Quantum Mechanics*. Addison-Wesley Publishing company, 1994.

[66] A.J. Berkley. *A Josephson Junction Qubit*. PhD thesis, University of Maryland, 2003.

[67] H. Xu, A.J. Berkley, M.A. Gubrud, R.C. Ramos, J.R. Anderson, C.J. Lobb, and F.C. Wellstood. Analysis of energy level quantization and tunneling from the zero-voltage state of a current-biased josephson junction. In *2002 Applied Superconductivity Conference, Aug 4-9 2002*, volume 13 of *IEEE Transactions on Applied Superconductivity*, pages 956–959, Houston, TX, United States, 2003. Institute of Electrical and Electronics Engineers Inc.

[68] P. Silvestrini, O. Liengme, and K.E. Gray. Current distributions of thermal switching in extremely underdamped josephson junctions. *Physical Review B (Condensed Matter)*, 37(4):1525–31, 1988.

[69] M.V. Fistul, A. Wallraff, and A.V. Ustinov. Quantum escape of the phase in a strongly driven josephson junction. *Physical Review B (Condensed Matter and Materials Physics)*, 68:060504(R), 2003.

[70] M. Gatzke, M.C. Baruch, R.B. Watkins, and T.F. Gallagher. Microwave multiphoton rabi oscillations. *Physical Review A (Atomic, Molecular, and Optical Physics)*, 48(6):4742–9, 1993.

[71] P.K. Tien and J.P. Gordon. *Phys. Rev*, 129:647, 1963.

[72] B.H. Bransden and C.J. Joachain. *Physics of Atoms and Molecules*. Prentice-Hall, 2003.

[73] A. Barone, R. Cristiano, and P. Silvestrini. Supercurrent decay in underdamped josephson junctions: nonstationary case. *Journal of Applied Physics*, 58(10):3822–6, 1985.

[74] C.C. Homes, S.V. Dordevic, D.A. Bonn, Ruixing Liang, W.N. Hardy, and T. Timusk. Coherence, incoherence, and scaling along the c axis of yba/sub 2/cu/sub 3/o/sub 6+x/. *Physical Review B (Condensed Matter and Materials Physics)*, 71(18):184515–1, 2005.

[75] I. Chiorescu, Y. Nakamura, C.J.P.M. Harmans, and J.E. Mooij. Coherent quantum dynamics of a superconducting flux qubit. *Science*, 299(5614):1869–71, 2003.

[76] Lev B. Ioffe, Vadim B. Geshkbein, Mikhail V. Feigel'man, Alban L. Fauchere, and Gianni Blatter. Environmentally decoupled sds-wave josephson junctions for quantum computing. *Nature*, 398(6729):679–681, 1999.

[77] M.L. Della Rocca, M. Aprili, T. Kontos, A. Gomez, and P. Spathis. Ferromagnetic 0- pi junctions as classical spins. *Physical Review Letters*, 94(19):197003–1, 2005.

[78] C.H. Van Der Wal, A.C.J. Ter Haar, F.K. Wilhelm, R.N. Schouten, C.J.P.M. Harmans, T.P. Orlando, S. Lloyd, and J.E. Mooij. Quantum superposition of macroscopic persistent-current states. *Science*, 290(5492):773–7, 2000.

[79] M.H.S. Amin and A.Yu. Smirnov. Quasiparticle decoherence in d-wave superconducting qubits. *Physical Review Letters*, 92(1):017001–1, 2004.

[80] Ya.V. Fominov, A.A. Golubov, and M.Yu. Kupriyanov. Decoherence due to nodal quasiparticles in d-wave qubits. *Pis'ma v Zhurnal Eksperimental'noi i Teoreticheskoi Fiziki*, 77(10):691–5, 2003.

[81] S. Kawabata, S. Kashiwaya, Y. Asano, and Y. Tanaka. Quasi-particle dissipation in d-wave superconductor phase qubit. *AIP Conference Proceedings Quantum Communication, Measurement and Computing. The Seventh International Conference on Quantum Communication, Measurement and Computing, 25-29 July 2004*, (734):421–3, 2004.

[82] S. Kawabata, S. Kashiwaya, Y. Asano, and Y. Tanaka. Macroscopic quantum tunneling and quasiparticle dissipation in d-wave superconductor josephson junctions. *Physical Review B (Condensed Matter and Materials Physics)*, 70(13):132505–1, 2004.

[83] S. Kawabata, S. Kashiwaya, Y. Asano, and Y. Tanaka. Effect of zero-energy bound states on macroscopic quantum tunnelling in high-tc superconductor junctions. *Cond-Mat*, (0501358), 2005.

[84] E. Il'ichev, N. Oukhanski, A. Izmalkov, T. Wagner, M. Grajcar, H.-G. Meyer, A.Yu. Smirnov, A.M. van den Brink, M.H.S. Amin, and A.M. Zagoskin. Continuous monitoring of rabi oscillations in a josephson flux qubit. *Physical Review Letters*, 91(9):097906–1, 2003.

Appendix A

Energy Conversion Table

The table below lists some experimentally interesting energy values tabulated using four different scales. The conversion between the the scales is done using the following formulas. The voltage-to-frequency conversion is done using the following relations

$$f = \frac{2e}{h}V \tag{A.1}$$

$$T = \frac{2e}{k_B}V \tag{A.2}$$

$$I_c = \frac{2e^2}{h}V \tag{A.3}$$

V	Frequency	Temperature	Critical Current
86 nV	41.7 MHz	1 mK	5.7 pA
1 μV	483 MHz	12 mK	77 pA
2.2 μV	1.02 GHz	25 mK	0.17 nA
10 μV	4.84 GHz	120 mK	0.77 nA
13 μV	5.24 GHz	0.15 mK	1 nA
22 μV	10.8 GHz	260 mK	1.7 nA
86 μV	41.7 GHz	1 K	6.7 nA
100 μV	26.5 GHz	1.2 K	77 nA
0.13 mV	65 GHz	1.6 K	10.4 nA
0.15 mV	70.9 GHz	1.7 K	11 nA
0.21 mV	100 GHz	2.4 K	15nA
0.36mV	175 GHz	4.2 K	28 nA
1mV	484 GHz	12 K	77 nA
6.4 mV	3.2 THz	77 K	0.51 μA
13 mV	6.2 THz	150 K	1 μA
26 mV	12.5 THz	300 K	2.0 μA

Table A.1: Energy conversion table

Appendix B

Appended Papers

Paper I

Feasibility studies of ultra-small Josephson junctions for qubits
A.Ya Tzalenchuk, T. Lindström, S.A. Charlebois, E.A Stepantsov, A.M. Zagoskin, Z. Ivanov and T. Claeson,
IEEE Transactions on Applied Superconductivity, v 13, pp. 48-51(2003)

Paper II

Dynamical Effect of an Unconventional Current-Phase Relation in YBCO dc SQUIDs
T.Lindström, S. A. Charlebois, A. Ya. Tzalenchuk, Z. Ivanov, M. Amin and A.M. Zagoskin
Physical Review Letters 90, 117002 (2003)

Paper III

Mesoscopic Josephson Junctions of high-Tc Superconductors
A. Ya. Tzalenchuk, T. Lindström, S.A. Charlebois, E.A. Stepantsov, Z. Ivanov and A.M. Zagoskin
Physical Review B 68 100501(R) (2003)

Paper IV

Silent Phase Qubit Based on d-wave Josephson junctions
M. H. S. Amin, A. Y. Smirnov, A. M. Zagoskin, T. Lindstrom, S. A. Charlebois, T. Claeson, and A. Y. Tzalenchuk,
Physical Review B, vol. 71, pp. 64516-1 (2005)

Paper V

Josephson Dynamics of Bicrystal d-Wave YBCO dc-SQUIDs
T. Lindström, J. Johansson, T. Bauch, F.Lombardi and S.A. Charlebois
Manuscript (2005)
This manuscript will be somewhat revised before being submitted to a journal

Paper VI

Quantum Dynamics of a d-wave YBCO Josephson Junction
T. Bauch, F. Lombardi, T. Lindström, F. Tafuri, G.Rotoli, T. Claeson and P. Delsing
Submitted (2005)